DEVELOPMENT OF AN ATTENUATED TOTAL REFLECTION INFRARED SENSOR FOR THE MEASUREMENT OF NEUTRAL LIPIDS IN MICROALGAE

A Dissertation

by

TALAL YASIR SULAIYAM ALSHIKAILI

Submitted to the Office of Graduate and Professional Studies of
Texas A&M University
in partial fulfillment of the requirements for the degree of

DOCTOR OF PHILOSOPHY

Chair of Committee,	J. Alex Thomasson
Committee Members,	Yufeng Ge
	Roland Lacey
	Christi K. Madsen
Head of Department,	Stephen Searcy

May 2015

Major Subject: Biological and Agricultural Engineering

ABSTRACT

Algal lipids can be used to produce biofuels and are considered a potential source of energy that could supplant some fossil fuel. Algae can be produced in large ponds, and their nutrient supply can be controlled so as to maximize lipid content. An automated, real-time, lipid-content measuring technique, as opposed to the current time-consuming and labor-intensive laboratory methods, is needed to efficiently control nutrient addition to ponds. Spectroscopy was used in this research to establish that optoelectronic methods could be used for real-time sensing of neutral-lipid content in microalgae. A Fourier-Transform Infrared (FTIR) spectrometer was used with an attenuated-total-reflection (ATR) attachment to acquire spectra from samples of varying lipid contents in two algae species, *Nannochloris oculata* and *Desmid*. Measurements at three absorbance bands (2920 cm^{-1}, 2855 cm^{-1}, and 1742 cm^{-1}) were correlated to lipid content, as measured with gas chromatography (GC). Several estimation models including various groupings of the three bands were found to provide reasonably good estimations of lipid content, suggesting that a sensor using this technique could be used for real-time measurements.

Ultimately a simple, fast, low-cost, infrared (IR) sensor was developed. The sensor uses an integrated convective heater to dry algae-mixture droplets onto an internal-reflection element (IRE). The main components of the sensor are an infrared light-emitting diode

(LED) that emits energy at 2940 cm^{-1}, a right-angle zinc-selenide IRE, and a photodiode to measure energy reflected through the IRE.

Sensor measurements were analyzed with simple linear regression (SLR) to determine their relationship with lipid content. These analyses, like those with spectroscopic data, revealed moderate estimation performance for *Nannochloris oculata*, (R^2 = 0.50; RMSE = 37.7 mg/g), but better performance for *Desmid* (R^2 = 0.73; RMSE = 42.4 mg/g). A generalized model of sensor measurements on both species had poorer performance (R^2 = 0.29; RMSE = 59.12 mg/g), but it showed a promising linear trend between sensor measurements and lipid content across multiple species. The time required for the sensor to take a measurement of one microalgae sample was 120 minutes, far less than that required with conventional laboratory methods.

ACKNOWLEDGEMENTS

I would like to acknowledge all those who made it possible for me to complete this research and dissertation toward accomplishing my doctoral program. Formerly and foremost, my late father who is my great idol in life for hard work, perseverance, pride, and dignity. I would like to extend my deepest gratitude with regret to my mom, wife, and little daughters Reem and Maryam, and all siblings for being patient and helpful while being far away from them. This work couldn't be accomplished without your support and understanding.

I would like to especially thank my supervisor and the chair of the committee Dr. John A. Thomasson for his continuous provision and useful guidance. Not to forget to mention that his personality and attitude in research field has reformed my potentials toward professionalism. I must not forget my committee members, Dr. Yufeng Ge for his unconditional support in providing instructions, information and sometimes practical assistance, Dr. Roland Lacey, and Dr. Christi M. Madsen for their useful comments and support. Special thanks go to Richard Epting and Brandon Hartley for their assistance with regard workshop metal works, Marisa Powell for her assistance with laboratory work.

In conclusion, I would like to thank all employees in the Department of Biological and Agricultural Engineering at Texas A&M University who provided any help and

cooperation in order to complete this work, as well as the National Alliance for Advanced Biofuels and Bioproducts (NAABB) for the research funding.

NOMENCLATURE

IRE	Internal Reflections Element
ATR-FTIR	Attenuated Total Reflection-Fourier Transform Infrared
SLR	Simple Linear Regression
GC	Gas Chromatography
MLR	Multiple Linear Regressions
R^2	Coefficient of Determination
RMSE	Root Mean of Squared Errors
NIR	Near Infrared

TABLE OF CONTENTS

Page

LIST OF FIGURES

Page

LIST OF TABLES

Page

1. INTRODUCTION

Algal biofuels are one type of biomass energy that has a promising future in becoming an important energy source due to the increasing global energy demand and depletion of sources of fossil fuels (Demirbas, 2010; Kosaric, and Velikonja, 1995; Brune et al., 2009). Neutral (non-polar) lipids in algae are the main constituent used to produce biodiesel – one type of biofuel – because they are the most desirable for the commercial production of biodiesel (Rodolfi et al., 2009). Different algae strains are grown in large open ponds under controlled chemical and physical conditions such as nutrients, sunlight, pH, and temperature. However, each algae strain (specie) at different growth stages produces unique biomass fractions of proteins, lipids, carbohydrates, and nucleic acids. The growth conditions play a major role in determining those fractions.

Hence, important issues in the process of biofuel production from algae are the selection of high yield microalgae strains and maintaining the optimum growth conditions (Elsey et al., 2007; Griffiths and Harrison, 2009; Laurens and Wolfrum, 2011). Doing so can maximize lipids in algae, and therefore potentially enhance the production of more biofuel. Therefore, there is a clear the need for screening techniques including lipid measurements in microalgae. Unfortunately, the current traditional lab-based methods to measure and analyze lipids in algae are time consuming, labor intensive, and require large samples (Laurens and Wolfrum, 2011; Cheng et al., 2011). It is of vital importance to devise new

simple, low-cost, and rapid methods to analyze and measure lipids content in microalgae. Such methods may improve the efficiency in selecting the higher yield lipid microalgae strains as well as providing faster feedback to control the optimal growth additions in ponds.

Several techniques have been used to characterize the lipid content in microalgae such as the gravimetric method (Bligh and Dyer, 1959), high performance liquid chromatography-mass spectrometry (HPLC-MS) (Pollio et al.,1988) , thin layer chromatography-mass spectrometry (TLC-MS) (Vieler et al., 2007), spectrofluorometric methods (Elsey et al., 2007; Chen and Vaidyanathan, 2012; Govender et al., 2012; Cooksey et al., 1987), colorimetric sulfo-phospho-vanillin (SPV) method (Wawrik and Harriman, 2010; Cheng et al., 2011), time-domain nuclear magnetic resonance (Gao et al., 2008) , and Near/Mid FTIR infrared spectroscopy (Mulbry et al., 2012; Laurens and Wolfrum, 2011).

Infrared spectroscopy is one of the widely used methods to analyze and quantify a broad variety of biochemical constituents in substances. It is based on the absorption of infrared light by certain chemical functional groups within molecules of substances due to the vibrational movements of atoms within these functional groups. Neutral lipids in algae are fatty-acid esters. The main chemical functional groups are thus carbonyl (C=O) and hydrocarbon groups, specifically methyl (CH_3) and methylene (CH_2). Smith (1999) indicated that the carbonyl group in esters has an absorption band at 1742 cm^{-1} due to the

stretching vibration, and methyl and methylene groups have absorption bands between 2800 cm^{-1} and 3000cm^{-1} due to the bending and stretching vibrations.

Few studies have been done on relating (ATR) FTIR measurements to lipid content in algae. Lauren and Wolfrum (2011) developed multivariate calibration models to predict the levels of neutral and polar lipids in spiked microalgae samples based on near infrared (NIR) and FTIR spectroscopy. They identified three distinct absorption bands for characterizing lipid content. Two bands located within the range (3,025–2,954 cm^{-1}) for characterizing the methyl and methylene groups, and one band for characterizing the ester (C=O) group that falls within (1,746–1,654 cm^{-1}) range. Their results showed high R^2 values of more than 0.90, which indicates good prediction performance of the models produced by the ATR-FTIR spectroscopy technique.

In this research, preliminary laboratory investigations were carried out to identify the diagnostic absorbance bands useful to detect and quantify neutral lipids in algae using transmission FTIR spectroscopy. Simple regression analyses were used to examine the correlation between the measurements of neutral lipids in algae using Gas Chromatography (GC) and the measurements taken by transmission FTIR spectroscopy. Transmission FTIR spectroscopy was used to analyze five algae samples of *Nannochloropsis salina* that had various lipid contents ranging from 26.71 mg/g to a maximum of 158.34 mg/g. Three absorbance bands related to algal neutral lipid were identified, and they are centered at approximately 2920cm^{-1}, 2855 cm^{-1}, and 1742 cm^{-1}.

These bands conformed with the absorbance bands for characterizing lipid content identified by Laurens and Wolfrum (2011), located within the ranges of 3025 to 2954 cm^{-1} and 1746 to 1654 cm^{-1}. Simple linear regression analyses showed that the 2920 cm^{-1} absorption band was strongly correlated with GC verified lipid content, with an R^2 of 0.92 and RMSE value of 10.65mg/g. The results were promising for the use FTIR spectroscopy for the measurement of neutral lipids in algae.

The results and outcomes of the study of using transmission FTIR spectroscopy for the measurement of neutral lipids in algae were used to support the design of a simple, fast, and low cost ATR-IR sensor to predict neutral lipids in algae. The rationale for this concept is that transmission IR spectroscopy and ATR-IR spectroscopy produce similar absorption spectra for the same constituent to be analyzed (Schuttlefield and Grassian, 2008). The difference between the two methods lies in the difference in the presentation of the sample to the measurement system.

Attenuated total reflection (ATR) is based on the reflection of infrared light when it travels from a medium of high refractive index to a medium with lower refractive index. The total reflection occurs when light is incident on the interface between the two mediums at an angle higher than the critical angle θ_c (Figure 1) that can be calculated using Snell's law (equation 3). Snell's law is used to describe the relation between the angle of incidence and refraction that occurs when light is transmitted through the interface between two mediums.

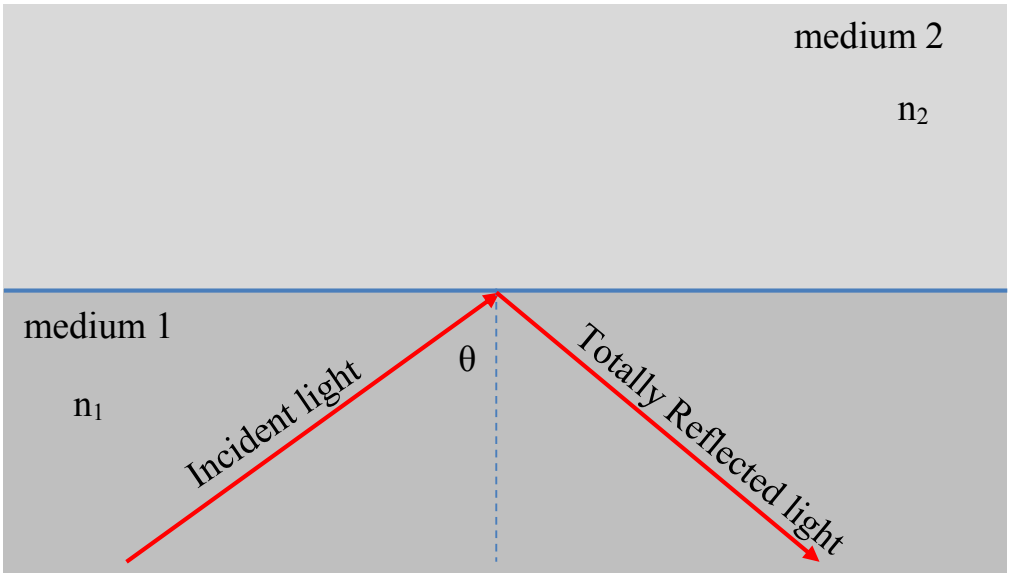

Figure 1. Reflection of light ray at the interface between two mediums ($n_1 > n_2$) when $\theta > \theta_c$

An evanescent wave propagates at each reflection on the interface between the two mediums originating from the high refractive index medium (IRE element). The evanescent wave has a penetration depth d_p at which its intensity decays to 1/e of its original value (Lau et al., 1997). The depth of penetration is expressed by equation (5). The penetration depth value of the evanescent wave is in the order of microns (0.5 – 5.0 μm) (Spectra-tech, 1996; PerkinElmer, 2005), which makes it suitable for analyzing highly absorptive or thick samples. ATR spectroscopy requires minimal sample preparation making it advantageous for rapid sample analysis. The low refractive index medium represents the sample whose specific functional groups need to be measured.

Those functional groups selectively absorbs the IR light of the evanescent wave causing attenuation of the light signal, which then can be measured using an appropriate detector.

This research investigates the suitability of using transmission and ATR FTIR spectroscopy for the measurements of neutral lipids in two microalgae species of various lipids content; *Nannochloris oculata*, and *Desmid*. In addition, a simple, fast, low cost ATR infrared sensor was developed and tested for performance evaluation.

2. BACKGROUND

2.1 Challenges facing fossil fuels as primary source of energy

Nowadays, fossil fuels are the primary source of energy in the world. In 2004, fossil fuels like petroleum, natural gas, and coal accounted for more than 80% of the total world energy consumption (Drapcho et al., 2008; Soetaert and Vandamme, 2009). However, the dependence on fossil fuels as the primary energy source has risks. The main risk is that fossil fuels are threatened by depletion (Demirbas, 2010; Drapcho et al., 2008). A statistical study predicted that the world's maximum oil production would occur between the years 2010 and 2020 and then it begin to decline gradually (Eia.gov, 2007). On the other hand, a current study by Exxon Mobile indicated that oil, natural gas, and coal will still be the dominant energy contributors, accounting for about 80% of the world energy demand up to the year 2040, and that wind, solar, and biofuels will account for about 4% of the energy world demand (Exxon Mobile, 2012). Regardless of the validity of the prediction that oil will run out in the next three or four decades, oil might still be the primary source for energy, but the dependence on it as major source of energy was viewed as decreasing over 40 years ago (Warman, 1972). Besides the eventual depletion of oil deposits, another risk is the political fluctuations of unstable oil-exporting countries which affect the availability of fossil fuel energy in the global market. For example, in 1973 and 1979, oil prices increased dramatically due to the Arab embargo and after the overthrow of the Shah in Iran, respectively, which reduced the oil supply in the market (Campbell

and Laherrère, 1998). As a consequence, the global economy went into recession. In addition to the above risks of availability and price, fossil energy sources are primary pollutants to the environment, enhancing the effect of what is known as the greenhouse phenomenon due to the addition of carbon dioxide in the atmosphere as those sources are burned (Klass, 1998; Hall, 1991).

In the meantime, there is an increase in the demand for energy with the increase in population and growing economy (Kulkarni and Dalali, 2006; Hossain et al., 2008). According to the previously mentioned study by ExxonMobil, the global demand for energy in 2040 is expected to increase by 30% compared to 2010 (ExxonMobile, 2012). The eventual decline in production along with increasing demand will lead to a rise in oil prices, and this phenomenon is likely to continue in the future if no alternative energy sources are developed or no appropriate measures are taken to conserve oil for energy use (Tsoskounoglou et al., 2008). There has recently been a move towards renewable sources of energy to avoid the negative aspects of dependence on fossil fuels and to have secure energy prospects for the future.

2.2 Renewable energy sources

Renewable energy is the energy that is produced from natural sources that are ongoing or can be replenished. Examples include wind energy, solar energy, geothermal energy, tidal energy, hydraulic energy, and biomass energy. Renewable energy has acquired great attention in recent years as an alternative to fossil fuels. In 2007, the contribution of

renewable energy to the world energy supply was 12% and is expected to reach 35% by 2050 (Destouni and Frank, 2010). Climate change, greenhouse gas (GHG) effect, and air pollution are other reasons for the transfer to more cleanly renewable energy sources. Renewable energy sources are carbon neutral and low-polluting alternatives. This is true because some renewable energy sources like, wind, sun, and hydro-electric generate no or little CO_2 emissions, while others like biomass consume CO_2 in the photosynthesis process, which then offsets the CO_2 produced by the combustion of fuel (Tillman et al., 2006). Nonetheless, it is important to understand that there is no one alternative source that can replace fossil fuels, but it is the combined contributions from several alternative sources that could do it (Achara, 2012).

2.3 Biomass energy (Bioenergy)

Biomass is a biological material that is derived from living organisms like plants, microalgae, or animals. The ultimate origin of energy in biomass is the sun, as solar energy is stored as organic compounds by carbon fixation due to the process of photosynthesis (Drapcho et al., 2008). Biomass can be used either directly or indirectly to produce energy. A direct form of producing energy is burning the biomass to generate heat. On the other hand, an indirect form of energy from biomass is to convert the biomass material into another form of energy such as biofuel. Certain biofuels, like oils from plants or algae can be directly used to produce energy or can be converted into biodiesel by the transesterification process. Other biomass material can be converted into bio-ethanol or bio-methane by fermentation of the biomass material by microbes under anaerobic

conditions (Drapcho et al., 2008). In 1995, biomass contributed 62.1% to the total renewable energy sources (Demirbas, 2010). Berndes et al. (2003) reported that the possible contribution of biomass to the world's energy by 2050 ranges from below 100 EJ yr^{-1} to above 400 EJ yr^{-1} (exajoule per year) This contribution is about 16 to 66 % of the total estimated total world energy supply of 612 EJ yr^{-1} (Destouni and Frank, 2010). The large difference in the estimated contribution of biomass energy is due to the uncertainty of future costs, land availability and crop yield levels. However, Destouni and Frank (2010), reported that biomass energy contributed about 10% of the world primary supply of energy and it is expected to reach 20% by 2050 (Destouni and Frank, 2010).Biomass energy is carbon neutral. The produced CO_2 from burning the biomass fuels is eventually taken up by plants or algae in the photosynthesis process.

2.4 Algae biofuel as a source of energy

Algae are a diverse group of simple, plantlike organisms. Unlike plants, algae lack stems, roots, and leaves. The term algae refer to both microalgae that are microscopic in size and can be found floating on the surface of lakes and oceans, and macroalgae which can stretch to up to 100m from the bottom of the ocean to the surface. Algae grow in diverse habitats because they can tolerate a wide range of environmental conditions like temperature, pH, salinity, turbidity, and O_2 and CO_2 concentrations. They can be commonly found in fresh, marine, or brackish water. They also can grow in the desert, hot springs, and mountains. Algae cells can be prokaryotic or eukaryotic. Prokaryotic cells such as, cyanobacteria, lack membrane-bounded organelles. Eukaryotic algae are those

that have membrane-bounded organelles (plastids, mitochondria, nuclei, Golgi bodies, and flagella). The wall of the eukaryotic algae cell is composed of polysaccharides, and a plasma wall surrounds the remaining part of a eukaryotic algae cell.

Algae capture much more of the light coming from the sun than plants, and since they exist in water, which covers two-thirds of the earth's surface they are considered as the most important photosynthesizing organisms on earth (Steinman, 2000). Photosynthetic algae contain chlorophyll, a pigment in their chloroplasts which is the primary component in photosynthesis and is found in all photosynthetic algae. Chlorophyll a absorbs light at two main light wavelengths, 663nm and 430 nm. Photosynthetic algae uses sunlight as a source of energy for growth. The photosynthesis process can be described by equation (1).

$$nCO_2 + nH_2O + Light \xrightarrow{Chlorophyll\ a} (CH_2O)_n + nO_2 \quad (1)$$

where:

n : number of moles

Chlorophyll a : catalytic agent

$(CH_2O)_n$: carbohydrates

Microalgae are microorganisms that growth rapidly and have high lipid content, making them a great potential source for producing biofuels. The U.S. Department of Energy (DOE) stated that algae can produce as much as 30 times more energy than land crops such as soybeans (Achara, 2012)

2.4.1 Growing and harvesting algae

Algae can be raised in either open ponds (raceways) or closed ponds (photobioreactors). Certain nutrients are added to the culture to enhance the growth and thus enhance the production of lipids in algae. Carbon dioxide (CO_2) is the main nutrient that plays a major role in the photosynthesis process. Other important nutrients are nitrogen, phosphorus, potassium, iron, silica, and other trace elements. Other physical and chemical properties of the algae culture medium also affect its growth and need to be controlled, such as temperature, pH, and salinity. Light is the most important external factor that affects the growth, because it is the energy source for the photosynthesis process. Ponds should be shallow, because sunlight can only penetrate water to a limited depth.

Algae can also be raised in photobioreactors. A photobioreactor is a closed cultivating system in which algae are grown and certain elements are added to enhance their growth,such as light, nutrients, and water. Using a photobioreactor is more expensive than using open ponds, but it produces algae of higher nutrient content (Achera, 2012) and offers other advantages.

2.4.2 Algae lipids

Algae biochemical structure is primarily composed of proteins, carbohydrates, fats and nucleic Acids. The proportions of these compounds vary in algae depending on species and culture conditions used to raise algae (Santhanam, 2013). Algae oil contains mostly unsaturated fatty acids. Lipids in algae can be converted to biodiesel using a chemical

process called transesterification (Figure 2). Transesterification is the reaction process of triglycerides with alcohol such as methanol in the presence of an acidic or basic catalyst to produce methyl esters (biodiesel) and glycerol as a trace element (Asakuma, 2011).

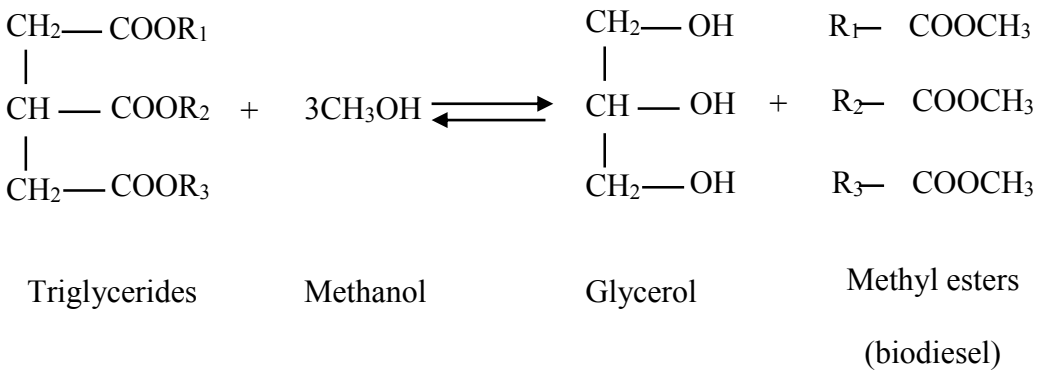

Figure 2. Transesterification chemical process of triglycerides

2.4.3 Extraction of lipids from algae

Generally, lipids in algae can be extracted using physical or chemical extraction methods or using both methods depending on the algae strain (Achara, 2012). In the physical process, the algae biomass is mechanically crushed to separate the oil content from the other biomass using different pressing techniques. Chemical extraction is carried out using solvents to break the algae cell walls and separate the oil. Examples of chemical solvents used are benzene, hexane, certain enzymes, and supercritical CO_2 (Achara, 2012).

2.5 Measurement techniques of algae lipids

2.5.1 The importance of measuring lipid content in algae

One of the important issues in the production of biofuels from algae is the selection of high yield microalgae strains and optimum culture conditions that potentially yield higher lipid contents and therefore more biofuel. Optimizing production requires rapid lipid measurements. Therefore, it is important to devise new methods to measure the lipid content in algae more quickly and continuously. It is desirable that these methods be incorporated into online measurement systems in algae ponds or algae biofuel production facilities. These methods can save time and effort and provide fast data feedback to control the optimal addition of nutrients such that it conserves resources and increases the amount of lipids in the cultured algae.

There are many spectroscopic and non-spectroscopic techniques to measure lipids in algae such as gravimetric, HPLC/TLC/Gas Chromatography, fluorescence spectroscopy, and NIR/FTIR infrared spectroscopy. Each method has its own advantages and disadvantages, but there is no one method that is specifically used to measure lipids in algae which could addresses and takes in account biological and structural diversity of algae species.

2.5.2 Non – Spectroscopic techniques

2.5.2.1 Gravimetric method

The gravimetric method is the most common method to quantify lipids in algae. It is also considered to be the most accurate. In this method, solvents are used to extract lipids from

dried algae powders. The extraction solvent is then evaporated and algae lipids are collected. The collected lipids represent the amount of lipid within the algae sample. The main drawbacks of the gravimetric method are that it is time consuming and labor intensive, requires large samples, and is invasive.

2.5.2.2 HPLC, TLC, and gas chromatography

HPLC (High-performance liquid chromatography), TLC (Thin-layer chromatography), and GC (Gas Chromatography) are based on the separation of the different constituents of a sample when mixed with a solvent (mobile phase) and forced through a porous medium called the stationary phase. The different constituents of the sample move at different speeds through the stationary medium due to the differences in their attraction to the stationary phase and differences in solubility in the solvent used (mobile phase). The time it takes each constituent to travel through the stationary phase to the detector is called the retention time. A particular constituent in the solution is identified by comparing its retention time is to a known retention time of the same constituent in a pure form measured under the same conditions. A detector is then used to identify and quantify each constituent present in the examined solution.

Laurens and Wolfrum (2011) reported that HPLC and TLC are powerful methods for analyses of lipids. However, these methods require considerable preparation of the sample prior to analysis (Han et al., 2011). Gas chromatography is also one of the most preferable

methods to measure and quantify lipids because it provides detailed information on fatty acid composition (Kramer et al., 2008; Mossaba et al., 2009).

2.5.3 Spectroscopic techniques

Spectroscopy is one type of analytical technique used to study the interaction of light with matter. Light interacts with matter in different ways: absorption, reflection, scattering, transmission, or diffusion. Spectroscopy can be used to identify and quantify the concentrations of certain chemical functional groups within molecules of a substance by measuring the amounts of these interactions at various wavelengths.

The use of infrared spectroscopy to analyze the composition of substances has many advantages over conventional methods. Infrared spectroscopy is highly versatile, provides rich information, and is fast, non-destructive, very sensitive, and relatively inexpensive (Laurens, and Wolfrum, 2011; Wagner et al., 2010). It can be used to study a wide range of substances in different forms such as solids, liquids, pastes, and gases. Furthermore, the features in the spectra produced by infrared spectroscopy such as locations of the peaks as well as their heights, widths, and shapes provide rich information about the substance being studied. Infrared spectroscopy can be used to study materials that have as low as 5 ng of a substance (Hsu, 1997). The preparation time required to prepare samples for spectroscopic analysis is very low compared to that of other methods. Lastly, spectroscopy instruments are relatively inexpensive compared to other laboratory equipment.

2.5.3.1 Staining and fluorescence spectroscopy

Staining methods require the use of fluorescent lipophilic dyes like Nile red, and boron-dipyrromethene (BODIPY) which selectively adhere to neutral lipids in algae cells. Fluorospectrophotometers are then used in conjunction with the stains to provide an indirect measurement of lipids in algae by measuring the fluorescence intensity of the staining dyes. These methods are relatively faster and require less preparation than gravimetric and chromatography methods, but they have lesser accuracy (Han et al., 2011). A major drawback of staining methods is the uneven dye uptake by lipids in algae cells for different algae strains.

2.5.3.2 Colorimetric methods

Colorimetric methods are used to determine the concentration of colored constituents in a solution. The reaction of some constituents with specific reagents produces unique colors which then can be read and provide an indirect measurement for constituent concentration. For lipid analysis and measurement, sulfo-phospho-vanillin (SPV) is used as coloring reagent.

Wawrik and Harriman (2010) used a colorimetric method to determine the amount of lipids in two microalgae species, *Phaeodactylum tricornutum* and *Chlorella vulgaris*.. Their method was based on hydrolysis of algae lipids using saponification with sodium hydroxide (NAOH), mixing with copper reagent to create copper salts of long chain fatty acids, and subsequent extraction of copper salts into chloroform. Diethyldithiocarbamate

was then added, which develops a yellow color proportional to the amount of fatty acids in the solution. The yellow color was then detected using a spectrometer at 440 nm, and the measurement provided a measure of lipids in the algae. The method produced reliable detection and quantification of lipids suitable for small volume samples.

2.5.3.3 TD-NMR method

Time domain nuclear magnetic resonance (TD-NMR) is based on the different relaxation times of hydrogen nuclei in different phases of the sample analyzed (Todt et al., 2001). Different constituents in solution exhibit different relaxation times. Carbohydrates and proteins exhibits a relaxation time on the order of microseconds, while free water, bound water, and lipids exhibit times of seconds, a few hundred microseconds, and a few hundred milliseconds, respectively.

2.5.3.4 IR spectroscopy

Infrared spectroscopy is a technique that is used to acquire an infrared spectrum of absorption, emission, reflection, transmission, or Raman scattering for specific, gaseous, solid, or liquid material. The rotational and vibrational movements of molecules induce the absorption of light in the infrared red region of the spectrum and create unique absorption bands (Sun, 2009). Infrared energy incites those rotational and vibrational movements when its frequency matches the molecules' frequency of movement.

Infrared spectroscopy is the spectrometry of materials using light in the mid-infrared region of spectrum from 4000 cm^{-1} to 400 cm^{-1} (2.5μm to 25μm). IR spectroscopy deals with the absorption of light by molecules at a given wavelength due to mainly the fundamental molecular vibrations and many of first overtones and combinations (Melling and Thomson, 2002). The absorption spectra produced in this region of the spectrum show highly distinctive sharp absorption bands for pure constituents, which makes the identification of specific molecules in mixtures possible. Infrared spectroscopy can be used to identify the unknown substances related to specific functional groups in molecules by comparing the spectra of the unknown spectra to known ones. Also, the absorption intensity in spectra provides a measure of the concentration of certain functional group within a molecule.

Lauren and Wolfrum (2011) developed multivariate calibration models to predict the levels of neutral and polar lipids in spiked microalgae samples based on near infrared (NIR) and Fourier-transform infrared (FTIR) spectroscopy. They identified three distinct absorption bands for characterizing lipid content. Two bands located within the range (3,025 to 2,954 cm^{-1}) for characterizing the methyl (CH_3) and methylene (CH_2) groups, and one band for characterizing the ester (C=O) group that falls within (1,746 to 1,654 cm^{-1}) range. Their results showed high R^2 values of more than 0.90, which indicates good prediction performance of the models produced by the ATR-FTIR spectroscopy technique.

In infrared spectroscopy, the infrared light may come into contact with the sample being studied in two different configurations. Those are transmission and ATR infrared spectroscopy. Both transmission-IR and ATR-IR techniques produce similar absorption spectra for the same constituents to be analyzed (Schuttlefield and Grassian, 2008). The difference between the two lies in how the sample is presented in the measurement system. The similarity is that they both use energy in the mid-infrared range of the spectrum and provide the same diagnostic bands (wavelengths) to characterize material constituents. However, ATR method requires less sample preparation. This feature makes ATR a faster and less costly method to measure lipid content in algae.

2.5.3.4.1 Transmission-IR spectroscopy

In the case of the use of transmission IR spectroscopy, the sample to be examined is placed between an IR source and a detector. Energy that ranges from 400 cm^{-1} to 4000 cm^{-1} is then emitted toward the sample and the transmitted energy through the sample is measured by an appropriate detector. The ratio of the transmitted energy to the emitted energy provide a measure of how much energy been absorbed along the infrared spectrum. The Beer-Lambert law describes this absorption as follows;

$$A = \log_{10} \frac{I_T}{I_0} \quad (2)$$

where:

A : absorption

I_T : transmitted light intensity through the sample

I_0 : emitted light intensity from the source

2.5.3.4.2 ATR IR spectroscopy

ATR infrared spectroscopy is based on the principal of internal reflection spectroscopy that was established in 1960's by Fahrenfort (Fahrenfort, 1961), and Harrick (Harrick, 1967). Total internal reflection occurs at the interface between two mediums when light is transmitted at an angle equal to or higher than the critical angle (θ_c) through a denser medium of higher refractive index (n_1) toward a rarer medium of lower refractive index (n_2) (Figure 3). The critical angle depends on the refractive indices of both mediums and is mathematically expressed using Snell's law of refraction as follows

$$\theta_c = \sin^{-1}\left(\frac{n_2}{n_1}\right) \quad (3)$$

At each reflection at the interface, an evanescent wave extends from the denser medium toward the rarer medium. Harrick, 1967 expressed mathematically the evanescent wave as

$$E = E_0\, e^{-\left(\frac{z}{dp}\right)} \quad (4)$$

where:

E : wave amplitude at given Z distance from the interface

E_0 : wave amplitude at the interface

z : distance from the interface

d_p: penetration depth

The penetration depth of the evanescent wave is mathematically expressed as follows;

$$d_p = \frac{\lambda_1}{2\pi(\sin^2\theta - {n_{21}}^2)^{\frac{1}{2}}} \quad (5)$$

where:

$\lambda_1 = \frac{\lambda}{n_1}$: wavelength of the incident light at the denser medium

$n_{21} = \frac{n_2}{n_1}$

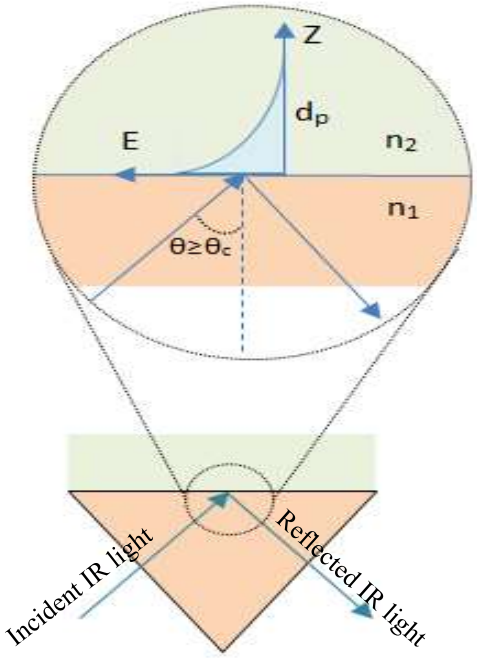

Figure 3. Schematic representation of the ATR of infrared light on a right angle shape IRE

A typical ATR-IR system is composed of three main components; a light source, internal reflection element (IRE), and a detector. Internal reflections elements (IRE) are usually made of materials of high refractive index such as diamond, germanium, Zinc-Selenide, etc. Each material has essential properties that need to be considered when choosing the

proper IRE for the given problem, such as refractive index, hardness, tolerance to temperature and PH, etc.

An advantage of using ATR spectroscopy over transmission FTIR spectroscopy is that, the absorbed light that doesn't makes its way toward the detector represents the portion that is absorbed by the sample. On the other hand, in transmission infrared spectroscopy some light is reflected back and doesn't make its way toward the detector and since it is not detected, someone might interpret it as absorbed light (Milosevic, 2012).

3. RESEARCH OBJECTIVES

The goal of this project was to investigate the suitability of using transmission and ATR spectroscopy for the measurement and prediction of neutral lipids in microalgae. The outcomes of these studies were then utilized to assist in the design and development of a simple, fast, and low-cost ATR-IR sensor for the measurement of neutral lipids in microalgae.

The specific goals of this project were to:

1. Investigate the suitability of using transmission FTIR spectrometry for the measurement of neutral lipids in microalgae, and determine appropriate diagnostic bands associated with lipid-based absorption.

2. Investigate the suitability of using ATR-FTIR spectrometry for the detection and measurement of neutral lipids in microalgae.

3. Design and develop a simple, fast, low-cost ATR infrared sensor to predict neutral lipid content in microalgae.

4. TRANSMISSION FTIR SPECTROSCOPY OF NEUTRAL LIPIDS IN MICROALGAE

This section describes the use of transmission FTIR spectroscopy for the measurement of neutral lipids in microalgae using the Nicolet 6700 FTIR spectrometer. Specific objectives were to identify the diagnostic absorbance bands associated with neutral lipid content in microalgae and evaluate their correlation strength with lipid content. Findings form this study will be used to assist in the design of a simple, fast, and low cost ATR-IR sensor for the measurement of neutral lipids in microalgae. This section includes materials and methods and results and discussion.

4.1 Materials and methods

4.1.1 Algal solutions and lipid content

The algae specie *Nannochloropsis salina* was used in this study. Five samples of *Nannochloropsis salina* having different lipids content were used. The samples were obtained from the Texas A&M Agrilife Research algae test facility in Pecos, Texas. Cultures were grown in rigorously maintained, outdoor, manmade ponds. Samples were received in the form of algal solutions and kept refrigerated at 4 °C to maintain their biochemical composition. A spreadsheet that shows the lipid composition of the algae samples was also provided along with the samples. The lipid content of each sample was determined using the gas chromatography (GC) technique. Gas chromatography (Agilent

6890N) mass spectrometry (Agilent 5975B) with flame ionization detector (GCMS–FID) was used to resolve and measure the fatty acid methyl esther (FAME) components from C_{14} to C_{24}. Neutral lipid was then calculated as the sum of all component FAMEs. The lipid content in the five samples ranged from a minimum of 26.7 mg/g to a maximum of 158.3 mg/g.

4.1.2 Algae-KBr pellets

In order to produce the absorption spectra for the algae samples using the FTIR transmission spectroscopy, Algae-KBr pellets were created by pressing a mixture of dried algae samples with Potassium Bromide (KBr). The process of making the algae-KBr pellets starts with drying the algae samples, grinding them, mixing them with KBr, and finally pressing the mixture under high pressure (5~6 bar) for 5 minutes to create algae-KBr pellets. Further description of this procedure is shown later in this section.

Water is known to strongly absorb light over a broad range of the IR spectrum, interfering with the measurement and affecting the accuracy (Pejcic et al., 2009). To minimize water interference, it was important to dry the algae samples prior to transmission FTIR measurements. The samples were dried into two stages; centrifugation and then oven drying. In the centrifugation process, the samples were placed in vials which were then inserted into a centrifuge (LABNET Hermle Z300) to remove excess water in algal solutions using a centrifugation speed of 2300 rpm for 20 minutes. The samples were then further dried in a drying oven for 12 hours at 40°C.

In transmission FTIR measurements, it is important that the sample under measurement is relatively transparent and does not prevent energy from reaching to the detector. Therefore, a small fraction of a sample is commonly mixed with an IR transparent material such as Potassium bromide (KBr).

Thus, after the samples were dried, they were mixed with KBr powder in a ratio of 1:150 (Algae:KBr). The mixture was then ground using a pestle and mortar to produce a fine and even blend. A quantity of 135 mg of the mixture was taken to create one Algae-KBr pellet by pressing it at high pressure of 6 bar (600 kPa) for 5 minutes using a hydraulic press (Carver, Inc). Each algae-KBr pellet is 13 mm in diameter and about 1 mm in thickness (Figure 4.a). The pellets are so fragile because of their small thickness and therefore must be handled carefully to avoid breakage. If stored for periods before acquiring the spectral measurements, they must be stored in a container in a cool and dry place to ensure no contamination by atmospheric moisture. It is of vital importance to check the quality of the algae-KBr pellets to ensure reliable transmission FTIR measurements. Important quality measures are degree of cloudiness and breakage. A high degree of cloudiness indicates insufficient drying or moisture contamination from the ambient atmosphere. A high degree of breakage indicates poor mixing and grinding of the samples. The quality of these pellets was examined by visual observation. A good algae-KBr pellet is one that is relatively clear (uncloudy) and retains its circular shape with no breakage. Samples of low quality were discarded and replaced with new ones produced with the earlier mentioned criteria.

4.1.3 Transmission-FTIR spectroscopy

The spectrum of each algae-KBr pellet was acquired using a Thermo-Nicolet FTIR spectrometer (Model 6700, Madison, Wisconsin) (Figure 4.b).The instrument – when in transmission mode – emits light in the infrared region of the spectrum, measures the light transmitted through the pellet and produces a curve that shows the absorbance of IR light along the spectrum. The spectra were then analyzed using the OMNIC™ software by Thermo Scientific™. The software has many features that help to identify the location and intensity of absorption peaks along the infrared spectrum.

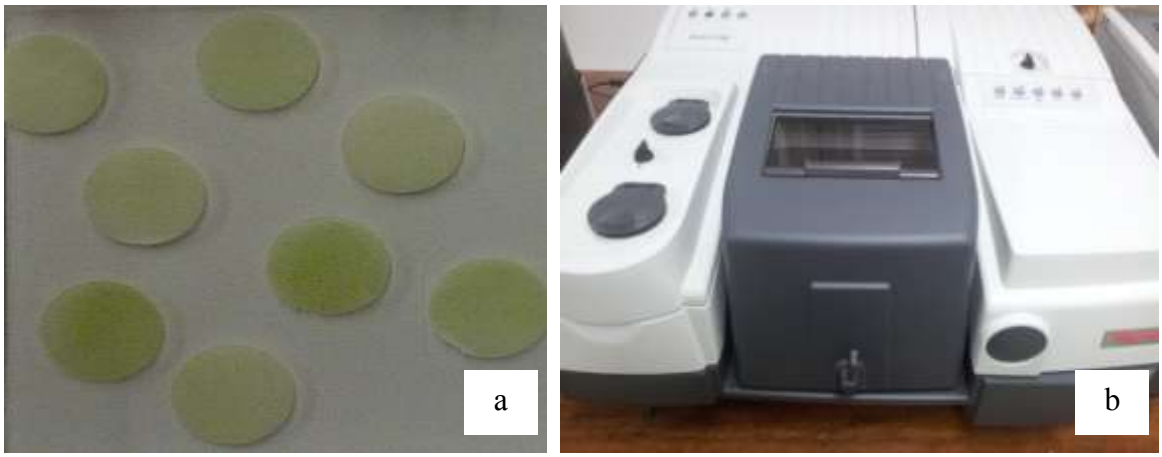

Figure 4. a) Algae-KBr pellets b) Nicolet 6700 FT-IR spectrometer

4.1.4 Identifying the absorbance bands and calculation of absorbance

After the spectra were obtained for each sample, OMNIC™ software was used to locate and measure the absorbance peaks at the diagnostic bands. Figure 5 shows an example of

one sample spectrum in which absorbance height was calculated at 2920 cm^{-1}. The calculation was achieved with the usage of the height calculation tool in the Omnic software of the Nicolet 6700 FTIR spectrometer. The tool calculates the height of the absorbance peak at the absorbance band 2920 cm^{-1} which depends on the amount of light being absorbed by lipids in the microalgae samples. The same procedure used for calculating the absorbance at diagnostic bands 2855 cm^{-1} and 1742 cm^{-1}. Absorbance was calculated using the Beer-Lambert law as follows:

$$A = -\log_{10}\left(\frac{I}{I_0}\right) = \varepsilon l c \quad (6)$$

where:

I : transmitted light intensity

I_0 : incident light intensity

ε : molar absorptivity of the sample

c : molar concentration of absorbing molecules

l : sample length

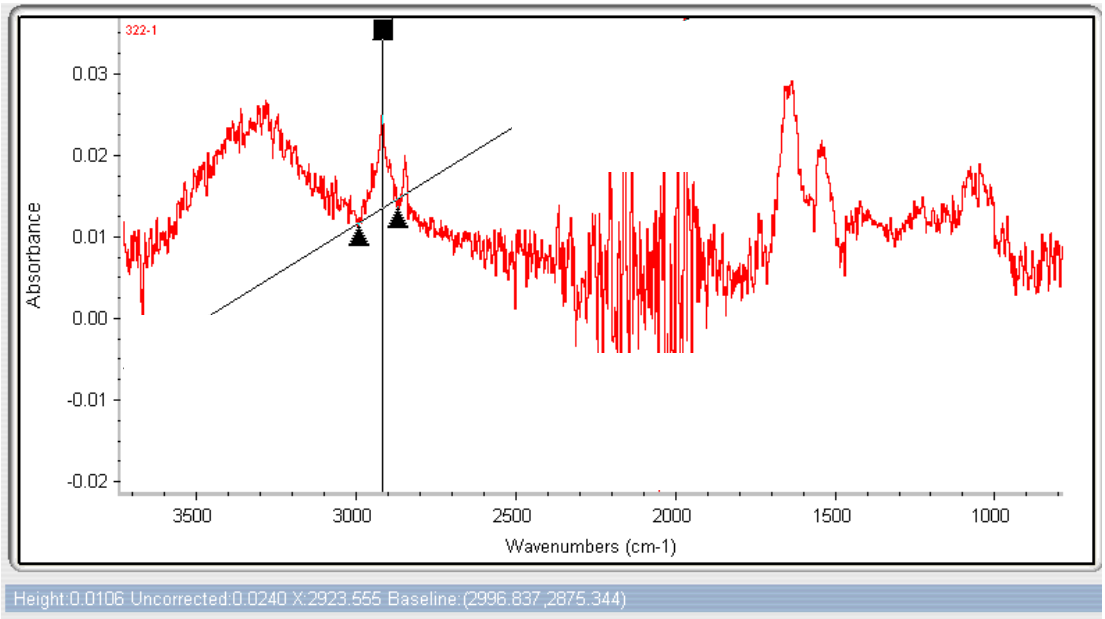

Figure 5. Calculation of absorption at the diagnostic band

4.1.5 Statistical analysis

Simple linear regression analyses were used to relate the absorbance values at each diagnostic absorption band to neutral lipid content for all the algae samples. The regression analyses were done using JMP (SAS Institute) statistical software. Two statistical parameters are of most interest; the coefficient of determination (R^2) and root mean squared error (RMSE). The R^2 value represents the degree of fitness of the measured data to the regression line. It explains how much of the variability in the dependent variable can be explained when related to the independent variables using that regression line (linear equation). The RMSE is the root mean of squared errors of the differences between the predicted values and the measured ones.

4.2 Results and discussion

4.2.1 Absorption spectra

A sample graph of the collected spectra for two Algae-KBr Pellets illustrating the diagnostic absorbance bands is shown in Figure 6. The graph shows the spectra of two different algae samples having different lipid contents, 39.5 mg/g and 94.7 mg/g. All spectra for the different samples show the same unique features and conformed with the findings of Laurens and Wolfrum (2011) such that the absorption of light by algae lipids in the samples occurred at three diagnostic bands 2920 cm^{-1}, 2855cm^{-1}, and 1742 cm^{-1}. It is obvious from figure 6 that the highest absorption intensity occurred at diagnostic absorbance band 2920 cm^{-1}, less at 2855cm^{-1} and least at 1740 cm^{-1}. The spectra also show some absorbance bands related to other biochemical groups in the algae samples. Those are protein at 1545 cm^{-1}, and carbohydrates at 1150 cm^{-1}.

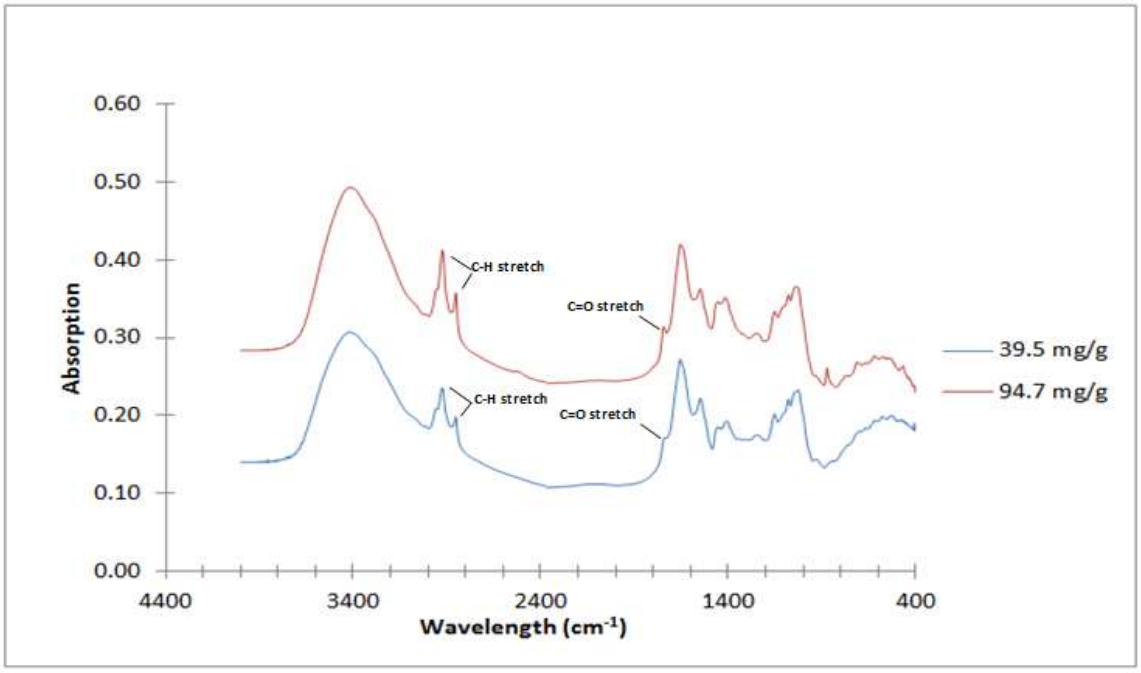

Figure 6. Absorption spectra graph of two Algae-KBr pellets having different lipid content

4.2.2 Simple regression analysis

The regression analyses produced three prediction models for lipid content in algae using each diagnostic absorbance band. The R^2 and RMSE values were used to evaluate each diagnostic absorbance band's prediction performance (Table 1). Diagnostic bands at 2920 cm^{-1} and 2855 cm^{-1} produced high R^2 values and low RMSE values, which indicate that they both estimate the lipid content in microalgae with reasonable precision (Figures 7 and 8). On the other hand, band 1742 cm^{-1} had a significantly lower R^2 value and higher RMSE value than the other bands, indicating lower prediction performance (Figure 9).

Table 1. Regression parameters of simple linear regression analyses

Diagnostic band [cm^{-1}]	R^2	RMSE [mg/g]
2920	0.92	10.56
2855	0.89	11.82
1742	0.58	23.42

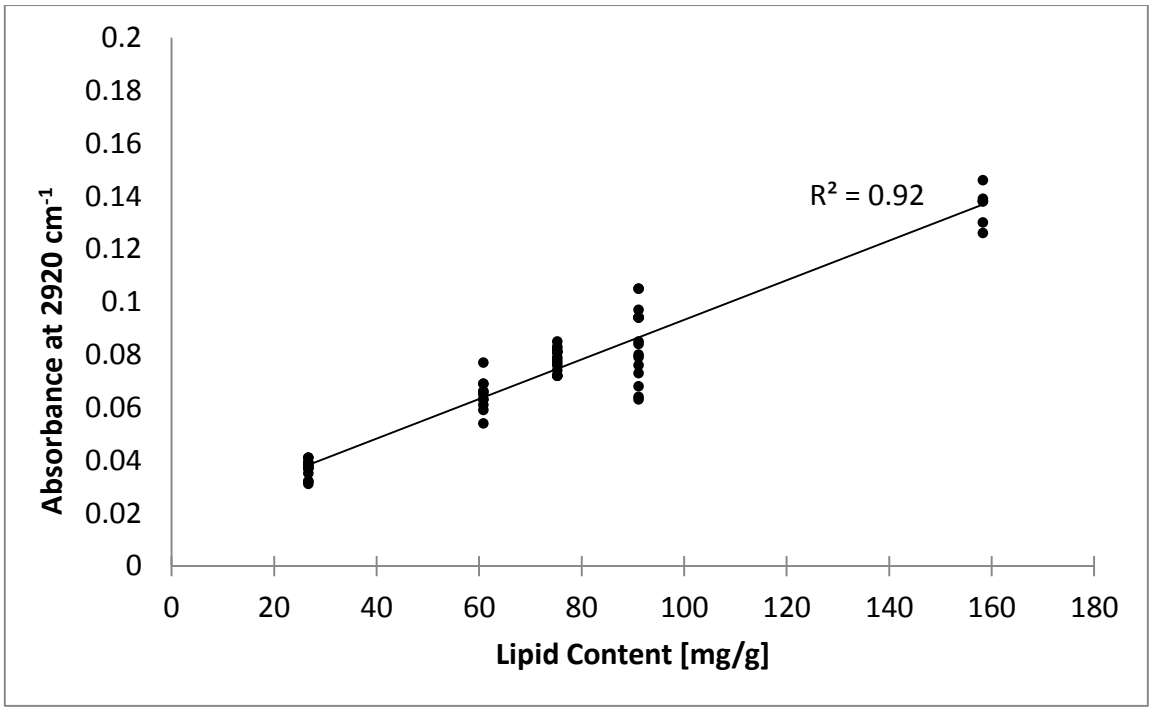

Figure 7. Actual lipid content versus transmission FTIR measurements (Absorbance) at 2920 cm^{-1} absorbance band

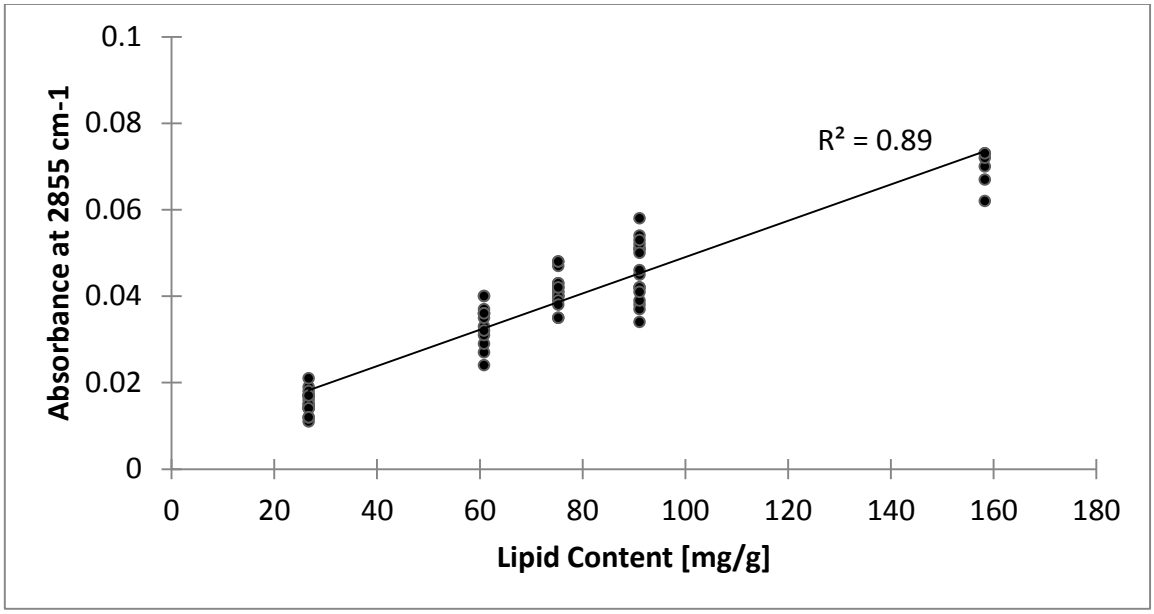

Figure 8. Actual lipid content versus transmission FTIR measurements (Absorbance) at 2855 cm^{-1} absorbance band

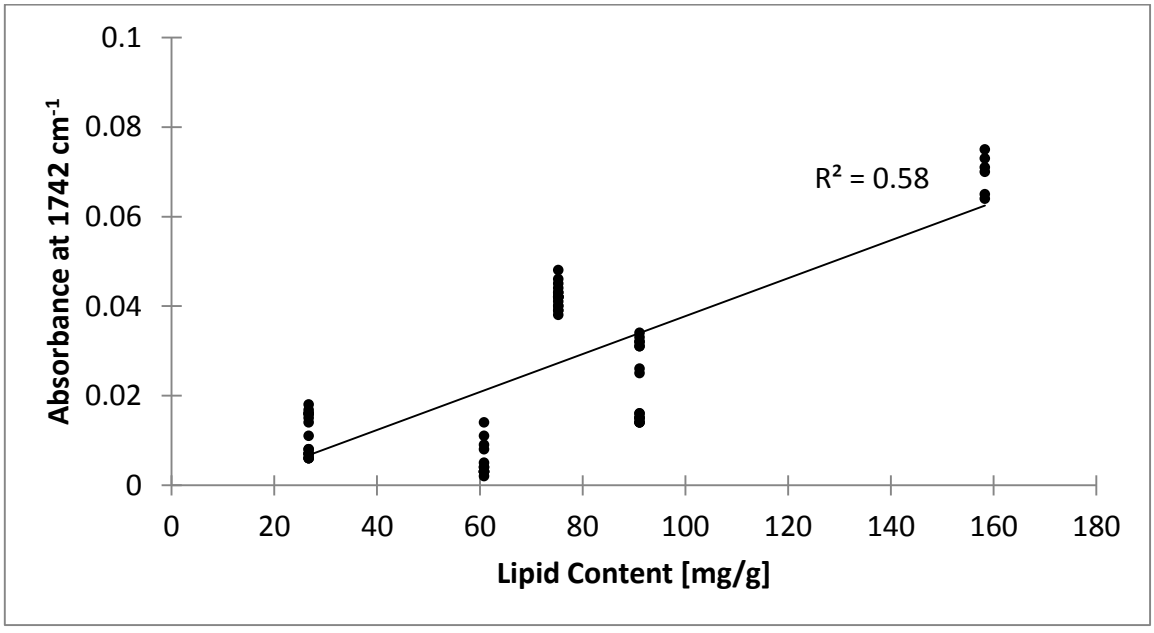

Figure 9. Actual lipid content versus transmission FTIR measurements (Absorbance) at 1742 cm^{-1} absorbance band

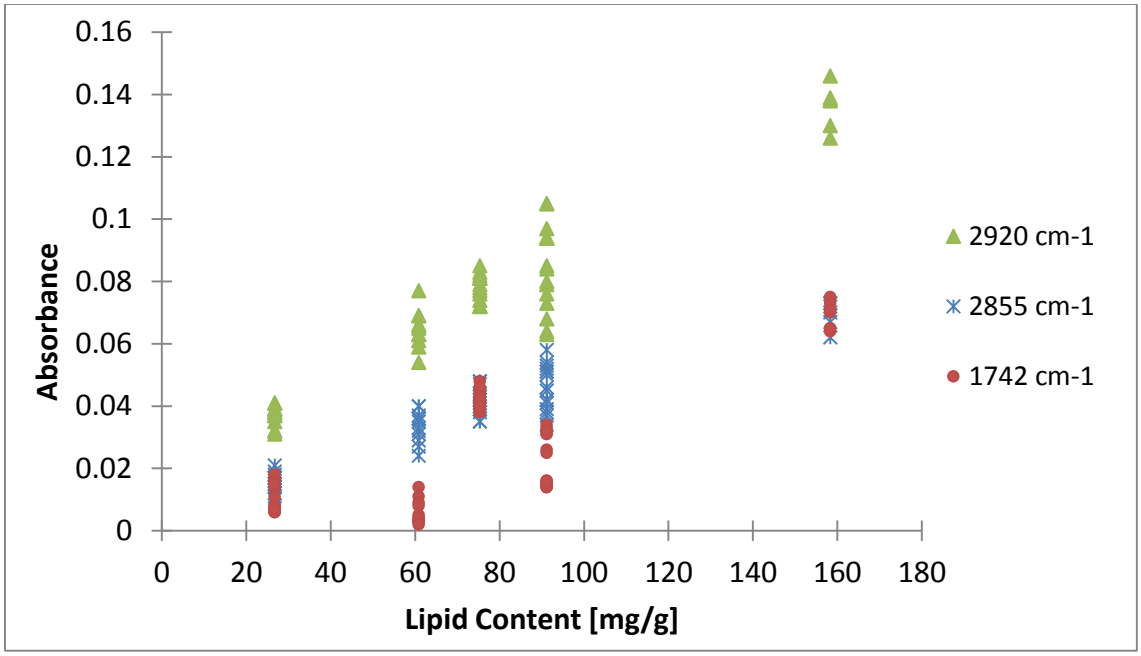

Figure 10. Comparison of absorbance at all diagnostic bands

4.2.3 The selection of a single best absorbance diagnostic band

One of the important objectives of this study was to select appropriate spectral bands to predict the lipid content in microalgae. The reason for choosing only one absorbance band in this work was to reduce cost and design complexity of the developed sensor. Thus, based on the above results and discussion, the 2920 cm^{-1} band was selected to be incorporated into the design of an ATR infrared sensor to predict neutral lipids in microalgae.

Figure 10 also shows that absorbance measurements at 2920 cm^{-1} had higher absorbance values for all microalgae samples compared to measurements at 2855 cm^{-1} and 1742 cm^{-}

[1]. Therefore, a sensor using this band would benefit from higher signal strength. Furthermore, electrical and optical components at lower infrared wavelengths are more available and less expensive.

5. DESIGN AND COMPONENTS OF THE DEVELOPED ATR-IR SENSOR

This part of the dissertation includes an explanation of the design of the sensor and its components, as well as a discussion of testing and comparisons of the performance of the sensor to that of the spectrometer when measuring the concentration of pure canola oil in chloroform ($CHCL_3$).

5.1 Overview of the ATR-IR measurement system

The developed ATR-IR sensor is composed of two main parts, the ATR-IR measurement system and the drying system. The design of the ATR-IR sensor was based on the use of a single internal reflection element (IRE), an infrared light emitting diode (IR-LED), a photo-detector (PD), and collimating and focusing lenses. The selection of the infrared light emitting diode and the photodiode detector was based on the findings from the transmission FTIR spectroscopy discussed earlier. The results suggested the use of 2920 cm^{-1} (≈ 3.4 μm) as the diagnostic absorbance band. Figure 11 shows the various components of the developed ATR-IR measurement system. The drying system uses a convection heat drying technique to evaporate water content from the algae samples after they are placed on the IRE prism prior taking the measurement. The drying system is composed of a ceramic heating element (200 watts), inlet air fan, air exhaust fan, and a temperature control system to control the temperature inside the drying chamber.

The sensor was designed with the software, Solidworks® 2014. Drawings and further details on the design measurements and dimensions of the sensor components are shown in appendices A, B, C, and D.

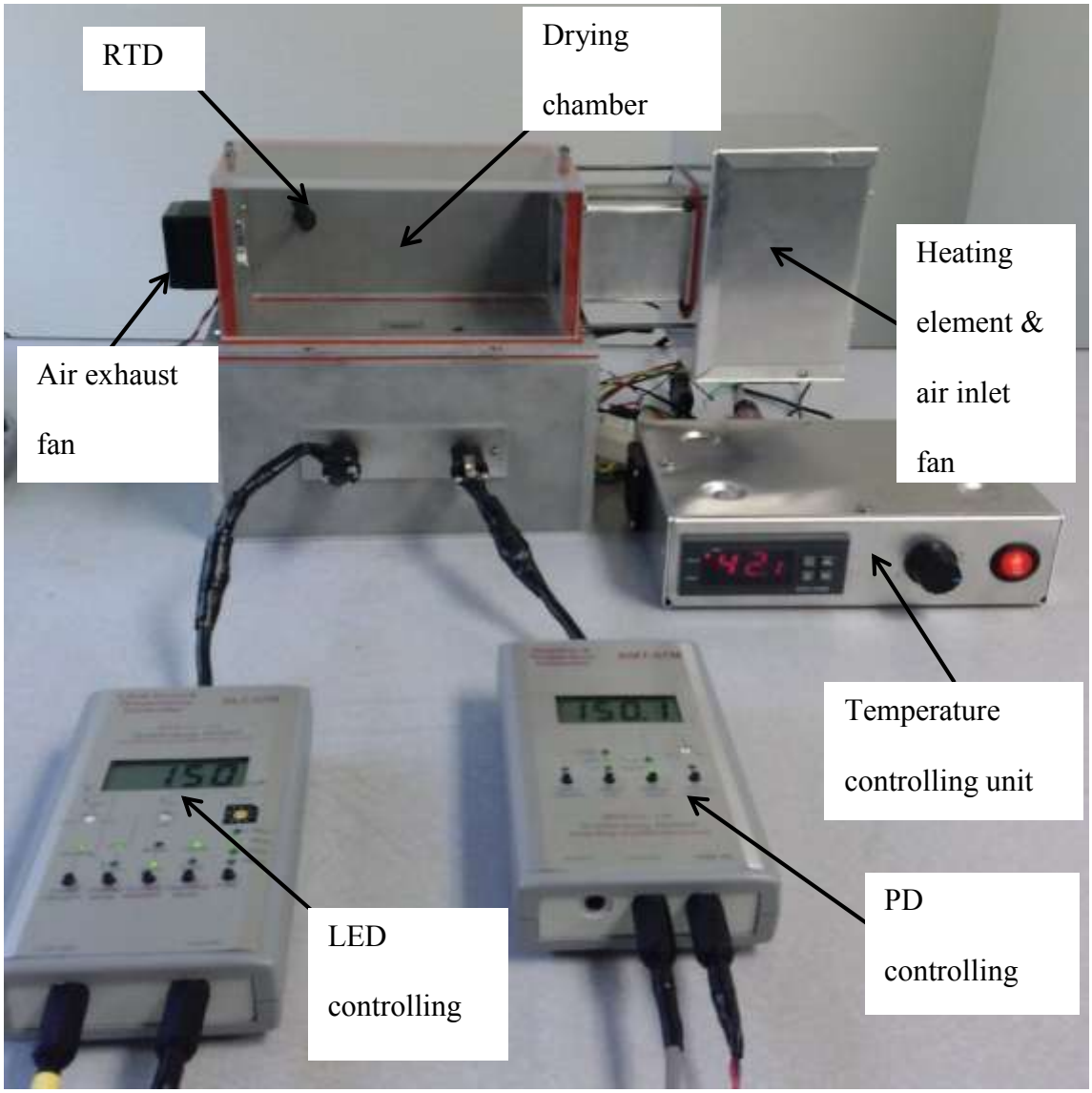

Figure 11. Various components of the attenuated total reflection- infrared sensor (ATR-IR sensor)

5.1.1 The light emitting diode (LED)

The light emitting diode (LED34-TEC) has an emission wavelength centered at 3.4 µm (≈ 2940 cm^{-1}) and an integrated thermoelectric cooling system to maintain a constant operating temperature (Figure 12). The LED operation is controlled with an LED driver and temperature control unit (DLT-37M). The LED was driven with a quasi-continuous-wave mode of 150 mA at a frequency of 2 KHZ. Further details about the LED (LED34-TEC) are shown in appendix C-1.

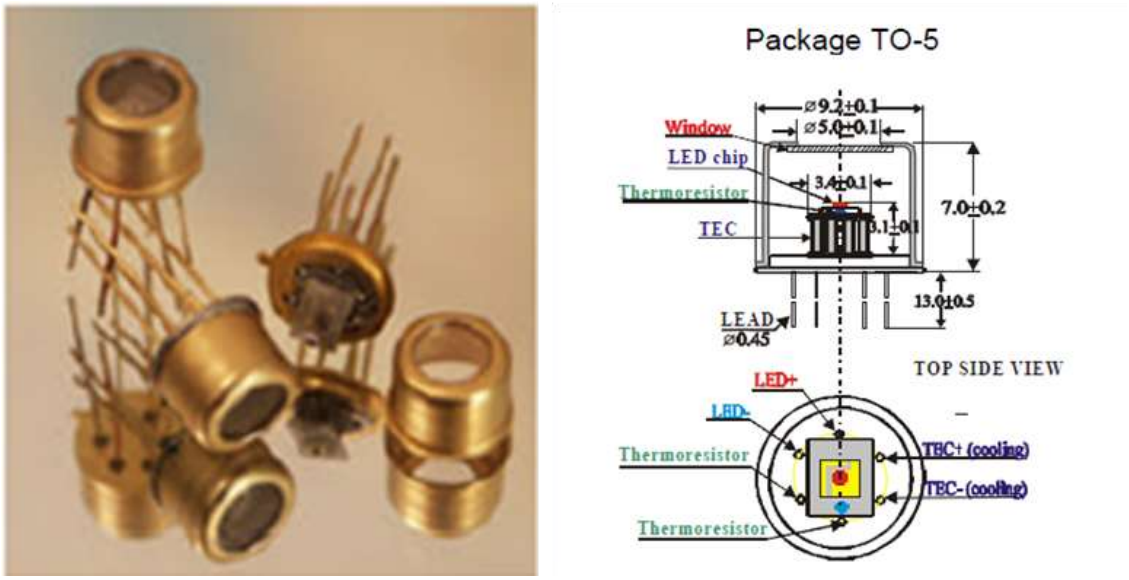

Figure 12. Photo and diagram illustrating the LED34-TEC (courtesy of IBSG)

5.1.2 The photodiode

The photodiode detector (PD-36-TEC) has region of wavelength responsivity that extends from 1.50 to 3.80 µm. The photodiode is made of Lead (II) Sulfide (PbS) (Figure 13). Like the LED34-TEC, it has an integrated thermoelectric cooling system that maintains ideal operating temperature. The photodiode is controlled with the AMT-07M amplifier and temperature controller unit. Further details about the PD-36-TEC are shown in appendix C-2.

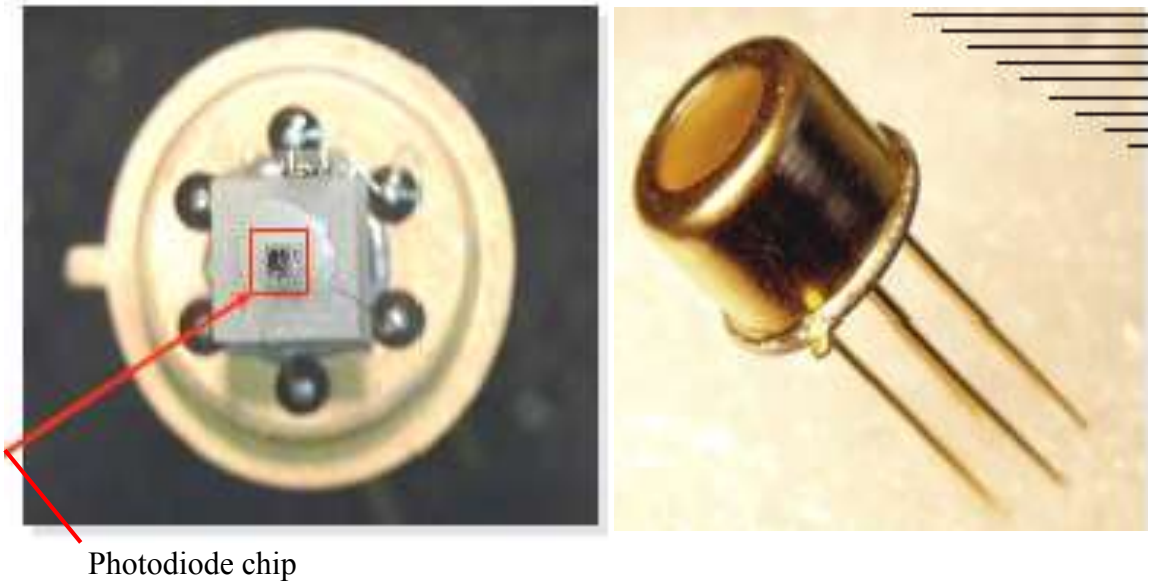

Figure 13. Photo illustrating the PD-03-TEC (courtesy of IBSG)

5.1.3 The IRE prism

The internal reflection element (IRE) is a right angle shaped prism made of zinc selenide and manufactured by Thorlabs, Inc. Zinc selenide is a clear yellow polycrystalline material that transmits light in the range of 0.5 to 15µm (Figure 14). Further information and specifications about the IRE element are shown in appendix C-3.

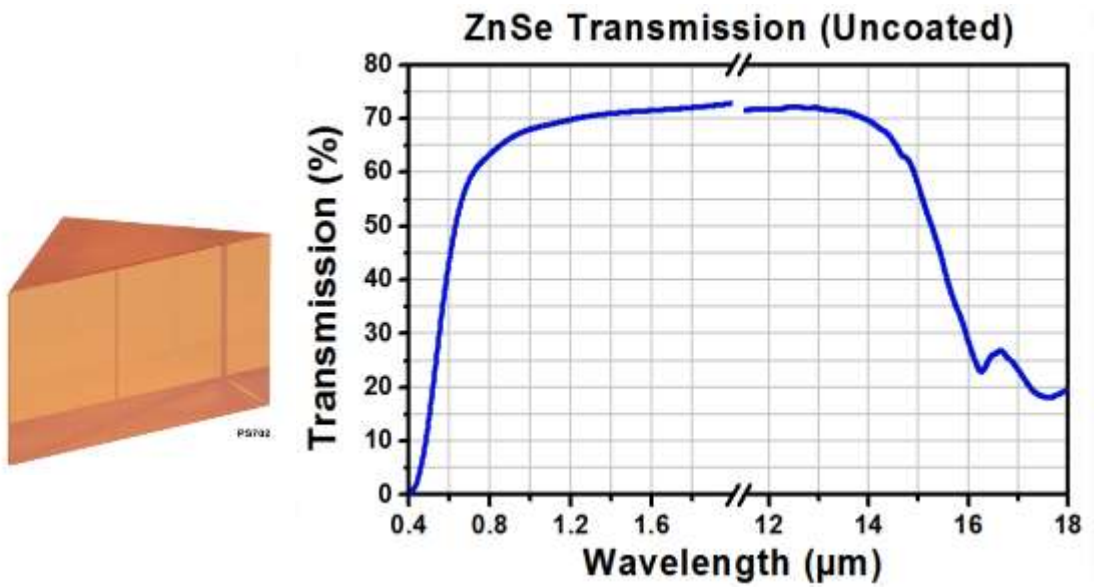

Figure 14. Znse right angle prism and the transmission range (Courtesy of Thorlabs, Inc)

5.1.4 Collimating and focusing lenses

Two lenses are used to collimate and focus the emitted light from the IR-LED (Figure 15). The first lens collimates the emitted infrared light from the LED and aligns it toward the focusing lens. The second lens then focuses the light toward the entrance face of the IRE

element. Required separation distances were taken into account during the design of the sensor. One requirement was that the distance between the focusing lens and the infrared light entrance face of the IRE prism should equal the focal length of the focusing lens. This configuration ensures that the maximum infrared light intensity reaches the reflection interface at the top surface of the right angle IRE. Figure 16 shows a cross sectional area of the measurements system that houses the various optoelectronic components.

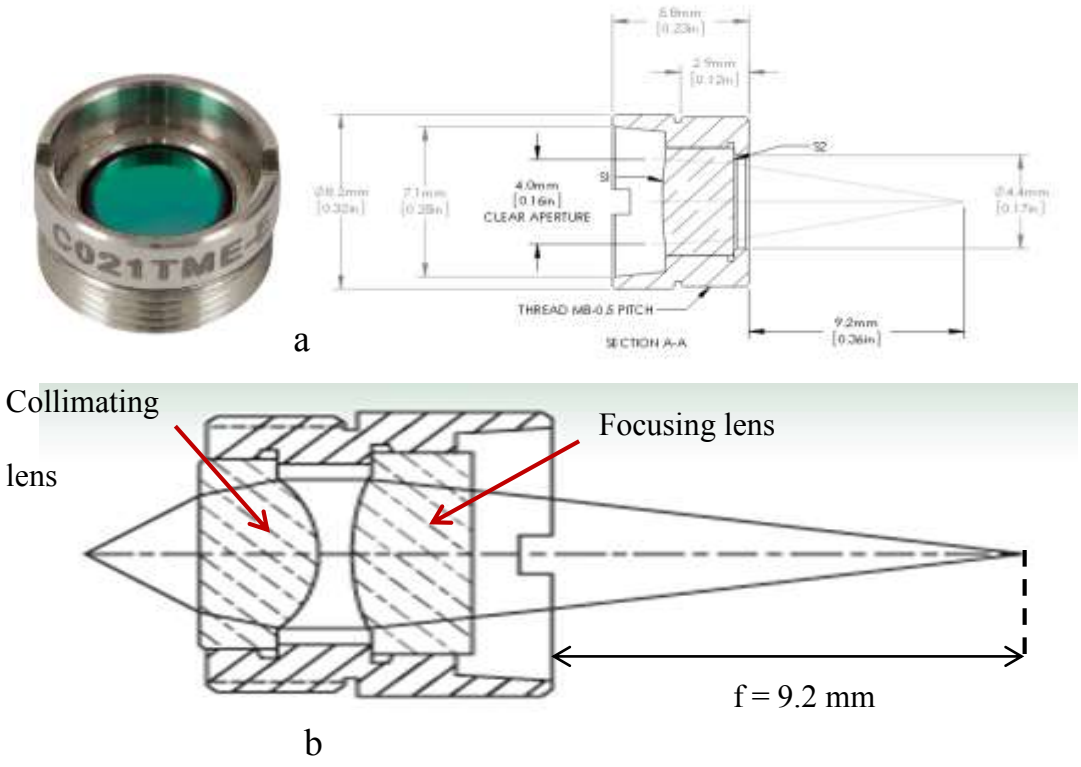

Figure 15. a) C021TME-E collimating and focusing lens b) Cross section for the configuration collimating & focusing lenses (Courtesy of Thorlabs, Inc)

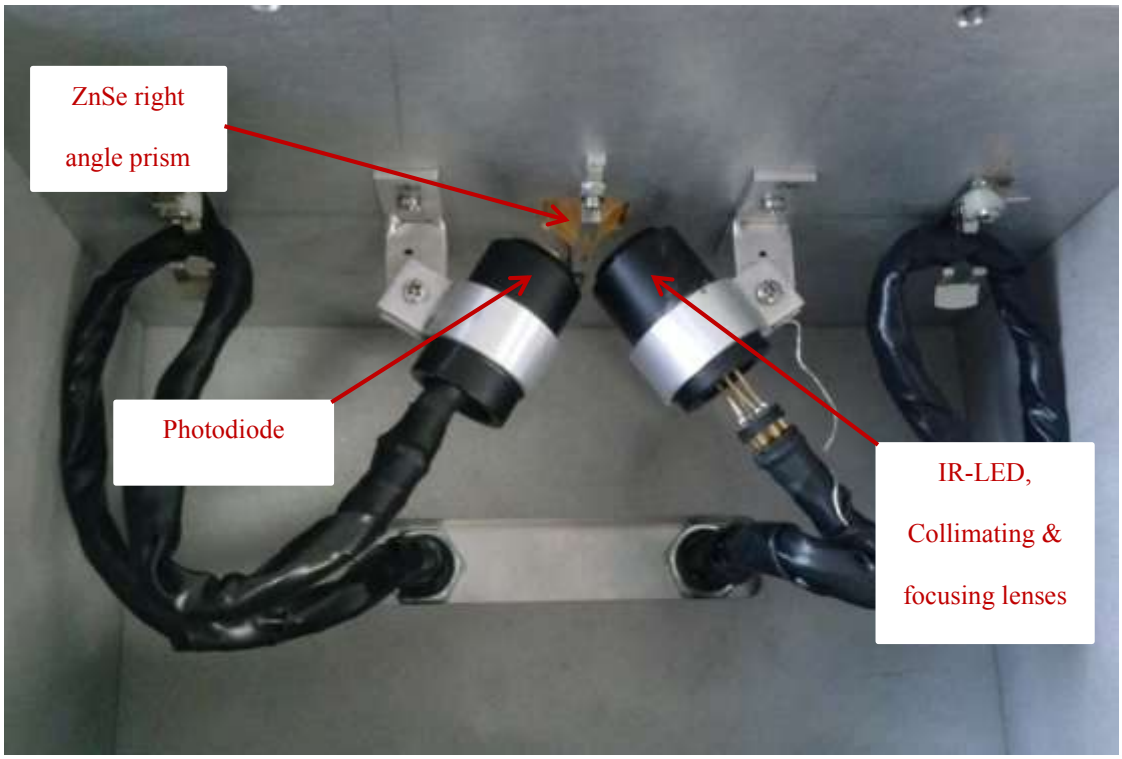

Figure 16. Cross section of the internal components of the developed ATR-IR measurement system

5.1.5 The LED and PD controllers

The DLT-37M driver is designed to control Mid-IR LEDs with built-in thermoelectric cooling capabilities (IBSG Co., Ltd.). It has two modes of operating the LED, quasi continuous wave mode (QCW) and pulse mode. In QCW mode, the current supplied to the LED can be changed from 20 to 250 mA, and frequency from 0.5 to 16 kHz with the current and frequency adjusters. In this project, the LED on the developed sensor was operated with QCW mode at a current of 150 mA, a frequency of 2 kHz and corresponding pulse duration of 100 μs (Figure 17). The controller also provides the ability to control

the temperature of the LED chip to maintain stable operating temperature as well as tuned wavelength or optical power during operation.

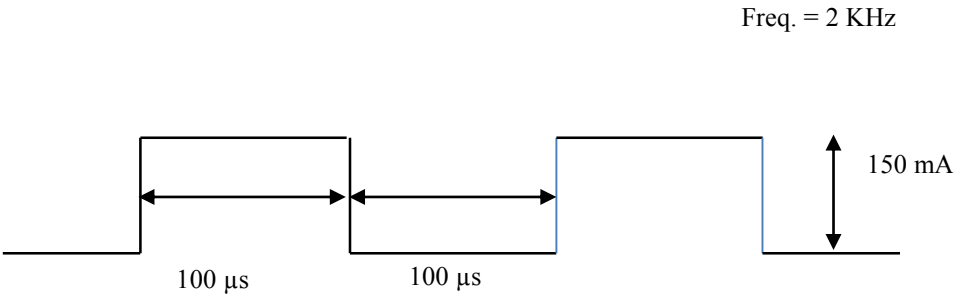

Figure 17. Current-time relation of operating the LED-34-TEC using QCW mode

The AMT-07M (Figure 18) amplifier is designed to read and amplify signals detected by the infrared photodiodes. Furthermore, it provides the ability to control the temperature of the photodiodes that have a built-in thermoelectric cooling system. This capability offers the possibility to tune and stabilize the desired photodiode spectral characteristics during periods of operation.

Figure 18. The LED & photodiode drivers and temperature controllers DLT-37M and AMT-07M (courtesy of IBSG)

5.2 The integrated drying system

The drying system is composed of the drying chamber, fan and heater, exhaust fan, and the temperature control unit. The drying system is attached to the top of the ATR-IR measurement system. The temperature controlling unit is composed of a resistive temperature detector (RTD) installed inside the chamber, digital temperature controller, ceramic heating element (200 watts), air inlet fan, and air exhaust fan (Figure 19). All

mentioned components are controlled with a temperature controlling unit (Figure 21) to regulate the temperature inside the drying chamber.

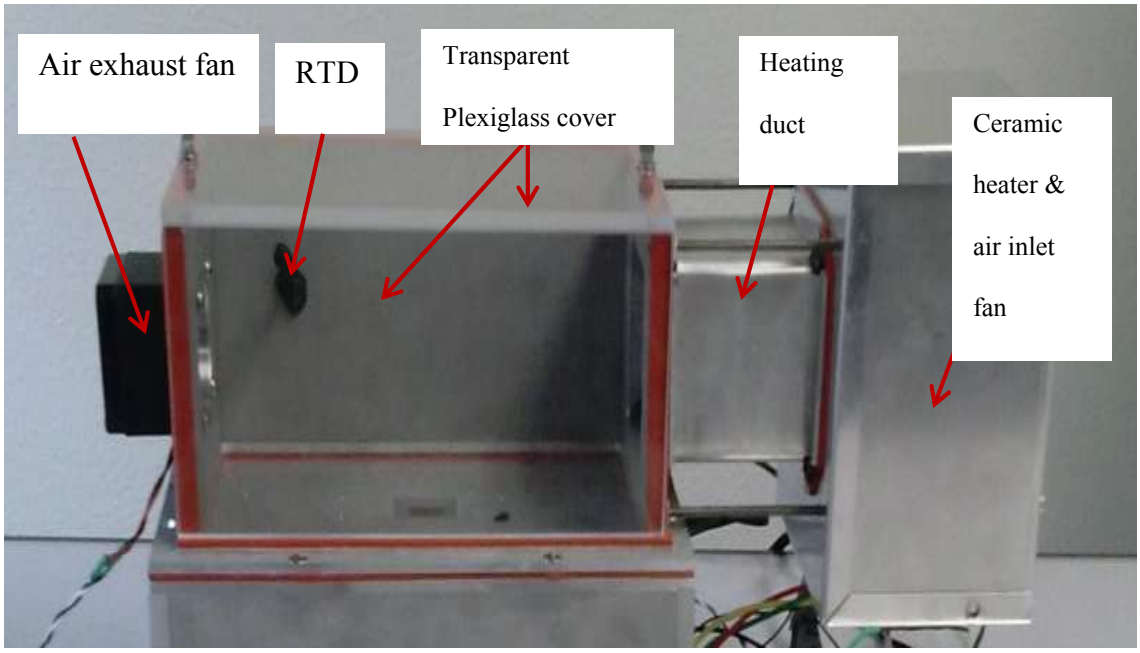

Figure 19. Various components of the drying system

The air inlet fan pulls in air from outside and pushes it through the ceramic heater. The air is heated by the ceramic heater as controlled by the temperature controlling unit. The hot air then travels through the duct toward the chamber. The air diffuses inside the chamber and passes over the sample that is placed on the surface of the IRE. The exhaust fan draws the air out through the exit. The RTD is used to detect the temperature inside the chamber and provide a continuous feedback so the temperature controlling unit can regulate and

maintain the desired temperature inside the drying chamber. Figure 20 depicts a closer view of the dimensions of the top surface of the internal reflection element. Further specifications about the drying system are given in appendix B.

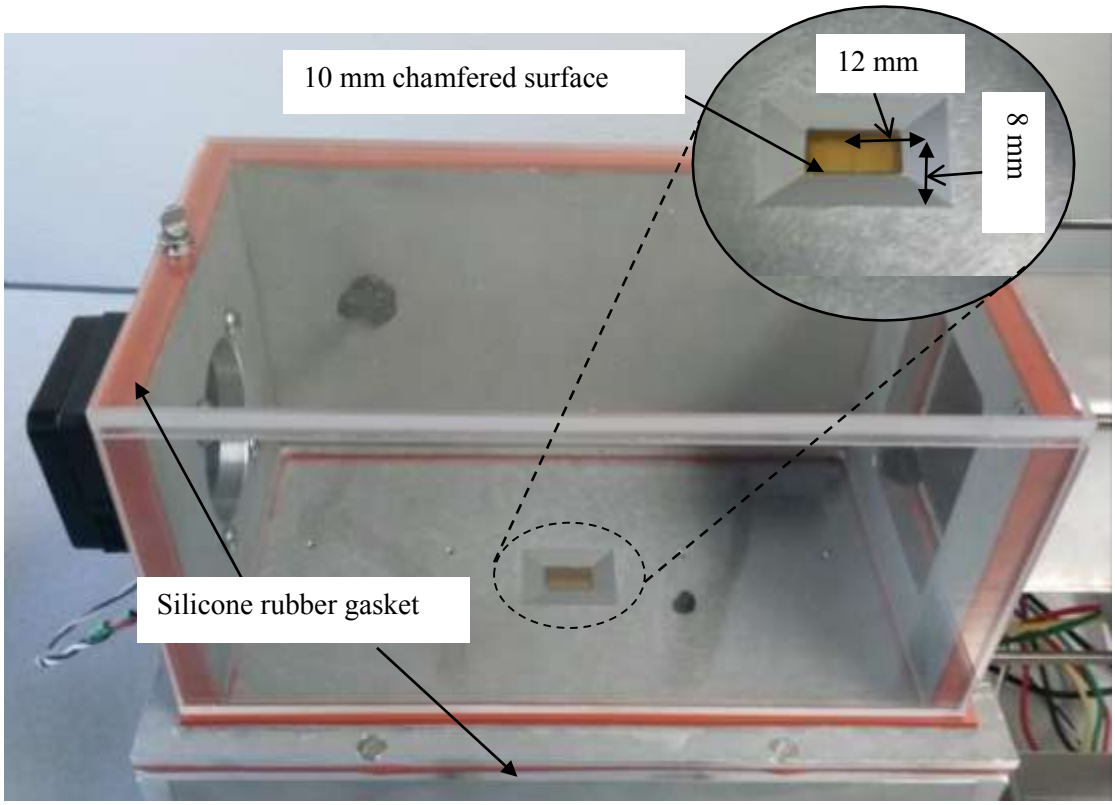

Figure 20. Closer view at the drying chamber

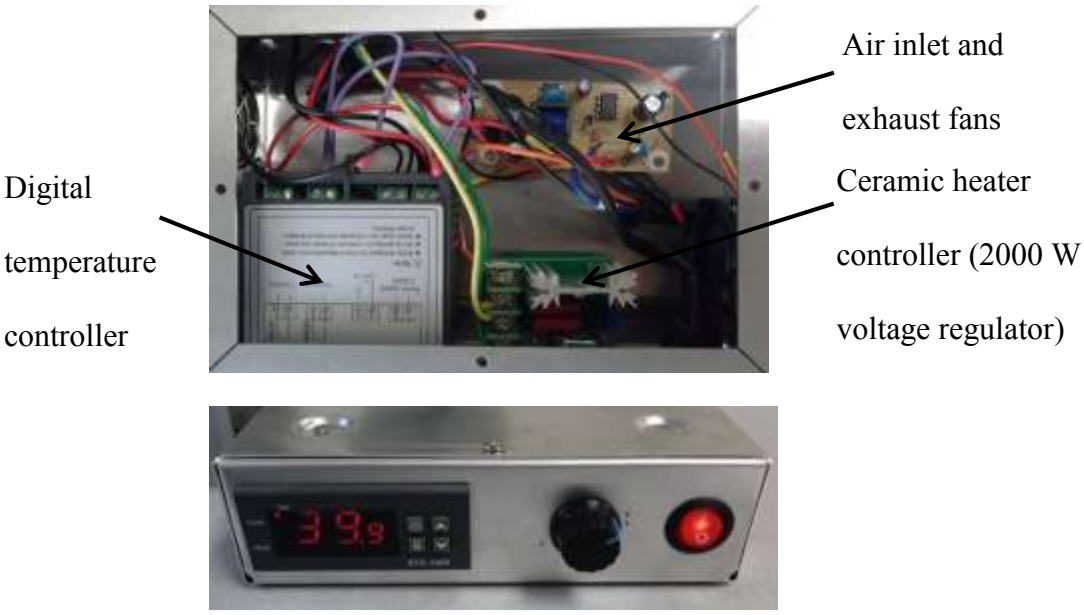

Figure 21. Temperature controlling unit of the drying chamber

6. ATR-IR MEASUREMENT OF CANOLA OIL CONCENTRATIONS IN CHLOROFORM USING THE NICOLET 6700 FTIR SPECTROMETER AND THE DEVELOPED ATR-IR SENSOR

The main objective in this section is to evaluate the performance of the developed ATR-IR sensor to estimate canola oil concentrations in chloroform and compare them to estimates produced with the Nicolet 6700 FTIR spectrometer and the ATR technique.

6.1 Materials and methods

6.1.1 Preparation of canola oil concentrations

Canola oil was used in combination with Chloroform ($CHCl_3$) to create various concentrations of 5, 10, 15, 20, 25, 50, 75, and 100%. For example, to create 50% oil concentration, 5 mL of canola oil and 5 mL of chloroform ($CHCl_3$) were mixed together into a 10 mL glass vial. The mixture was then shaken to ensure homogeneous solution.

6.1.2 Collecting the canola oil spectra with the Nicolet 6700 ATR-FTIR spectrometer

An FTIR spectrometer (Nicolet Model 6700, Madison, Wisconsin) was used to acquire absorption spectra of one replicate for each oil concentration with the Smart Orbit ATR accessory. The spectrometer acquires the absorption along a wide range of infrared spectrum from 400 cm^{-1} to 25,000 cm^{-1}. Figure 22 shows the collected spectra of one

replicate for each canola oil concentration. However, for the purpose of comparing the performance of the developed sensor to the spectrometer, and since the sensor is using only one wavelength in its design centered at 3.4 μm (≈ 2940 cm^{-1}), the absorbance at 2920 cm^{-1} for each oil concentration was calculated with the area calculation tool in the OMNIC® software of the Nicolet 6700 FTIR spectrometer.

With a pipette, an amount of 0.1 mL of each canola oil concentration was transferred from the glass tube and placed directly on the surface of the internal reflection element (IRE prism) of the spectrometer. Since chloroform is highly volatile, the sample was covered with a plastic cap to minimize exposure to air. The sample spectrum was first collected, and then the surface of the IRE prism was cleaned with distilled water and ethanol, and then the background spectrum was acquired. The background spectrum represents the acquired spectra by the spectrometer when there is no sample placed on its IRE. The spectrometer's software then subtracts the background spectrum values from the sample IR spectrum values at each wavelength to create an IR absorption spectrum for the sample.

Four distinctive absorbance bands can be seen in the collected spectra. Those bands are 750 cm^{-1}, 1742 cm^{-1}, 2855 cm^{-1} and 2920 cm^{-1}, and 3000 cm^{-1}, resulting from the stretching vibration of C-Cl, C=O, CH_2 and CH_3, and C-H functional groups, respectively. The absorbance bands 750 cm^{-1} and 3000 cm^{-1} are mainly associated with the C-Cl and CH functional groups in chloroform ($CHCl_3$). It can be seen that samples that had higher canola oil content and thus less chloroform content had lower absorbance peaks at these

bands (Figure 22). Also, the samples of higher canola oil content showed higher absorbance peaks at 2920 cm^{-1}, 2855 cm^{-1}, and 1742 cm^{-1}.

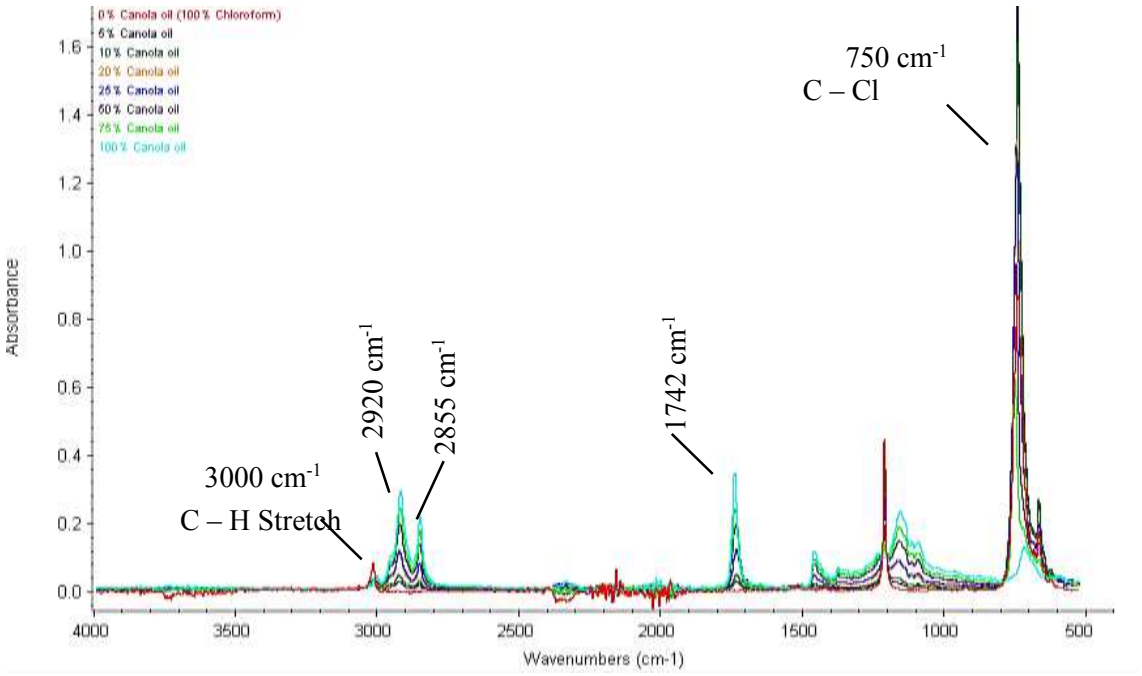

Figure 22. ATR-FTIR Spectra of 0, 5, 10, 15, 20, 25, 50, 75, and 100% canola oil concentration in chloroform acquired using the Nicolet 6700 FTIR spectrometer

6.1.3 Measurement of canola oil concentration in chloroform using the developed ATR-IR sensor

Three repeated measurements for each oil concentration were used in this experiment, but the drying system was not used since the canola oil and chloroform solution contains no water. The sensor was turned "ON" by setting the LED current to 150 mA with QCW

mode and a frequency of 2 KHz. In order to maintain constant spectral emission and intensity during operation, the LED was cooled down and maintained at 15℃ with the temperature adjuster in the DLT-37M controller. After that, the background output of the photodiode (O_b) was recorded when there was no sample on the surface of the IRE. After recording the background output, 0.1 mL of the sample at each concentration was placed on the surface of the IRE. As previously mentioned, the sample was then covered with a plastic cap to minimize vaporization. The photodiode sample output (O) was then recorded 3.0 s after covering the sample. The 3.0 s delay was used because it was found that the sensor measurement fluctuates greatly due to evaporation of chloroform and the consequent change in oil concentration. Table 2 shows the three repeated measurements for each concentration of canola oil in chloroform and the calculated sensor output. The percentage of light theoretically absorbed by the oil sample was then calculated with the following equation;

$$sensor\ output = \frac{O_b - O_s}{O_b} x100\% \quad (7)$$

where;

O_b : sensor output when measuring the background

O_s : sensor output when measuring the sample

Table 2. Sensor output measurements of canola oil concentration in chloroform

Oil content in chloroform [%]	Repeated measure								
	1			2			3		
	O_b	O_s	Sensor output [%]	O_b	O_s	Sensor output [%]	O_b	O_s	Sensor output [%]
5	92.4	91.9	0.5	92.3	91.6	0.8	92.5	91.6	1.0
10	91.0	89.2	2.0	91.0	90.5	0.5	93.0	92.1	1.0
15	93.2	91.8	1.5	93.2	91.6	1.7	92.0	91.0	1.1
20	92.0	90.0	2.2	92.5	90.4	2.3	91.1	88.5	2.9
25	90.3	87.0	3.7	91.0	88.0	3.3	91.3	88.0	3.6
50	91.3	87.7	3.9	91.8	86.8	5.4	91.4	87.2	4.6
75	90.0	83.5	7.2	89.0	83.1	6.6	88.8	82.7	6.9
100	89.7	83.7	6.7	91.0	83.3	8.5	92.0	84.2	8.5

6.2 Simple linear regression analyses (SLR) of the measurements obtained by the Nicolet 6700 ATR-FTIR spectrometer and the developed ATR-IR sensor

Simple linear regression (SLR) analyses were used to correlate the canola oil concentration (dependent variable) to both ATR-IR sensor measurements and absorbance measurements at 2920 cm^{-1} with the FTIR spectrometer. The regression analyses were carried out with Minitab® (version 17.1.0, 2013, Minitab Inc.) software.

6.3 Results and discussion

The results of the SLR analysis between canola oil concentrations and FTIR measurements indicated a linear trend that has an R^2 value of 0.95 and an RMSE value of 8.62%. The correlation model of FTIR measurements versus canola oil concentrations has a slope and

constant values of 0.09 and 0.75, respectively. The analysis between oil concentrations and ATR-IR sensor measurements indicated a linear trend with an R^2 value of 0.93 and RMSE value of 8.64%. The correlation model of sensor measurements versus canola oil concentrations has a slope and constant values of 0.08 and 0.71, respectively. The developed ATR-IR sensor and FTIR measurements showed relatively similar sensitivity to the change in canola oil concentration based on their slope and constant values. The ATR-IR sensor results shows that the developed model could explain 93% of the variability in actual canola oil concentrations, which in turn indicates good performance of the developed ATR-IR sensor, comparable to that of the FTIR spectrometer. Figures 23 and 24 show the linear regression lines between canola oil concentrations and FTIR spectrometer measurements and then sensor measurements, respectively. Three repeated measurements per canola oil concentration were used in the regression analyses to correlate the measurements of developed ATR-IR sensor to canola oil concentration, while only one measurement per canola oil concentration was used to for the FTIR spectrometer.

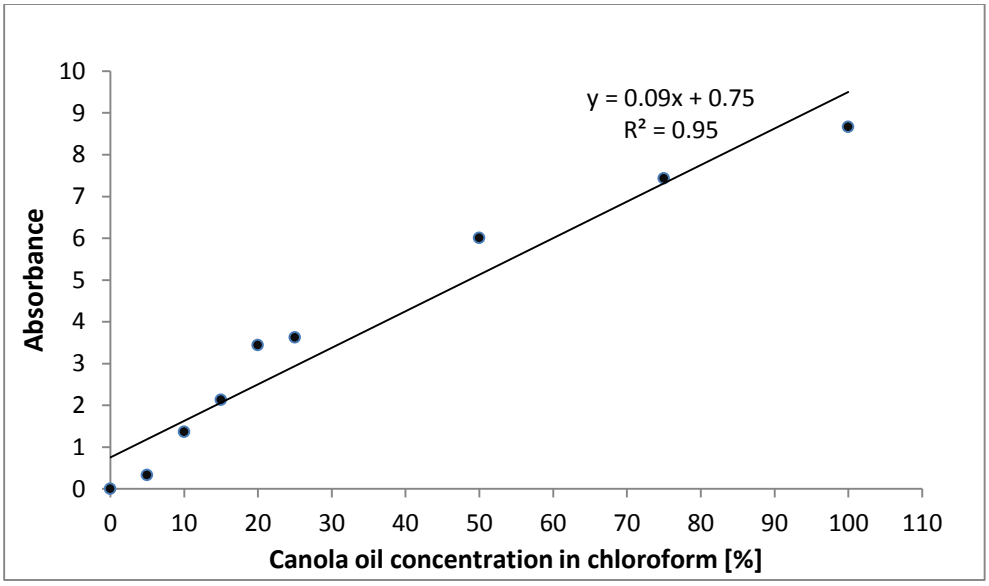

Figure 23. Regression line of absorbance measurements at 2920 cm^{-1} acquired using the Nicolet 6700 ATR-FTIR spectrometer versus canola oil concentrations in chloroform [%]

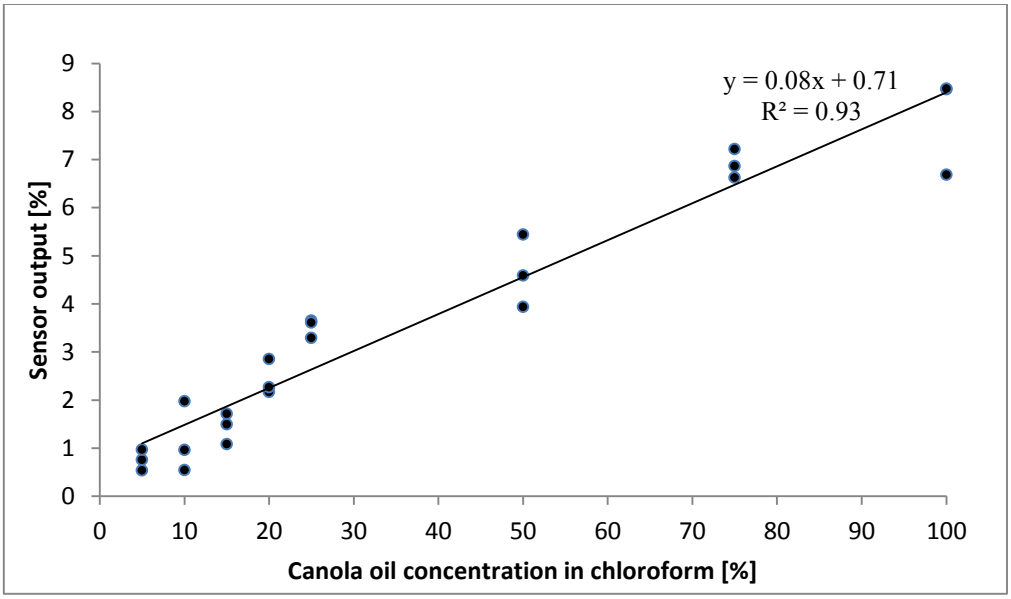

Figure 24. Regression line of sensor output [%] measured using the developed ATR-IR sensor versus canola oil concentrations in chloroform [%]

7. ATTENUATED TOTAL REFLECTION ATR-FTIR SPECTROSCOPY OF NEUTRAL LIPIDS IN MICROALGAE

The objective of this section is to consider the accuracy of an ATR-FTIR spectrometry and the developed ATR-IR sensor for the measurement of neutral lipids in microalgae. The section includes materials and methods, results and discussion, and finally conclusions. The findings of this study provide for recommendations for future improvement of the current sensor.

7.1 Materials and methods

7.1.1 The microalgae samples

Two algae species were used in this study, Desmid sp. and Nannochloris oculata. The microalgae species were obtained from Texas AgriLife Research's algae production facility in Pecos, Texas (Table 3). The samples were received in the form of freeze dried algal pastes that had been concentrated approximately 100 times after being harvested from the growing ponds. Five samples of various lipid contents for each microalgae species were used in this study. GCMS–FID was used to resolve and measure the FAME components from C_{14} to C_{24}. Neutral lipid was then calculated as the sum of all component FAMEs. For Nannochloris oculata, the five samples had a lipid content that ranged from a 71.59 mg/g to 213.30 mg/g. The lipid content in the Desmid samples ranged from 48.16 mg/g to 277.25mg/g.

Table 3 shows the ash free dry weight (AFDW) [g/L], total lipids [mg/g], and lipid content [%] in the five samples of each microalgae specie. AFDW represents the dry weight of organic matter (microalgae biomass) found in 1.0 L of an algae sample, excluding intracellular and extracellular water and inorganic matter. The total lipids represent the amount of neutral lipids [mg] present in 1.0 g of ash free dried material in an algae sample.

Table 3. Studied microalgae species and their lipid content

Harvest Code	Specie Code	Algae Name	AFDW (g/L)	Total Lipids (mg /g AFDW)	Lipid content [%]
TAL-NB-313	AM43	Nannochloris oculata	81.45	71.39	7.14
TAL-NB-311	AM43	Nannochloris oculata	78.85	94.95	9.49
TAL-NB-327	AM43	Nannochloris oculata	89.84	154.24	15.42
TAL-NB-314	AM43	Nannochloris oculata	77.93	170.86	17.09
TAL-NB-322	AM43	Nannochloris oculata	69.17	213.30	21.33
TAL-NB-309	12-AM	Desmid	58.07	48.16	4.82
TAL-NB-302	12-AM	Desmid	49.14	128.45	12.84
TAL-NB-303	12-AM	Desmid	60.96	197.87	19.79
TAL-NB-307	12-AM	Desmid	64.80	219.95	21.99
TAL-NB-308	12-AM	Desmid	60.85	277.25	27.73

7.1.2 Sample preparations

Although the concentration of algal cells found in growing ponds varies, it is found that a typical algal concentration in a growing pond is around 1.0 g/L. Since the received microalgae samples been concentrated after harvesting about 100 times, they had to be diluted and brought back to their original concentrations as found in the growing ponds. This re-dilution was done to enable consideration of using this optical technique to measure neutral lipids in microalgae close to the growing ponds with minimal sample preparation, which means taking the algae samples directly from the pond and measuring lipid content. However, when diluting the samples back to their original concentrations, preliminary ATR-IR spectroscopic measurements revealed weak absorption spectra. The spectra had no distinctive features, and it was almost impossible to identify the absorption peaks associated with algae lipids. Thus, it was decided to only re-dilute the algae samples down to three times their original concentration, which means 3.0 g of algae sample per 1.0 L of distilled water.

To create algae solution that about three times more concentrated than the original, 0.6 g of algae biomass was added to 200 mL distilled water. A total of five algal solutions were made for each specie, representing the various lipid contents for each specie. After that, six subsamples were made from each concentrated algae sample. The subsamples were made by transferring 1.75 mL from each roughly 200 mL sample into a 2 mL vial. The subsamples enable repeated measures for each algae sample.

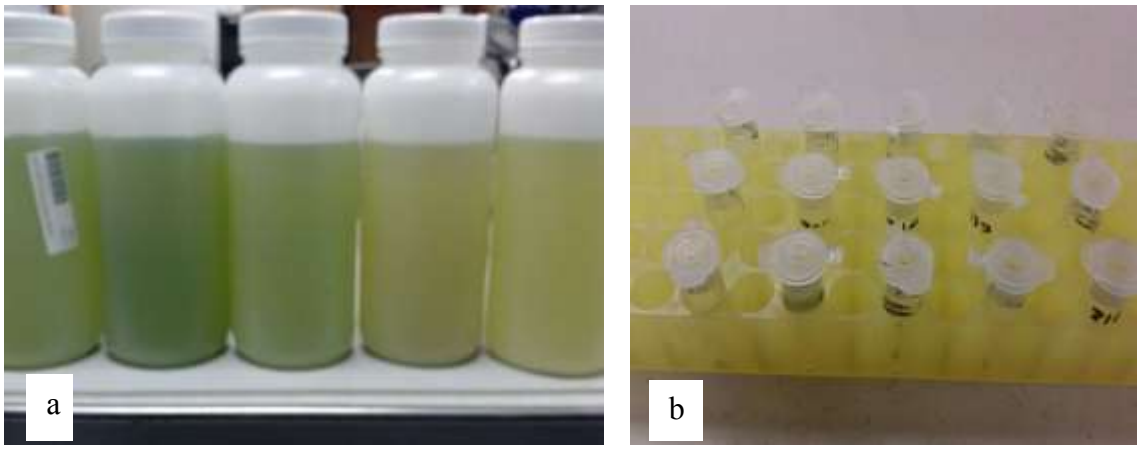

Figure 25. Examples of a) five 200 mL algae samples b) washed subsamples

7.1.3 Washing the algae subsamples

Preliminary ATR measurements of neutral lipid content in algae samples with the FTIR spectrometer showed that the absorbance spectra were heavily affected by salts and inorganic matter present in the algae samples. ATR is highly dependent on the refractive index value of the sample being analyzed (Equations 4 and 5). The variation in the amount of nutrients added to algae ponds probably creates this variation in salts present in each algae sample. To minimize this effect, the algae samples were washed three times with distilled water. The washing procedure was carried out as follows: the subsamples were centrifuged (LABNET Hermle Z300) for 20 minutes at a speed of 2500 rpm. After centrifugation, the algae biomass settles at the bottom of the vials while the salts were suspended in the top aqueous layer. Using a pipette, the top aqueous layer that contains the salts was removed. After that, the algae biomass was re-suspended again by adding

distilled water and brought back to its original volume. The same washing procedure was executed three times for each subsample (Figure 26).

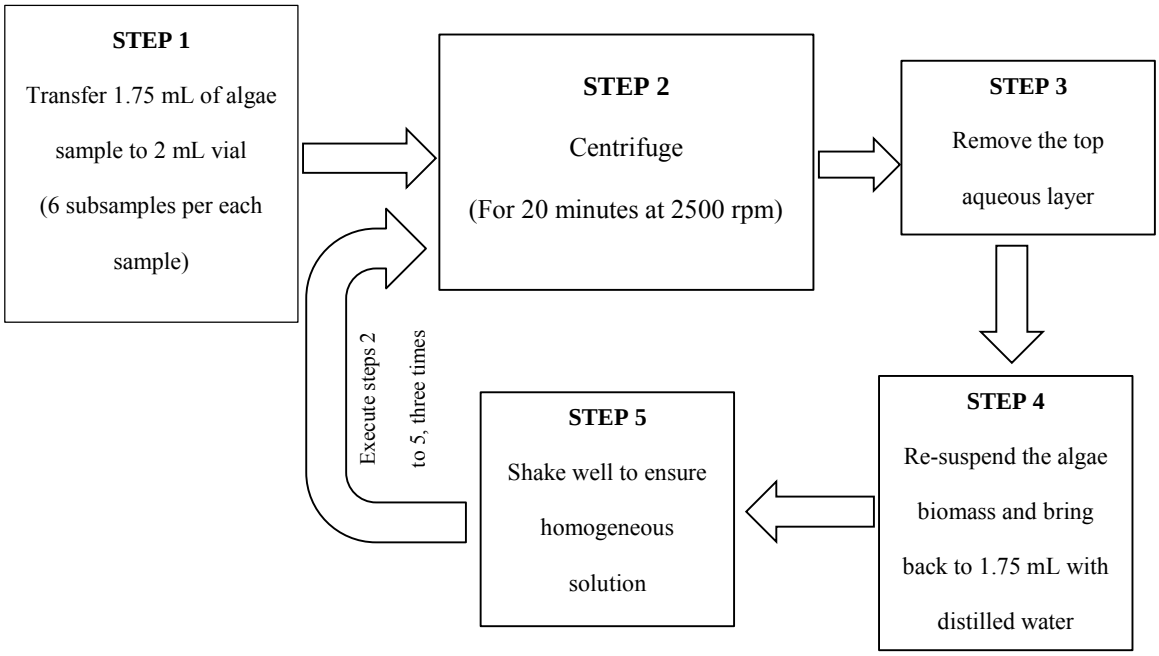

Figure 26. Flow chart shows the procedure for washing the algae subsamples

7.1.3.1 The effect of washes on the algae spectra

To understand the effect of the number of washes on algae spectra, one algae sample (NB-322) of Nannochloris oculata was used. Three subsamples (repeated measures) were used for each washing. Using the FTIR spectrometer, three spectra were acquired for each number of washes, one, two, and three (Figures 27, 28 and 29).

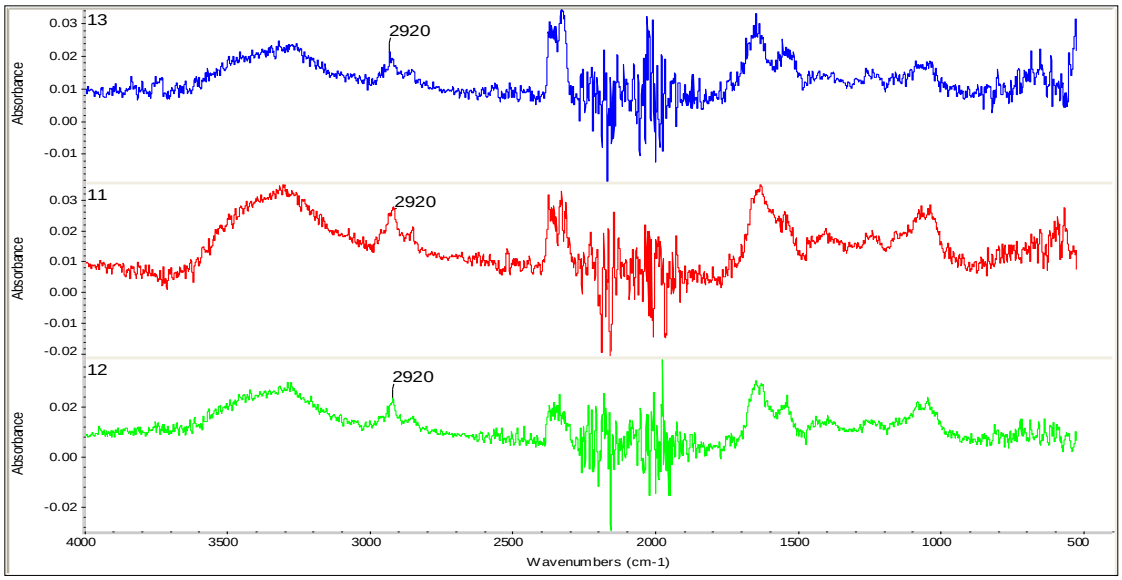

Figure 27. Three stacked spectra for three subsamples of NB-322 Nannochloris oculata microalgae washed once

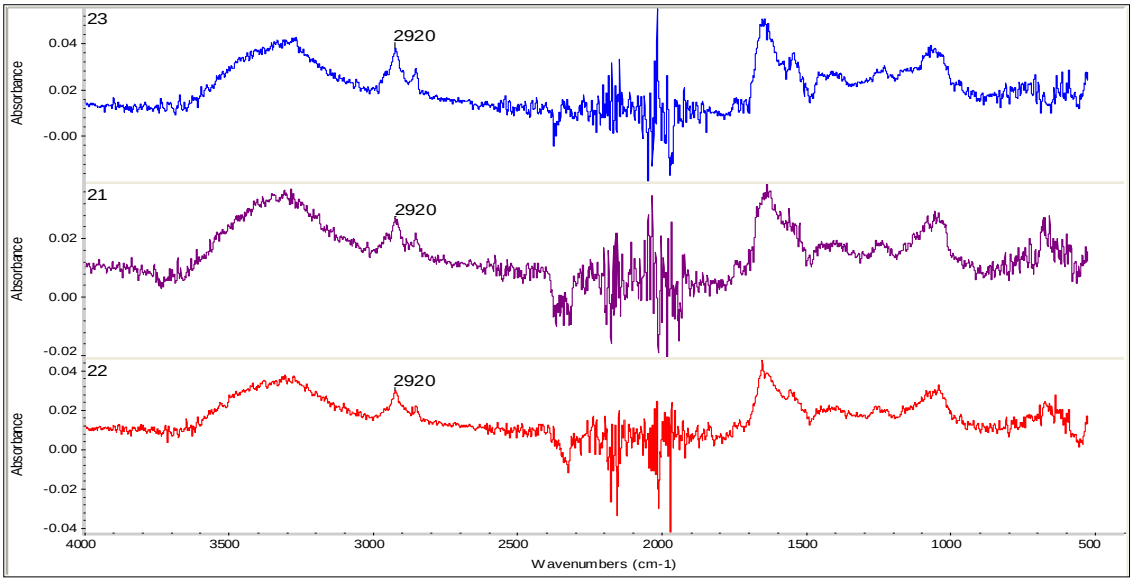

Figure 28. Three stacked spectra for three subsamples of NB-322 Nannochloris oculata microalgae washed twice

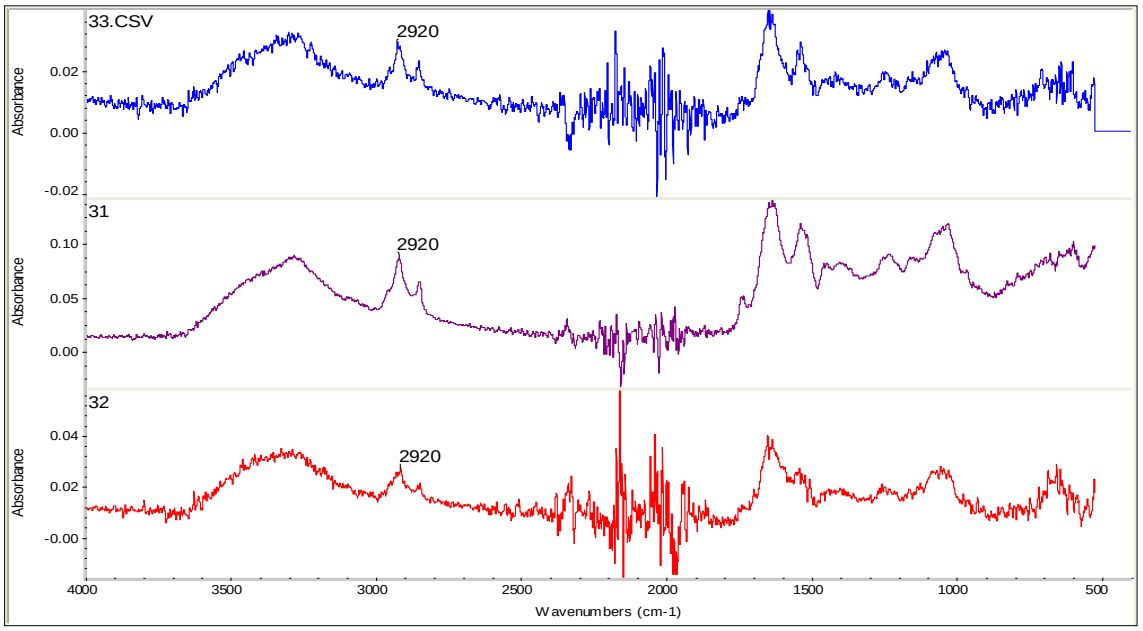

Figure 29. Three stacked spectra for three subsamples of NB-322 Nannochloris oculata microalgae washed three times

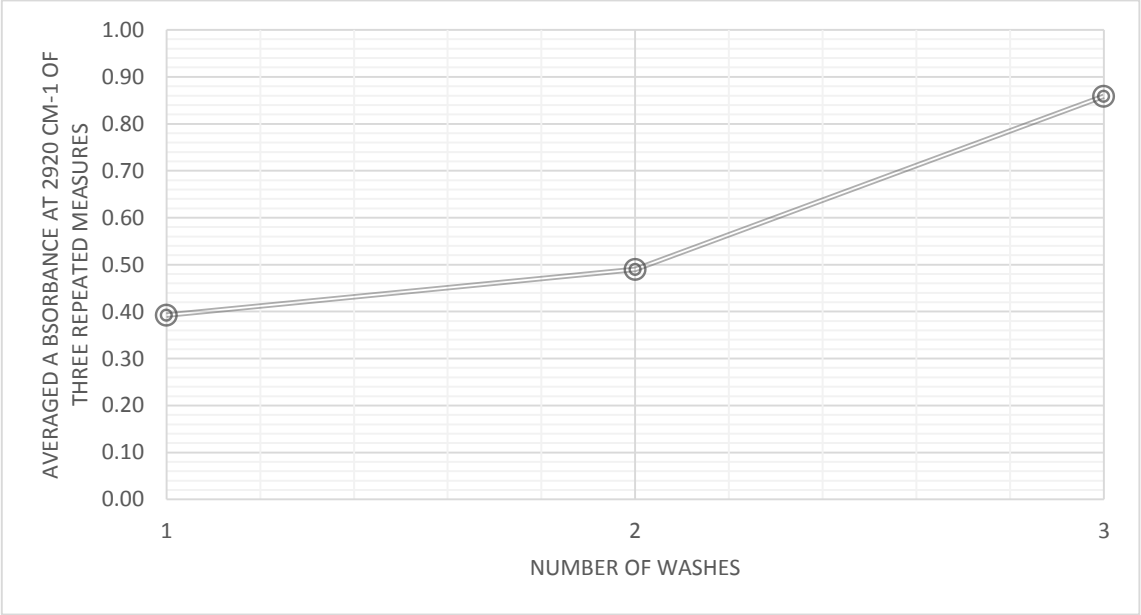

Figure 30. Effect of number of washes of algae samples on absorbance intensity at 2920 cm^{-1}

Figure 30 shows that the average absorbance at 2920 cm^{-1} was highly affected by the number of washes of the microalgae NB-322 subsamples of Nannochloris oculata. The averaged absorbance measurements are 0.39, 0.49, and 0.86 for samples that were washed once, twice, and three times, respectively. The decision to wash the microalgae samples came after observing that some unwashed samples produced weak spectra with no features, which made it difficult to identify the absorbance bands associated with lipid content. Therefore, it was decided to compare the averaged absorbance measurements at three different washing numbers. If no significant increase in absorbance was seen at two or three washes compared to one, then the samples would be washed only once prior to acquiring FTIR measurements. Conversely, if absorbance increased significantly, then a higher number of washes would be used. While there was a large absorbance difference between two and three washes, indicating the possibility that four or more washes might have further increased absorbance, using three washes provided repeatable absorbance values and was selected as adequate. The graph shows that the averaged absorbance at 2920 cm^{-1} is 0.39. The absorbance increased by approximately 20% to 0.49 when washed twice, and further increased by approximately 43% to 0.86 when washed three times. The trend here shows that an increase in averaged absorbance values with the number of washes. Based on this response it was decided to wash the algae samples of various lipid content three times each prior to acquiring spectral measurements with the FTIR spectrometer as well as the developed ATR-IR sensor.

7.1.4 ATR-FTIR spectroscopy of the algae samples using the Nicolet 6700 FTIR spectrometer

Each subsample was scanned with the removable ATR accessory of the Nicolet 6700 FTIR spectrometer. This accessory is mainly used to study dry or paste like samples that retains their shape integrity during acquisition of the spectra. However, in this study algal solution samples were used, requiring some modifications to the ATR plate accessory. A circular metallic washer was attached to the ATR plate with a silicone sealing paste (Figure 31). The washer keeps the algal sample centered on the diamond IRE of the FTIR spectrometer's ATR accessory. Since a known volume is used for each sample, the washer ensures that samples are of the same thickness as it provides a consistent location and area for all samples. With a pipette, 0.05 mL from each subsample was dropped on the ATR accessory's IRE within the hole of the washer (Figure 31). After that, the entire ATR plate accessory including the sample was removed from the spectrometer and placed inside a drying oven that had been set at 40° C. The sample was left to dry inside the oven for 90 to 100 minutes until the algae sample was completely dried on the ATR plate. Then the ATR plate was then left to cool down at room temperature for about 10 minutes or until its temperature went below 30°C. The ATR plate was then placed back on the spectrometer in preparation of acquiring the spectra. With the spectrometer's OMNIC® software, the sample spectra were first collected. Then the sample was removed by cleaning the ATR plate with distilled water and ethanol. Then, the background spectra were collected. Figures 32 to 36 show the acquired spectra of all six subsamples for all

five samples of Nannochloris oculata. Similarly, figures 37 to 41 show the acquired spectra for all six subsamples for all five samples of Desmid microalgae.

In general, the spectra show that samples of higher lipid content produced stronger absorption intensities at 2920 cm^{-1}, 2855 cm^{-1}, and 1742 cm^{-1} than those of lower lipid content. The spectral variations conform with those generated with transmission FTIR spectroscopy in section 4, which showed that absorption intensity was the highest at the absorbance band at 2920 cm^{-1}, then at 2855 cm^{-1} and finally lowest at 1742 cm^{-1}. All acquired spectra encompassed undesirable noise at wavenumbers ranging from 2000 cm^{-1} to 2500 cm^{-1}. This noise indicates that the algae samples being examined were of low biomass concentration, leading to low absorption intensities and thus low signal to noise ratio.

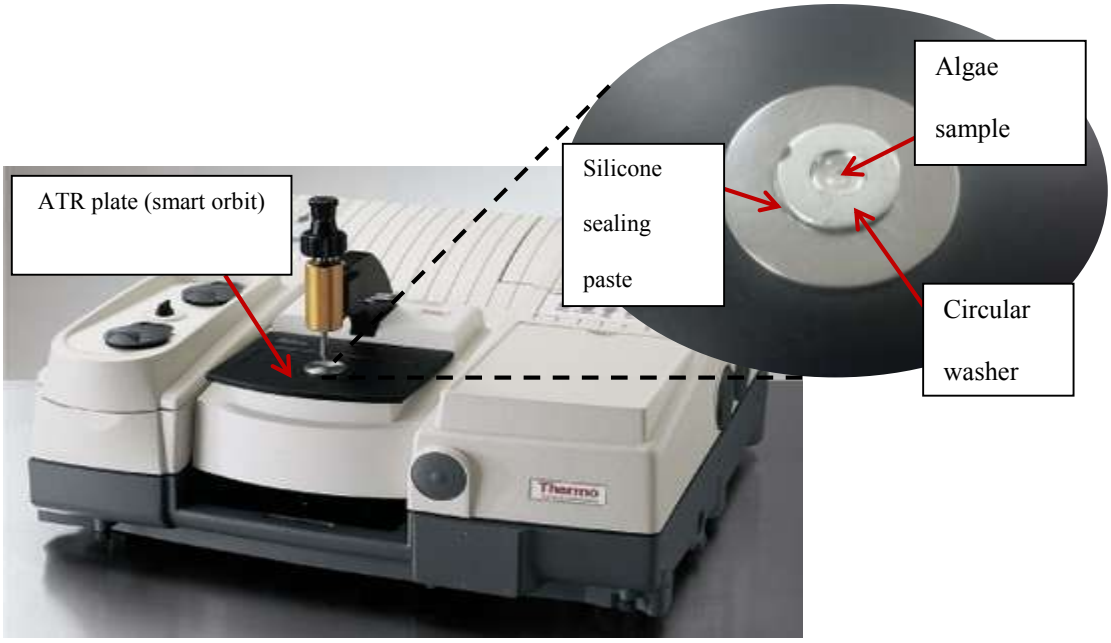

Figure 31. The ATR plate and sample presentation on the Nicolet 6700 FTIR spectrometer

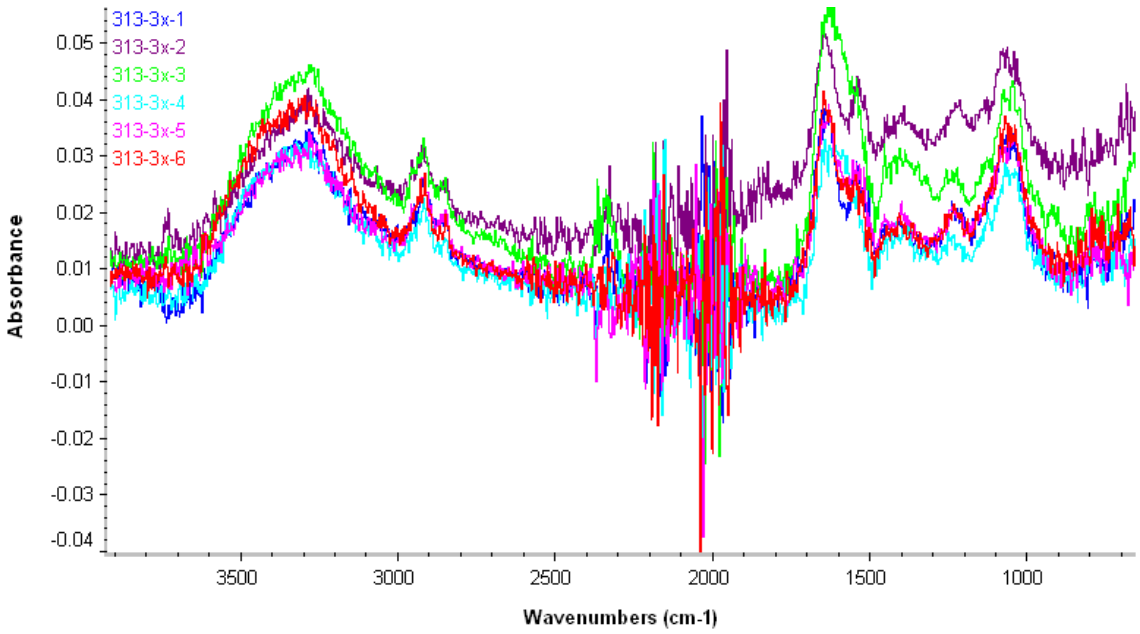

Figure 32. Six repeated measures of ATR-FTIR spectra for NB-313 sample of Nannochloris oculata

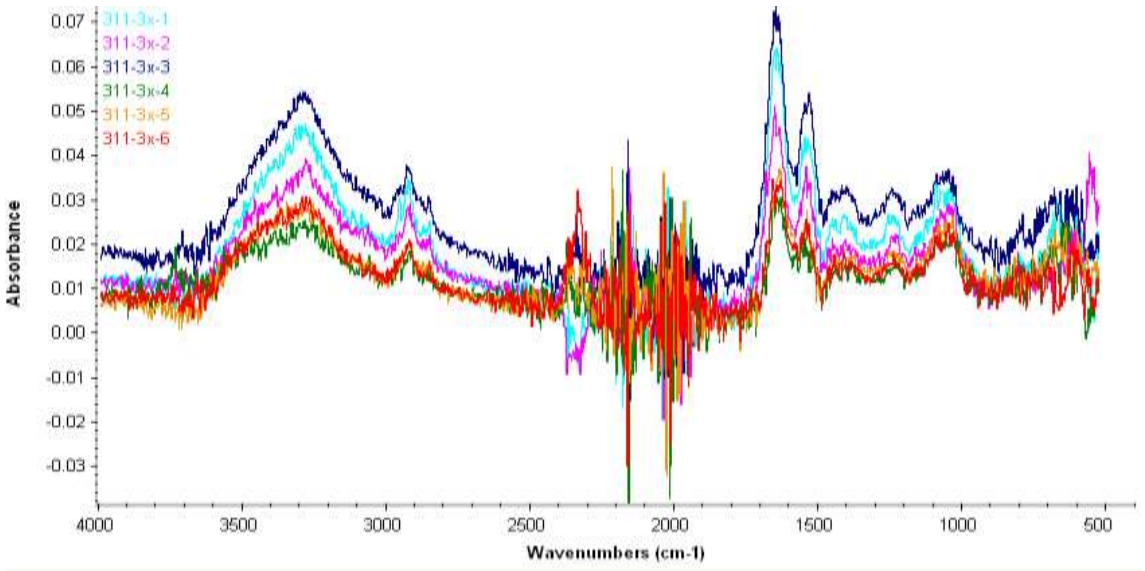

Figure 33. Six repeated measures of ATR-FTIR spectra for NB-311 sample of Nannochloris oculata

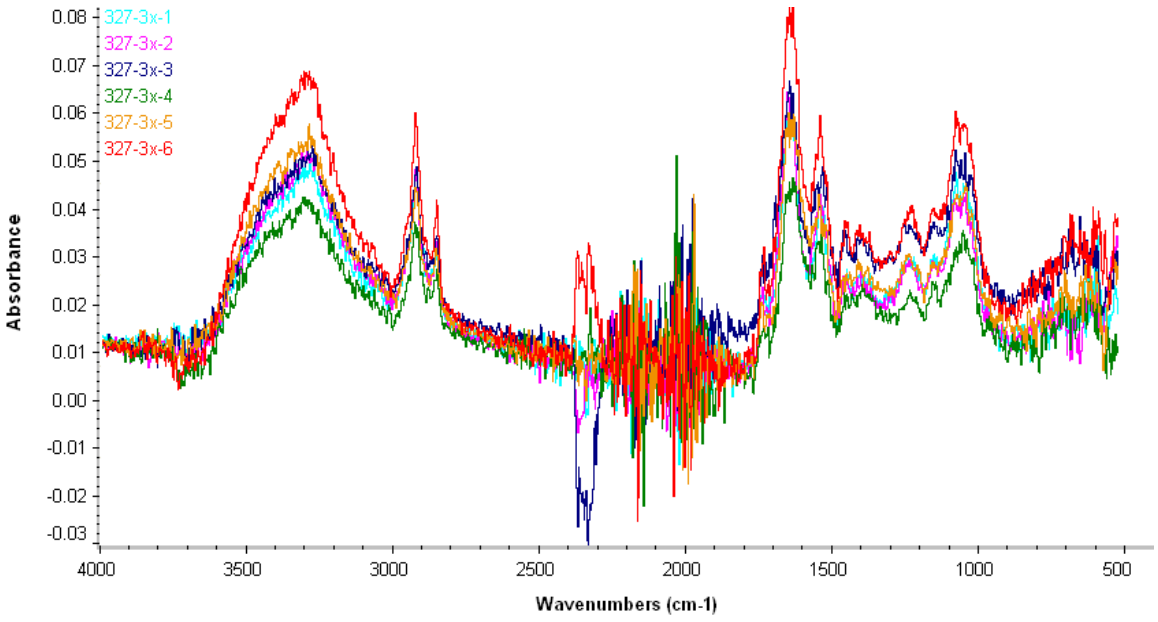

Figure 34. Six repeated measures of ATR-FTIR spectra for NB-327 sample of Nannochloris oculata

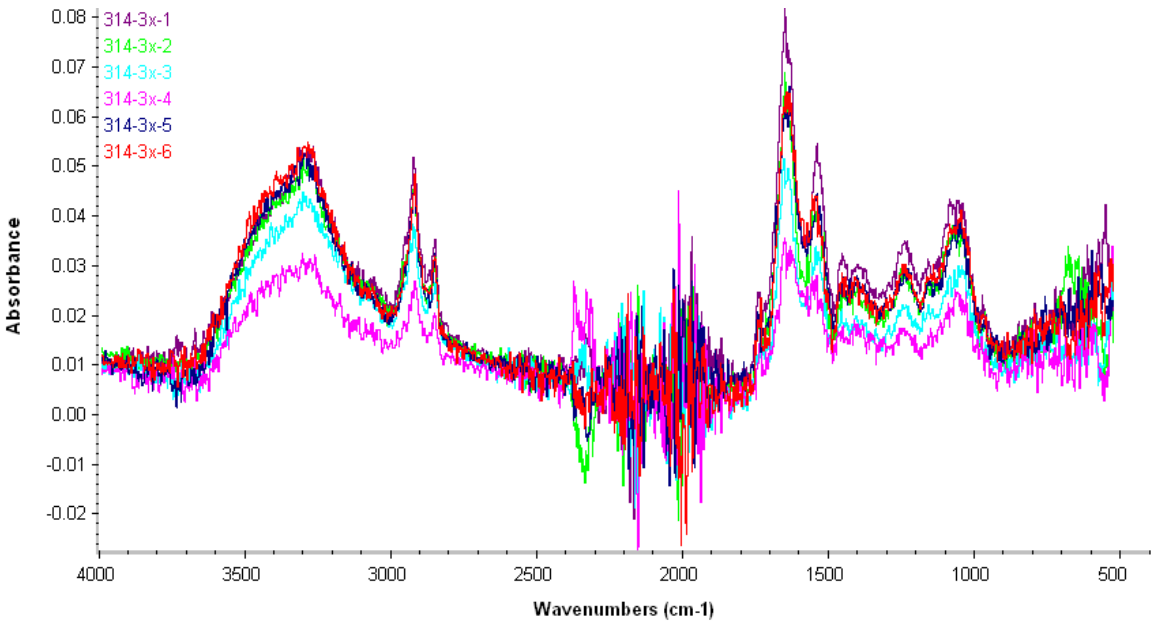

Figure 35. Six repeated measures of ATR-FTIR spectra for NB-314 sample of Nannochloris oculata

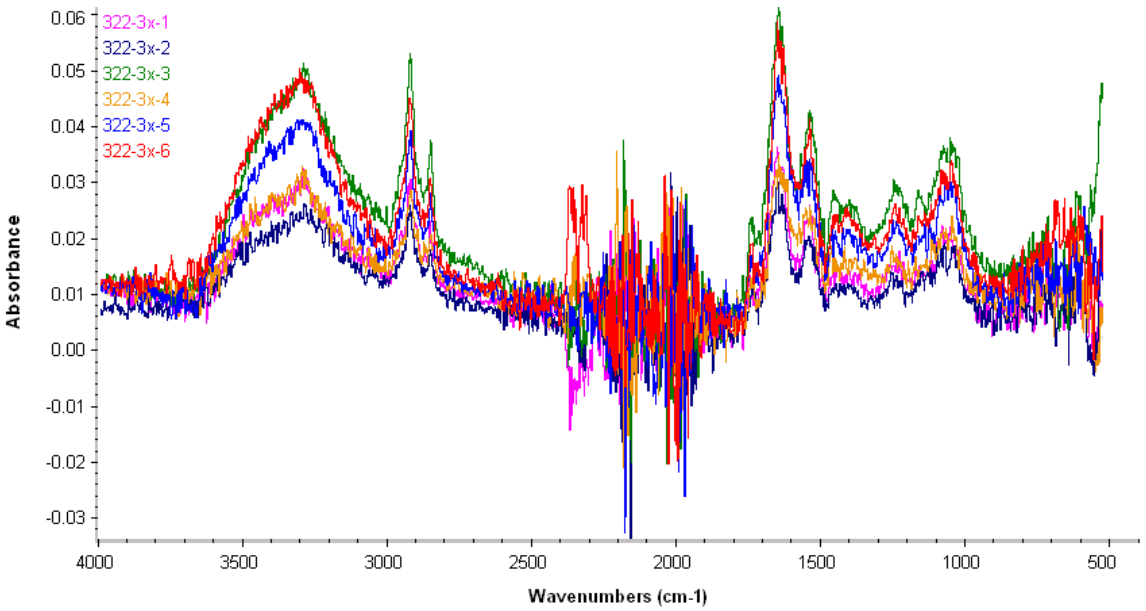

Figure 36. Six repeated measures of ATR-FTIR spectra for NB-322 sample of Nannochloris oculata

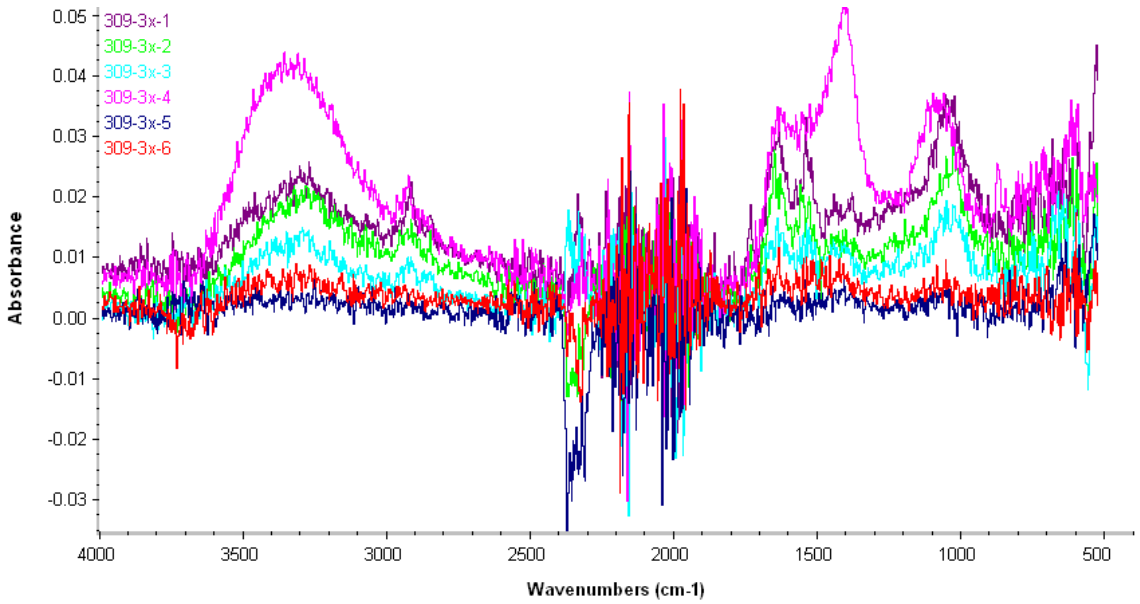

Figure 37**.** Six repeated measures of ATR-FTIR spectra for NB-309 sample of Desmid

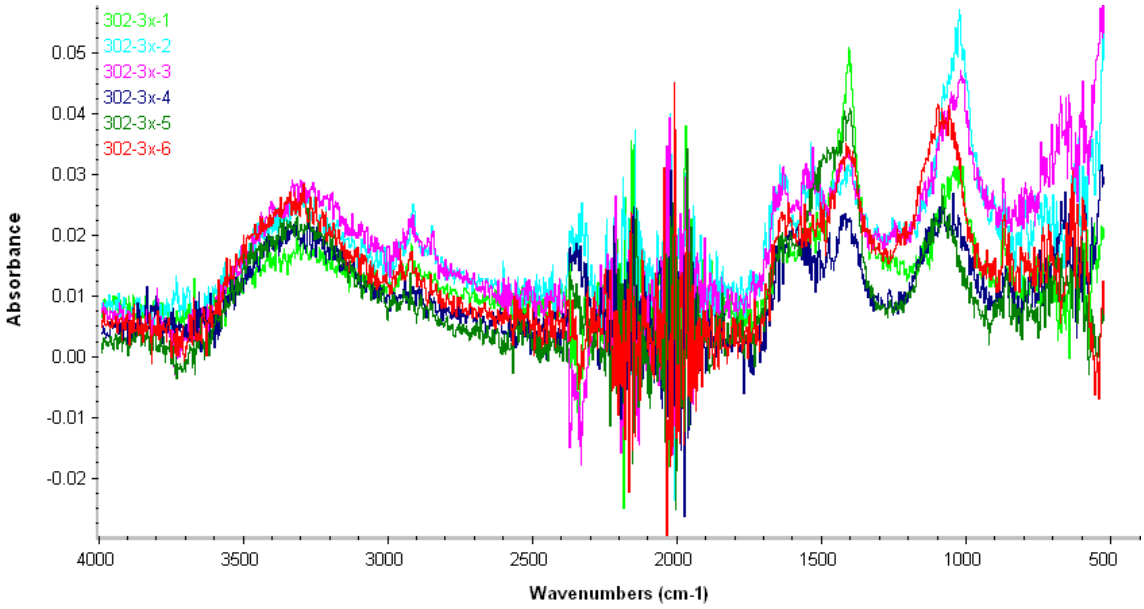

Figure 38. Six repeated measures of ATR-FTIR spectra for NB-302 sample of Desmid

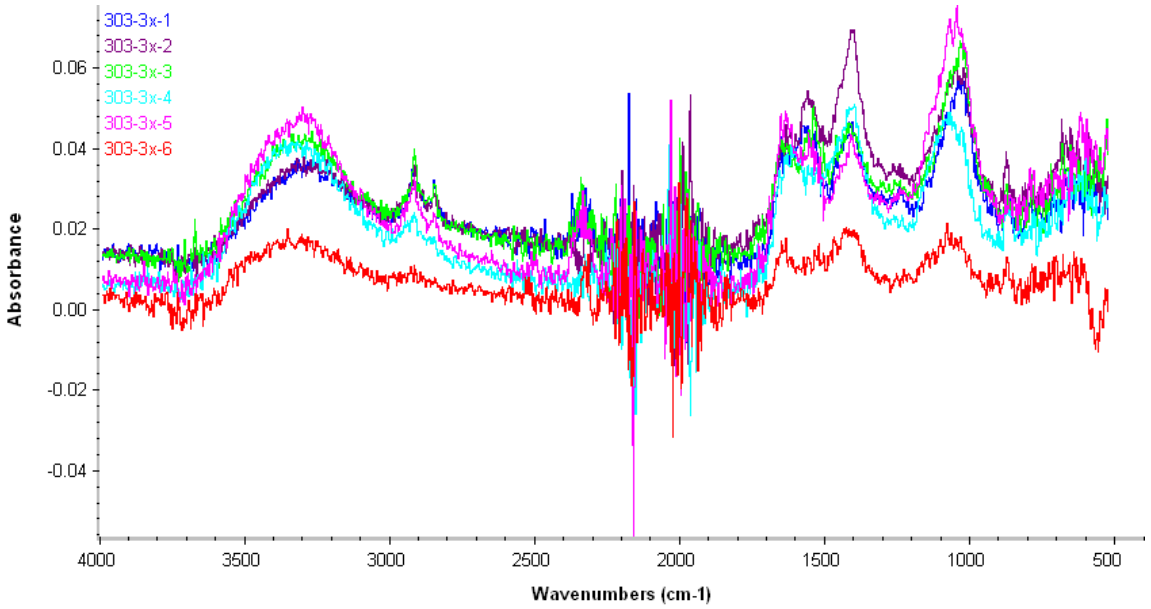

Figure 39. Six repeated measures of ATR-FTIR spectra for NB-303 sample of Desmid

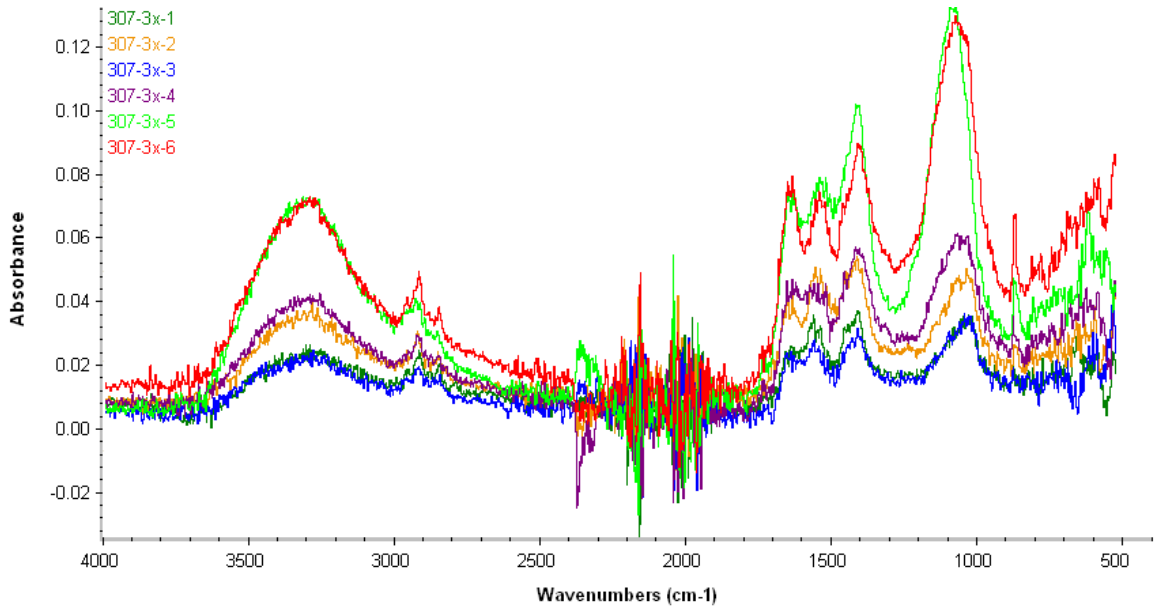

Figure 40. Six repeated measures of ATR-FTIR spectra for NB-307 sample of Desmid

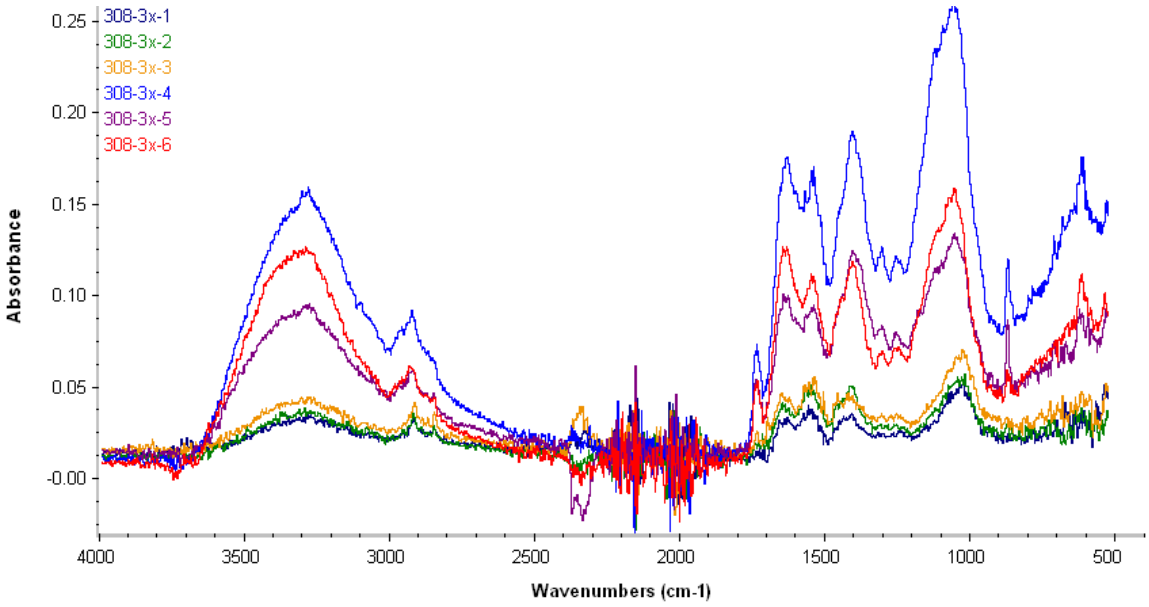

Figure 41**.** Six repeated measures of ATR-FTIR spectra for NB-308 sample of Desmid

7.1.5 Calculating the absorbance under the absorption peak

The absorbance at each absorbance band was determined by calculating the area under the absorption peak. Figure 42 shows a sample spectrum in which the absorbance area was calculated at 2920 cm^{-1}. This was achieved by using the area calculation tool found in the Omnic software.

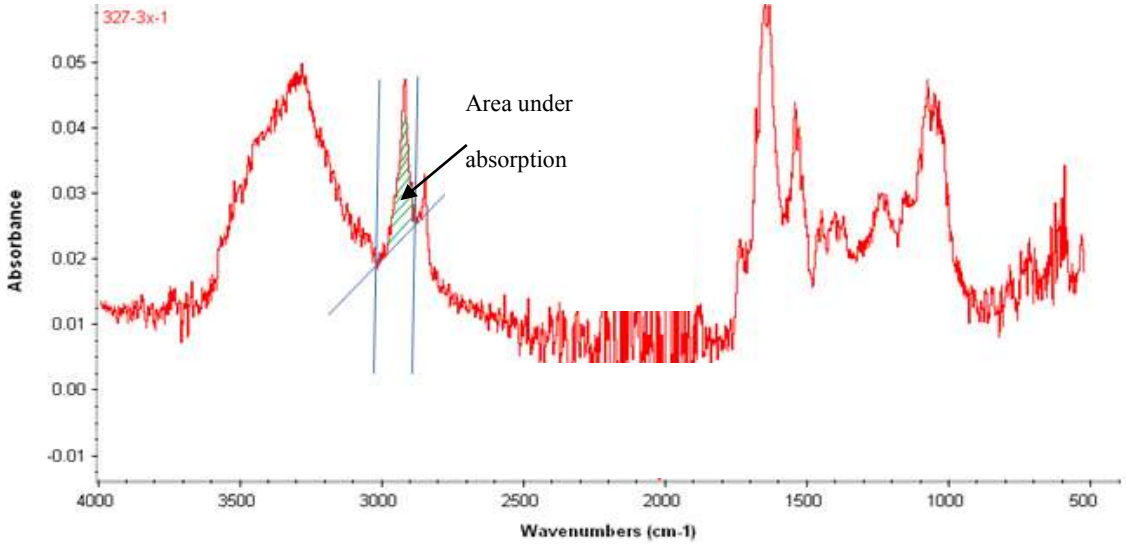

Figure 42. Sample spectrum depicts the method used to calculate the absorbance area under 2920 cm^{-1}

7.1.6 Protocol for using the developed ATR-IR sensor to measure lipid content in Nannochloris ocualta and Desmid samples

As mentioned previously, there were five samples each of Nannochloris oculata and Desmid microalgae, each subsample representing different lipid content. Six repeated measurements were taken for each sample, and each of these involved one washed subsample. The measurement procedure with the developed ATR-IR sensor involved turning it "ON" by setting the light emitting diode (LED) current to 150 mA with QCW mode and a frequency of 2 kHz. The LED was cooled down and maintained at 15˚C with the temperature adjuster in the DLT-37M controller. When the measurement system reached a state of consistent output (within 10 minutes), 0.1 mL of a given subsample was placed on the surface of the IRE prism (Figure 43). Then the drying chamber was closed

by fastening the Plexiglass cover on top. After that, the drying process was initiated by turning "ON" the temperature controlling unit and setting the temperature at 40ºC. The temperature inside the drying chamber increased until it reached and stabilized around (40 ºC ± 2ºC). The sample was then left to dry for 110 minutes. After the sample had been dried, the drying system was turned "OFF" and the entire measurement system was left to cool down until it reached temperature equilibrium with the ambient room temperature. At that point O_s (photodiode sample output) was recorded by manually recording the readout on the AM-07M digital display. After that, the surface of the IRE prism was cleaned with ethanol and distilled water in order to remove the sample. Then O_b (background output) was recorded. A schematic of the measurement protocol used with the developed ATR-IR is shown in figure 44.

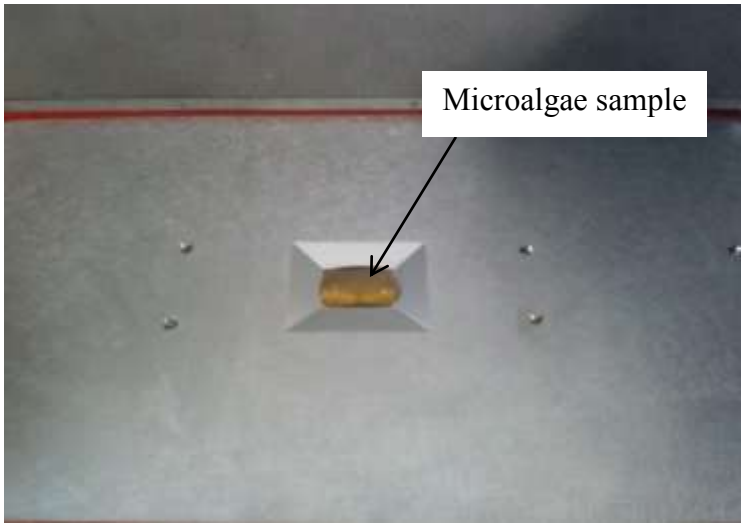

Figure 43. Microalgae sample on the surface of the right angle IRE

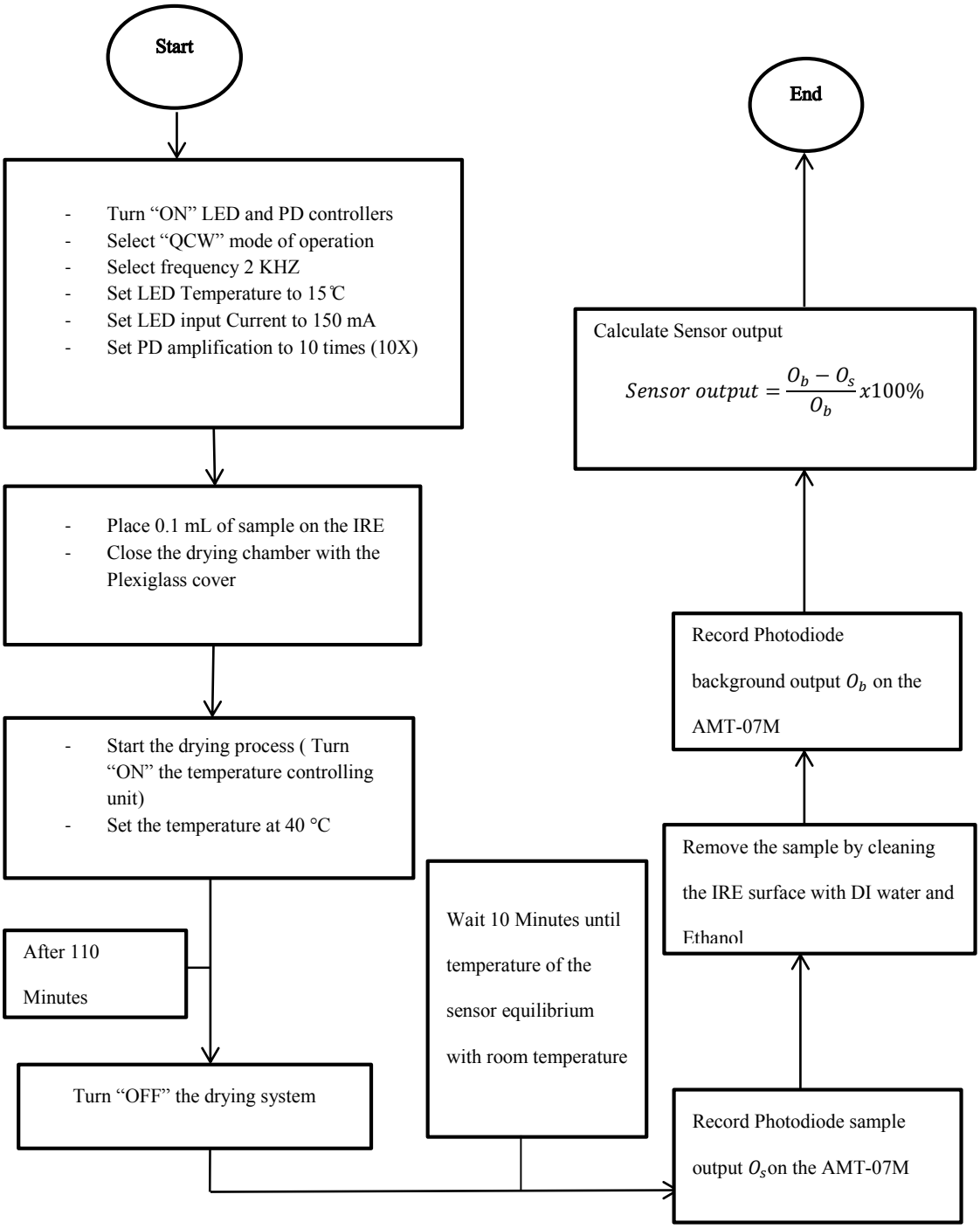

Figure 44. Flow chart for the protocol of using the developed ATR-IR sensor to measure neutral lipids in microalgae

7.1.6.1 Calculation of sensor output for all Nannochloris oculata and Desmid microalgae samples

The sensor output value for each measurement was calculated with equation (7). Tables 4 and 5 show the calculated sensor output values for all washed subsamples of Nannochloris oculata and Desmid microalgae, respectively.

Table 4. ATR-IR sensor output for lipid content in Nannochloris microalgae

Lipid content [mg/g]	Sensor output [%]					
	Repeated measure					
	1	2	3	4	5	6
71.39	10.87	10.00	10.00	9.40	11.70	7.20
94.95	12.35	13.70	10.05	14.20	12.96	12.12
154.24	12.91	14.30	13.33	13.90	16.30	13.64
170.86	14.09	15.00	17.10	13.50	13.50	13.70
213.30	13.18	12.85	15.60	13.90	14.40	15.50

Table 5. ATR-IR sensor output for lipid content in Desmisd microalgae

Lipid content [mg/g]	Sensor output [%]					
	Repeated measure					
	1	2	3	4	5	6
48.16	4.56	3.23	5.10	1.36	4.49	5.71
128.45	9.60	5.96	8.52	5.28	5.40	3.44
197.87	13.12	12.85	10.86	10.27	7.48	3.63
219.95	10.21	10.86	11.11	12.47	9.61	11.36
277.25	12.28	11.55	14.81	15.65	13.73	14.76

7.2 Multiple linear regression analysis

7.2.1 Multiple linear regression analysis for measurements acquired using the Nicolet 6700 FTIR spectrometer

Minitab® (version 17.1.0, 2013, Minitab Inc.) software was used to generate the multiple linear regression models relating lipid content to the three absorbance bands. The method of best subsets regression was used. Best subsets regression evaluates all possible models with all predictors specified by the user. The output of these analyses includes only the two best fitting models of one predictor, two predictors, three predictors, and so on. The user then compares these models and chooses the best-fitting model based on statistical and/or scientific evidence.

In this study, the dependent variable (response) is lipid content and the independent variable (predictor) is wavenumber of the absorbance bands: 2920 cm^{-1}, 2855 cm^{-1}, and 1742 cm^{-1}. Since there are three values of the independent variable, the maximum number of predictors in the largest generated model is three and the minimum is one. Seven criteria were used to evaluate the prediction performance of each model: slope of the regression line, intercept of the regression line, coefficient of determination (R^2), adjusted coefficient of determination (R^2-adj), prediction coefficient of determination ($R^2_{Prediction}$), Mallow's Cp, and root mean of squared errors (RMSE). The coefficient of determination provides a measure on how much of the variation in the response (dependent variable) is explained by the model. In general, a model with higher R^2 value is always preferable to a model with lower R^2 value, assuming that the two models are of the same size and number of

predictors. When comparing models of different sizes it is advisable to use the adjusted R^2 value as a criterion, because it compensates for the increase in R^2 value in larger model sizes by penalizing the adding of more predictors into the larger model and thus makes the comparison between two models more reasonable. The predicted R^2 ($R^2_{Prediction}$) value provides a measure of how much variation can be explained by the model in predicting new observations other than the ones used for generating the predicting model. The root mean squared error (RMSE) value provides a measure of how well the predicted values fit the measured ones. A smaller value of RMSE denotes smaller differences between the actual and predicted values, and thus a better model performance. Mallow's Cp is a measure of the amount of information in the data that is not incorporated in the model. Consequently, a model of lower Mallow's Cp value is always preferable. Lastly, the slope of the regression line provides a measure of sensitivity of the relationship between the dependent and the independent variable.

7.2.2 Simple linear regression analyses for the measurements obtained using the developed ATR-IR sensor

Simple linear regression (SLR) was used to correlate sensor output to neutral lipid content in Nannochloris oculata and Desmid. In order to test the performance of the developed sensor regardless of the algae species to be measured, a generalized model was generated by relating lipid content to sensor output across both microalgae species.

7.3 Results and discussion

7.3.1 Results and discussions for MLR analyses of correlating Nicolet 6700 ATR-FTIR spectrometer measurements to lipid content

Table 6 shows the independent variable values and regression coefficients resulting from multiple linear regression analysis relating lipid content in Nannochloris oculata, Desmid, and combined species to absorbance at the three absorbance bands, 2920 cm^{-1}, 2855 cm^{-1}, and 1742 cm^{-1}.

Table 6. Best subsets multiple linear regression parameters

Algae specie	Regression coefficients of predictors				R^2	R^2 (adj)	R^2 (Pred)	Mallow's Cp	RMSE [mg/g]
	2920 cm^{-1}	2855 cm^{-1}	1742 cm^{-1}	Constant					
Nannochloris oculata	-	-	531	77.2	0.43	0.41	0.35	3.1	41.08
	-	458	-	84.9	0.37	0.35	0.27	5.8	43.05
	-	245	363	67.3	0.49	0.45	0.35	2.1	39.51
	44.8	-	386	64.3	0.46	0.41	0.33	3.8	40.83
	-22.1	309	391	71.1	0.49	0.43	0.31	4	40.22
Desmid	213.1	-	-	89.2	0.53	0.51	0.47	7.5	57.23
	-	1817	-	66.9	0.5	0.48	0.43	9.6	59.08
	136.1	1033	-	59	0.62	0.59	0.54	3.2	52.37
	314.4	-	-148.8	69.6	0.59	0.55	0.51	5.5	54.65
	211.2	841	-89.3	52.9	0.64	0.59	0.52	4	52.16
Mixed species (Generalized model)	-	-	193.1	132.8	0.22	0.2	0.17	4.3	63
	103.1	-	-	102.6	0.22	0.2	0.16	4.3	63
	64.5	-	121.6	107.5	0.27	0.24	0.22	2.3	61.28
	-	267	170	111.6	0.27	0.24	0.22	2.3	61.31
	36	136	141.4	107.8	0.27	0.23	0.2	4	61.71

7.3.1.1 Nannochloris oculata regression models

Table 6 shows the independent variable values and regression coefficients resulting from multiple linear regression analysis relating lipid content in Nannochloris oculata to absorbance at the three absorbance bands, 2920 cm^{-1}, 2855 cm^{-1}, and 1742 cm^{-1}. The prediction models had moderate R^2 values ranging from 0.43 to 0.49. In general, the larger prediction models are associated with higher R^2 values. The best one-predictor model is the one containing absorbance band 1742 cm^{-1} as the independent variable, with an R^2 value of 0.43 and RMSE value of 41.08 mg/g. Similarly, the best two-predictor model is the one containing the 2855 cm^{-1} and 1745 cm^{-1} absorbance bands, with an R^2 value of 0.49 and RMSE value of 39.51 mg/g. Finally, the best three-predictor model of course contains all three absorbance bands (2920 cm^{-1}, 2855 cm^{-1}, and 1742 cm^{-1}), with an R^2 value of 0.49 and RMSE value of 40.22 mg/g.

It is obvious from the results that the best model is the two-variable model containing the 2855 cm^{-1} and 1742 cm^{-1} absorbance bands. This model explained about 49 % of the variability in lipid content data, and compared to the three-variable model it had the same R^2 value and a lower RMSE, even though it contained fewer independent variables. A plot of the predicted versus actual lipid content of the selected model shows a moderate goodness of fit over the range of experimental data (Figure 45). The model has a slope and a constant value of 0.49 and 72.20 mg/g, respectively. These values indicate that a 1% change in the actual lipid content in nannochloris microalgae creates a change of 0.49%

change in the predicted measurement using absorbance bands of 2855cm^{-1} and 1745 cm^{-1}.

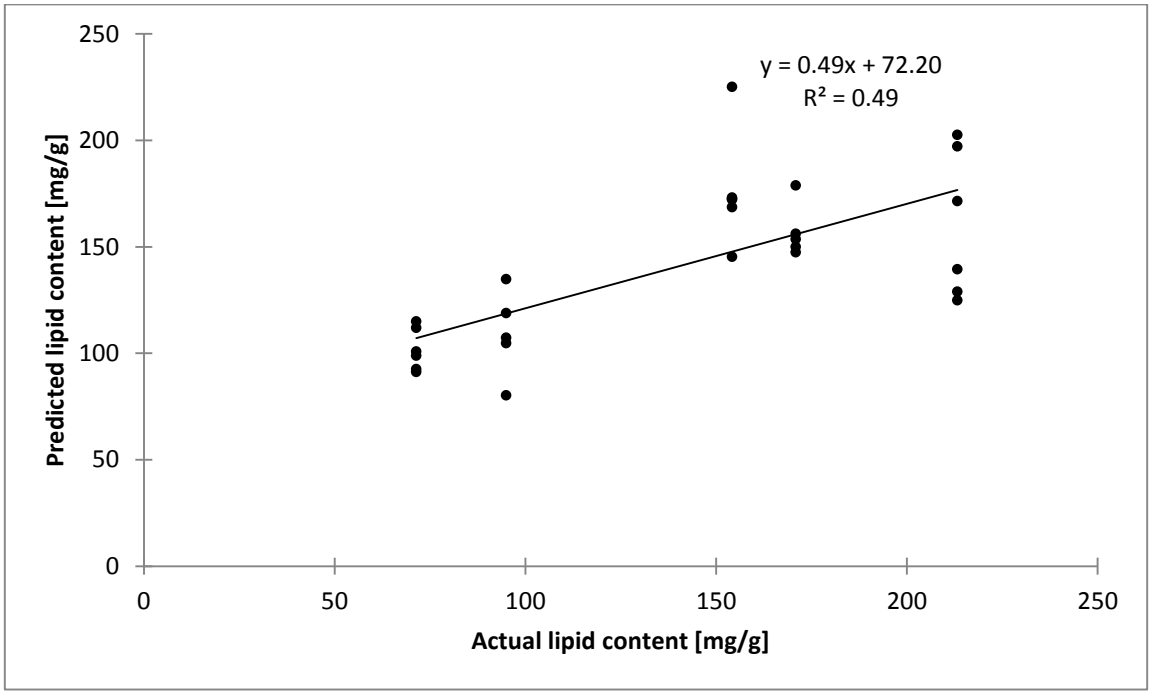

Figure 45. Predicted versus actual lipid content for the selected two variables (2855 cm^{-1} and 1742 cm^{-1}) model for the Nannochloris oculata microalgae

7.3.1.2 Desmid microalgae regression models

The results of the analysis for the Desmid specie show that the best one-predictor model contains the absorbance band at 2920 cm^{-1}, with R^2 value of 0.53 and RMSE value of 57.23 mg/g. The absorbance at band 2855 cm^{-1} had an R^2 value of 0.50 and RMSE value of 59.08 mg/g. The best two-predictor model contained the absorbance bands at 2920 cm^{-}

^{1} and 2855 cm^{-1}, with R^2 value of 0.62 and RMSE value of 52.37 mg/g. The three-predictor model had an R^2 value of 0.64 and RMSE value of 52.16 mg/g. The two-predictor model containing absorbance bands at 2920 cm^{-1} and 2885 cm^{-1} and the three-predictor models have equivalent adjusted R^2 values of 0.59. However, the three-predictor model has a slightly lower RMSE value (52.16 mg/g versus 52.37 mg/g). Although the three-predictor model has the lower RMSE value, the two predictor model was selected because it is simpler and has a smaller Mallow's Cp value of 3.2 versus 4.0 for the three-predictor model. A plot of the predicted versus actual lipid content for the selected model showed a moderate goodness of fit over the range of experimental data (Figure 46). The model has a slope and a constant value of 0.62 and 66.14 mg/g, respectively. These values indicate that a 1% change in the actual lipid content in desmid microalgae creates a change of 0.62% change in the predicted measurement using absorbance bands of 2920 cm^{-1} and 2855 cm^{-1}.

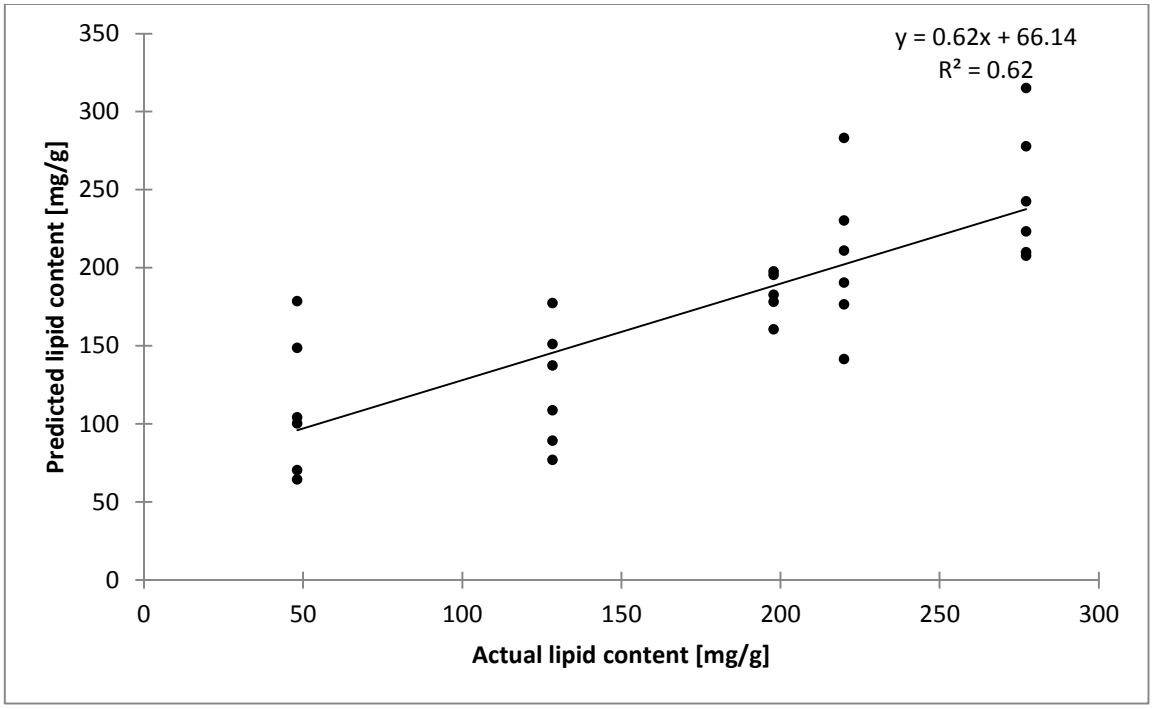

Figure 46 Predicted versus actual lipid content for the selected two variables (2920 cm^{-1} and 2855 cm^{-1}) model for the Desmid microalgae

7.3.1.3 Combined Nannochloris oculata and Desmid microalgae regression models

When spectra from both species were considered simultaneously, regression results showed that the one-predictor models including the 1742 cm^{-1} and of 2920 cm^{-1} absorbance bands had similar prediction performance, with an R^2 value of 0.22 and RMSE value of 63.00 mg/g. The two-predictor and three-predictor models had the highest R^2 values of 0.27. However, the adjusted R^2 value for both of the two-predictor models considered were higher (0.24) than that of the three-predictor model (0.23). The two model predictor containing absorbance bands at 2920 cm^{-1} and 1742 cm^{-1} was the best-fitting model, with an R^2 value of 0.27 and RMSE value of 61.31 mg/g. A plot of the predicted versus actual

lipid content of the selected model had relatively poor goodness of fit over the range of experimental data when compared to separate models for each microalgae specie (Figure 47). The model has a slope and a constant value of 0.27 and 113.89 mg/g, respectively. These values indicate that a 1% change in the actual lipid content in combined microalgae species creates a change of 0.27% change in the predicted measurement using absorbance bands of 2920 cm^{-1} and 1745 cm^{-1}.

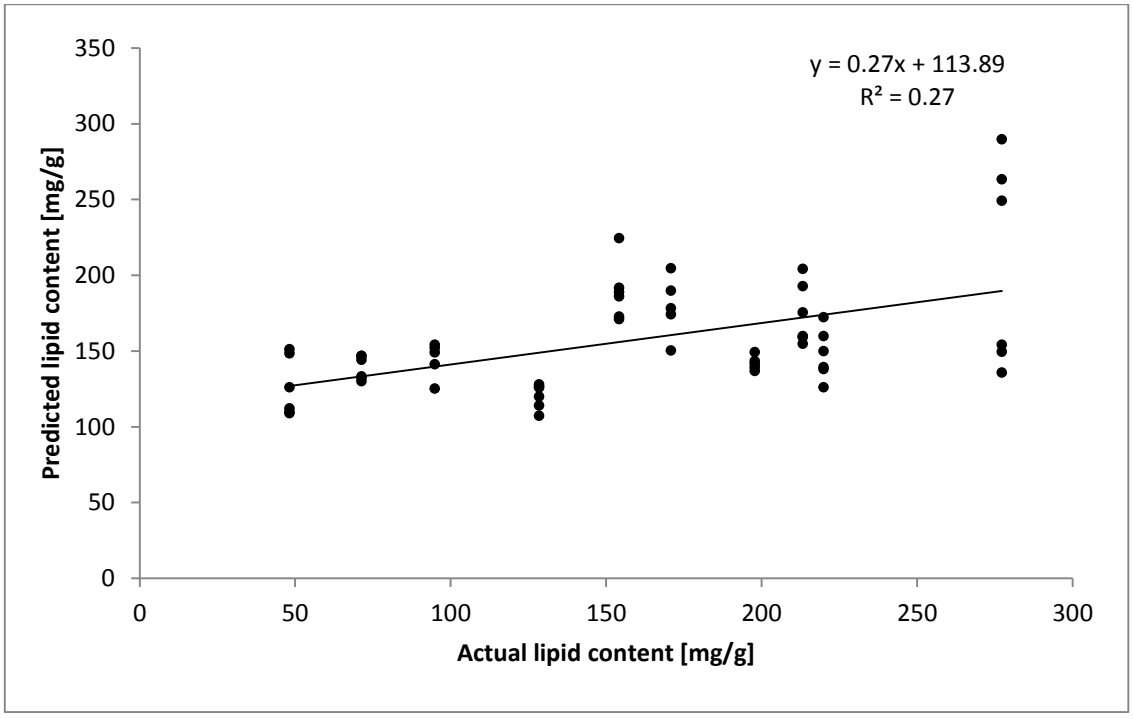

Figure 47. Predicted versus actual lipid content for the selected two variables (2920 cm^{-1} and 1742 cm^{-1}) model for the Nannochloris oculata & Desmid (mixed species)

7.3.2 Results and discussion for simple linear regression analysis relating sensor output to lipid content

Table 7 shows important statistics regarding how the developed ATR-IR sensor output relates to neutral lipid content in Nannochloris oculata, Desmid, and both species (generalized model).

Table 7. Regression statistics

Algae specie	Slope	Constant	R^2	RMSE [mg/g]
Nannochloris oculata	17.13	-82.50	0.50	37.72
Desmid	17.06	21.20	0.73	42.36
Combined species (generalized model)	9.74	50.40	0.29	59.12

The analyses produced a relatively good fitting linear model for Desmid, with an R^2 value of 0.73 and an RMSE value of 42.36 mg/g. The linear model for Nannochloris oculata fitting moderately well, with an R^2 value of 0.50 and RMSE value of 37.72 mg/g. On the other hand, the generated generalized model for both of the species combined had poor prediction performance, with an R^2 value of 0.29 and RMSE value of 59.12 mg/g. The Nannochloris oculata model has a slope and a constant value of 17.13 and -82.5 mg/g, respectively. The Desmid model has a slope and a constant value of 17.06 and 21.2 mg/g,

respectively. These values indicate similar sensitivity of the developed sensor to measure lipid content between microalgae species. On the other hand, the model of the combined species has a slope and constant values of 9.74 and 50.4 mg/g, respectively. These values indicate lower sensitivity of the sensor in measuring lipid content in the algae species when combined.

It is obvious that the sensor performs differently for different algae species. This difference could be due to the fact that algae species vary in physical and biochemical structure. Despite the lower R^2 and higher RMSE value of the generalized model, the results indicate a statistically significant trend between lipid content and sensor output across both species of microalgae. Figures 48, 49, and 50 show the linear regression lines of models correlating lipid content to sensor output measurements for Nannochloris oculata, Desmid, and the species combined (generalized model), respectively.

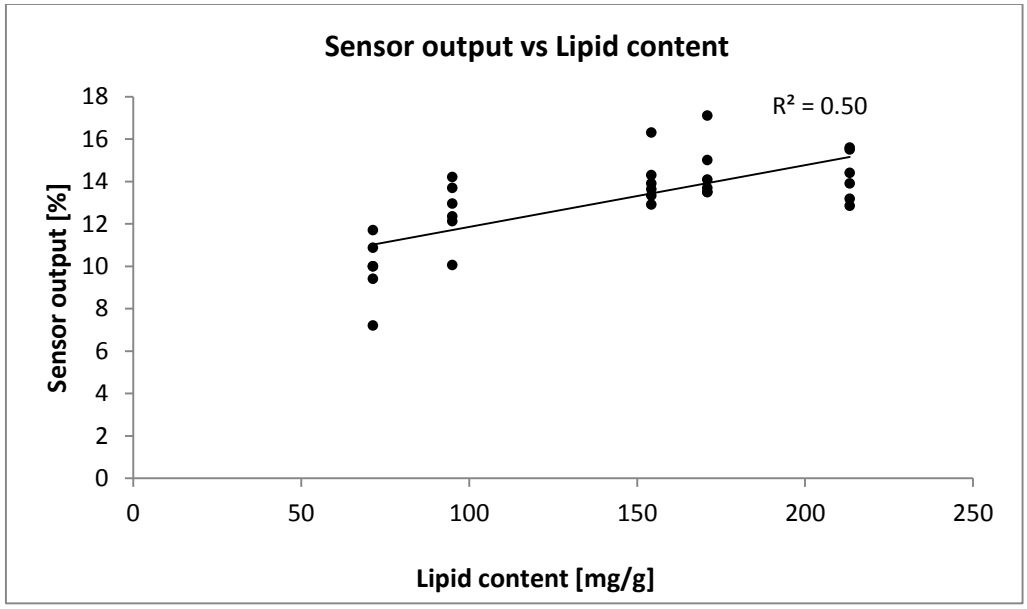

Figure 48. Regression line for sensor output [%] vs lipid content for Nanaochloris oculata microalgae

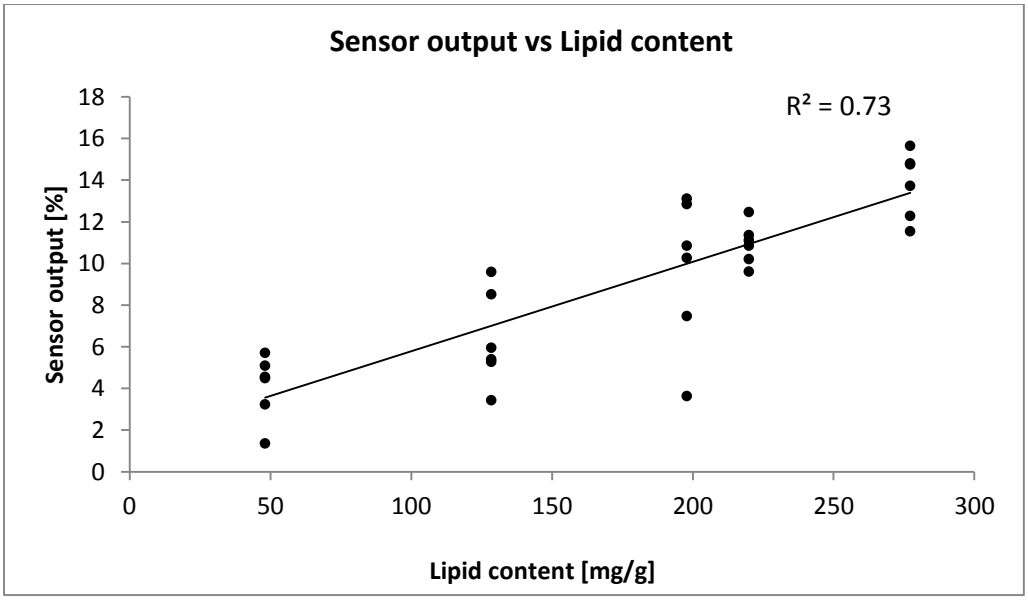

Figure 49. Regression line for sensor output [%] vs lipid content for Desmid microalgae

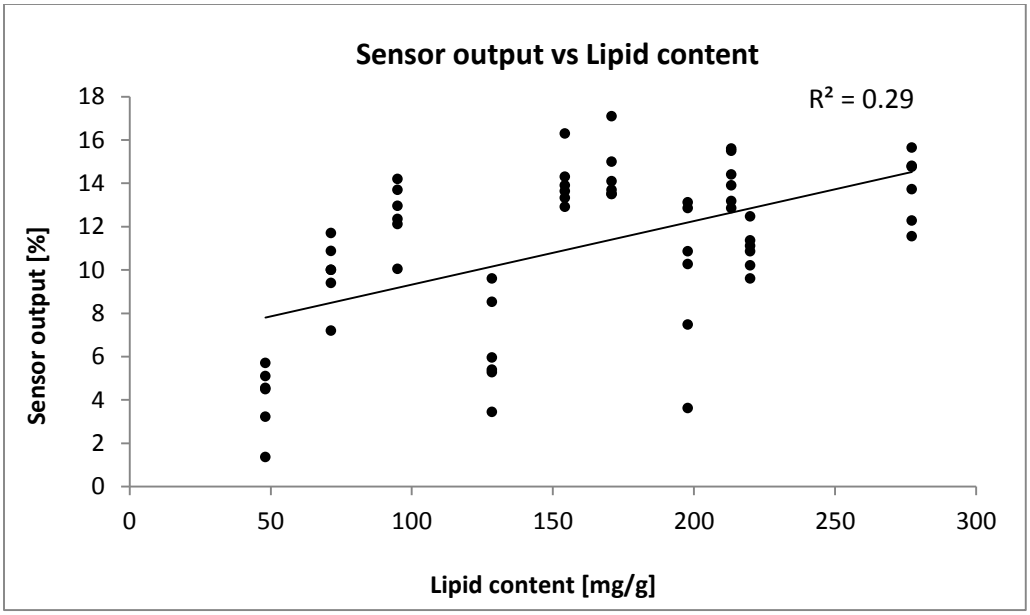

Figure 50. Regression line for sensor output [%] vs lipid content for mixed species (generalized model)

8. RECOMMENDATIONS

The results of the this study indicate that the use of the attenuated total reflection technique for the measurement of neutral lipids in microalgae is promising. The developed ATR-IR sensor indicated moderate to good prediction performance in measuring neutral lipids in the two species of algae, Nannochloris oculata and Desmid. However, the prediction performance was poor for the species combined. It is recommended that more algae species with a broader range of lipid content be included in any future study. From a design prespctive, it is recommended that at least one more absorbance band be included in any attempt to improve the performance of the current ATR-IR sensor. The results of the study with ATR-FTIR spectroscopy clearly showed that the best prediction models were two-variable models. Both species and the species combined had different combinations of two absorption bands, but since the two-variable model of 2920 cm^{-1} and 1742 cm^{-1} absorbance bands was best for the species combined, it is recommended to include both these bands to improve the sensor performance.

In the current design of the ATR-IR sensor, a single reflection IRE element was used. However, using a multiple internal reflection element would increase the sensor sensitivity, increase signal to noise ratio, and thus likely raise the sensor capabilities for measuring lipid content of algae samples at low biomass concentrations. In addition, in the current design of the sensor a focusing lens was used in combination with a collimating

lens to concentrate the IR light on a smaller spot area on the surface of the IRE prism. This was done intentionally to increase IR light intensity and consequently signal strength measured by detector. Nonetheless, dispensing with the focusing lens and using only the collimating lens, which would increase the light spot area on the surface of the IRE prism, would also lead to a larger area of interaction between IR light and the sample's molecules. Such a design change may improve sensor sensitivity and performance.

9. SUMMARY AND CONCLUSIONS

Measurements of absorbance at three absorbance bands (2920 cm^{-1}, 2855 cm^{-1}, and 1742 cm^{-1}) on two algae species (Nannochloris oculata and Desmid) at five lipid contents collected with an ATR-FTIR spectrometer. Multiple linear regression analysis of was used to relate the three absorbance bands to lipid content to generate prediction models.

In general, the best models showed moderate to good prediction performance for Nannochloris oculata and Desmid microalgae, when considered separately. The best prediction model for Nannochloris oculata was the two-variable model containing absorbance bands at 2855 cm^{-1} and 1742 cm^{-1}, with an R^2 value 0.49 of and RMSE value of 39.51 mg/g. The best prediction model for Desmid was the two-variable model containing absorbance bands at 2920 cm^{-1} and 2855 cm^{-1}, with an R^2 value of 0.62 and and RMSE value of 52.37 mg/g. On the other tand, the best model to predict lipid content for the species combined had poor prediction performance, with an R^2 value of 0.27 and RMSE value of 61.28 mg/g.

These results showed that using two absorbance bands for the prediction of neutral lipid content improved the prediction performance over using only one band. This improvement was evident with both algae species as well as for the algae species combined. Thus, adding another absorbance band in future improvements of the devloped ATR-IR sensor

is likely warranted. Since the sensor would ideally be used for predicting lipid content in various microalgae species, the results indicate that absorbance bands at 2920 cm^{-1} and 1742 cm^{-1} have potential for predicting neutral lipids in multiple microalgae species.

Measurmements with the developed sensor were related to lipid content in Nannochloris oculata and Desmid with simple linear reghression analyses. The sensor in the configuration used in this work used only a single absorbance band at 2920 cm^{-1} (wavelength ≈ 3.4 μm). Even so, the sensor had comparable prediction performance to the spectrometer for neutral lipids in Nannochloris oculata, Desmid, and the species combined. Regression analyses showed moderate prediction performance for Nannochloris oculata and good performance for Desmid microalgae . For Nannochloris oculata, the regression analysis generated a prediction model with an R^2 value of 0.50 and RMSE value of 37.72 mg/g. For Desmid microalgae, the regression analysis generated a prediction model with an R^2 value of 0.73 and RMSE value of 42.36 mg/g. For the generalized model including both of the microalgae species, the model demonstrated lower prediction performance, with an R^2 value of 0.29 and RMSE value of 59.12 mg/g.

REFERENCES

Achara, N. (2012). Biofuel from algae. *The Journal of American Science, 8*(1), 240-244.

Asakuma, Y. (2011). Theoretical study of the transesterification of triglycerides to biodiesel fuel under various conditions. *International Journal of Thermodynamics, 14*(4), 193-196.

Berndes, G., Hoogwijk, M., & van den Broek, R. (2003). The contribution of biomass in the future global energy supply: a review of 17 studies. *Biomass and Bioenergy, 25*(1), 1-28.

Bligh, E., & Dyer, W. J. (1959). A rapid method of total lipid extraction and purification. *Canadian Journal of Biochemistry and Physiology, 37*(8), 911-917.

Brune, D., Lundquist, T., & Benemann, J. (2009). Microalgal biomass for greenhouse gas reductions: potential for replacement of fossil fuels and animal feeds. *Journal of Environmental Engineering, 135*(11), 1136-1144.

Campbell, C. J., & Laherrère, J. H. (1998). The end of cheap oil. *Scientific American, 278*(3), 60-65.

Chen, Y., & Vaidyanathan, S. (2012). A simple, reproducible and sensitive spectrophotometric method to estimate microalgal lipids. *Analytica Chimica Acta, 724*, 67-72.

Cheng, Y., Zheng, Y., & VanderGheynst, J. S. (2011). Rapid quantitative analysis of lipids using a colorimetric method in a microplate format. *Lipids, 46*(1), 95-103.

Demirbas, A. (2007). Progress and recent trends in biofuels. *Progress in Energy and Combustion Science, 33*(1), 1-18.

Demirbas, M. F. (2010). Microalgae as a feedstock for biodiesel. *Energy Education Science and Technology Part A-Energy Science and Research, 25*(1-2), 31-43.

Destouni, G., & Frank, H. (2010). Renewable Energy. *Ambio, 39*(1), 18-21.

Drapcho, C. M., Nhuan, N. P., & Walker, T. H. (2008). *Biofuels engineering process technology.* McGraw-Hill New York, NY.

Elsey, D., Jameson, D., Raleigh, B., & Cooney, M. J. (2007). Fluorescent measurement of microalgal neutral lipids. *Journal of Microbiological Methods, 68*(3), 639-642.

Eia.gov. (2007). Official energy statistics from the U.S. government. *Energy Information Administration (EIA).* Retrieved from: http://*www.eia.gov.*

Exxon Mobile. (2012).*The outlook for energy: a view to 2040*. Retrieved from: http://www.exxonmobil.com/Corporate/files/news_pub_eo.pdf.

Fahrenfort, J. (1961). Attenuated total reflection: A new principle for the production of useful infra-red reflection spectra of organic compounds. *Spectrochimica Acta*, 17(7), 698-709.

Gao, C., Xiong, W., Zhang, Y., Yuan, W., & Wu, Q. (2008). Rapid quantitation of lipid in microalgae by time-domain nuclear magnetic resonance. *Journal of Microbiological Methods, 75*(3), 437-440.

Griffiths, M. J., & Harrison, S. T. (2009). Lipid productivity as a key characteristic for choosing algal species for biodiesel production. *Journal of Applied Phycology, 21*(5), 493-507.

Hall, D. O. (1991). Biomass energy. *Energy Policy, 19*(8), 711-737.

Han, Y., Wen, Q., Chen, Z., & Li, P. (2011). Review of methods used for microalgal lipid-content analysis. *Energy Procedia, 12*, 944-950.

Harrick, N. J. (1967). *Internal reflection spectroscopy.* Interscience Puplishers, New York.

Hossain, A. S., Salleh, A., Boyce, A. N., & Naqiuddin, M. (2008). Biodiesel fuel production from algae as renewable energy. *American Journal of Biochemistry and Biotechnology, 4*(3), 250.

Hsu, C. S. (1997). Infrared spectroscopy. In: F. Settle, ed., *Handbook of Instrumental Techniques for Analytical Chemistry*, 1st ed. Upper Saddle River, New Jersey: Prentice-Hall, Inc., p.249.

IBSG Co., Ltd. (2012). *Operations manual for the DLT-37M universal driver for LEDs with built-in cooler*. IBSG Co., Ltd., St-Petersburg, RUSSIA.

Klass, D. L. (1998). *Biomass for renewable energy, fuels, and chemicals*. San Diego: Academic Press.

Kosaric, N., & Velikonja, J. (1995). Liquid and gaseous fuels from biotechnology: challenge and opportunities. *FEMS Microbiology Reviews, 16*(2-3), 111-142.

Kramer, J. K., Hernandez, M., Cruz-Hernandez, C., Kraft, J., & Dugan, M. E. (2008). Combining results of two GC separations partly achieves determination of all cis and trans 16: 1, 18: 1, 18: 2 and 18: 3 except CLA isomers of milk fat as demonstrated using Ag-ion SPE fractionation. *Lipids, 43*(3), 259-273.

Kulkarni, M. G., & Dalai, A. K. (2006). Waste cooking oil an economical source for biodiesel: a review. *Industrial & Engineering Chemistry Research, 45*(9), 2901-2913.

Lau, S., Right, J., Stavens, K., Whitaker, J., Liu, Z., & Lauterbach, J. (1997). 'Do-It-Yourself'Attenuated Total Reflectance Cell Designed and Constructed in a Laboratory Course: A Versatile and Economical Alternative to Commercial Designs. *The Chemical Educator*, *2*(4), 1-16.

Laurens, L. M., & Wolfrum, E. J. (2011). Feasibility of spectroscopic characterization of algal lipids: chemometric correlation of NIR and FTIR spectra with exogenous lipids in algal biomass. *BioEnergy Research, 4*(1), 22-35.

Melling, P.J. & Thomson, M. (2002). *Fiber-optic Probes for Mid-infrared Spectrometry, Handbook of Vibrational Spectroscopy*; John Wiley & Sons: Chichester, UK; pp. 1–9.

Milosevic, M. (2012). Internal reflection and ATR spectroscopy: Chemical analysis: A series of monographs on analytical chemistry and its applications. Hoboken: John Wiley & Sons. & Sons.

Mossoba, M. M., & Kramer, J. K. G. (2009). *Official methods for the determination of trans fats (2nd ed.)*. Urbana, IL: AOCS Press.

Mulbry, W., Reeves, J., Liu, Y., Ruan, Z., & Liao, W. (2012). Near-and mid-infrared spectroscopic determination of algal composition. *Journal of Applied Phycology, 24*(5), 1261-1267.

Pejcic, B., Myers, M., & Ross, A. (2009). Mid-infrared sensing of organic pollutants in aqueous environments. *Sensors, 9*(8), 6232-6253.

PerkinElmer. (2005). *FT-IR spectroscopy attenuated total reflectance (ATR). Technical note*. PerkinElmer, Inc., 710 Bridgeport Avenue Shelton, CT 06484-4794 USA.

Pollio, A., Greca, M., Monaco, P., Pinto, G. & Previtera, L. (1988). Lipid composition of the acidophilic alga Dunaliella acidophila (Volvocales, Chlorophyta) I. Non-polar lipids. *Biochimica et Biophysica Acta (BBA) - Lipids and Lipid Metabolism*, 963(1), pp.53-60.

Rodolfi, L., Chini Zittelli, G., Bassi, N., Padovani, G., Biondi, N., Bonini, G., & Tredici, M. R. (2009). Microalgae for oil: Strain selection, induction of lipid synthesis and

outdoor mass cultivation in a low-cost photobioreactor. *Biotechnology and Bioengineering, 102*(1), 100-112.

Santhanam, N. (2013). *Algal chemical composition*. Retrieved 11/12, 2013, from http://www.oilgae.com/algae/comp/comp.html

Schuttlefield, J. & Grassian, V. (2008). ATR-FTIR Spectroscopy in the Undergraduate Chemistry Laboratory. Part I: Fundamentals and Examples. *J. Chem. Educ.*, 85(2), p.279.

Soetaert, W. & Vandamme, E. (2009). *Biofuels*. Hoboken, N.J.: Wiley.

Spectra-tech. (1996). *Introduction to attenuated total internal reflectance (ATR)*. Technical note. Spectra-Tech Inc., 2 Research Drive, Shelton, CT 06484-0869 USA.

Steinman, Alan. (2000). *Algae*. Retrieved 11/28, 2014, from: http://autocww.colorado.edu/~toldy3/E64ContentFiles/AlgaeAndFungi/Algae.html

Sun, D. (2009). *Infrared spectroscopy for food quality analysis and control*. Amsterdam: Academic Press/Elsevier.

Tilman, D., Hill, J., & Lehman, C. (2006). Carbon-negative biofuels from low-input high-diversity grassland biomass. *Science*, *314*(5805), 1598-1600.

Todt, H., Burk, W., Guthausen, G., Guthausen, A., Kamlowski, A., & Schmalbein, D. (2001). Quality control with time-domain NMR. *European Journal of Lipid Science and Technology, 103*(12), 835-840.

Tsoskounoglou, M., Ayerides, G., & Tritopoulou, E. (2008). The end of cheap oil: Current status and prospects. *Energy Policy, 36*(10), 3797-3806.

Vieler, A., Wilhelm, C., Goss, R., Süss, R. & Schiller, J. (2007). The lipid composition of the unicellular green alga Chlamydomonas reinhardtii and the diatom Cyclotella meneghiniana investigated by MALDI-TOF MS and TLC. *Chemistry and Physics of Lipids*, 150(2), pp.143-155.

Wagner, H., Liu, Z., Langner, U., Stehfest, K., & Wilhelm, C. (2010). The use of FTIR spectroscopy to assess quantitative changes in the biochemical composition of microalgae. *Journal of Biophotonics, 3*(8-9), 557-566.

Warman, H. (1972). The Future of Oil. *The Geographical Journal*, 138(3), p.287.

Wawrik, B., & Harriman, B. H. (2010). Rapid, colorimetric quantification of lipid from algal cultures. *Journal of Microbiological Methods, 80*(3), 262-266.

APPENDIX A

COMPONENTS OF MEASUREMENT SYSTEM

Component	Model	Manufacturer	Specifications
Light emitting diode	LED-36-TEC	IBSG	- Material : InAs substrate - Wavelength (typical): 3.40µm - Optical power (typical): 24µw (@Quasi-CW) - Emitting area: 300 µmX300 µm - Switching time (typical): 30ns - Cooling : thermoelectrically
Photodiode	PD-36-TEC	IBSG	- Window material: sapphire glass - Spectral range: 1500nm to 3800 nm - Diameter of photosensitive area: 0.3 mm - Cooling: one-stage TE-cooled - Operating temperature: -20 to 40 °C
Collimating & focusing lens	C021TME-E	Thorlabs, Inc.	- Material: black diamond-2 - Coefficient of thermal expansion: 13.5 x 10^{-6} / °C - Refractive index: 2.630 at 2.5 µm - Focal length: 9.2 mm
LED controller	DLT-37M	IBSG	- Input voltage : + 12 v - Adjustment temperature range: -10°C to +25°C - Mode of operation : QCW or Pulsed - Pulse duration : 31 - 1000µs (QCW), 0.6 – 20 µs (Pulsed) - Frequency : 0.5 – 16 kHz - Output current : 20 – 250 mA (QCW), 0.1 – 2.0 A (Pulsed)
PD controller	AMT-07M	IBSG	- Input voltage : +12 v - Adjustment temperature range: -15°C to +15°C - Maximal amplification : 6.4 x 10^6 V/A - Maximal output voltage: |±4V

			- Output resistance : 50 ohm|
Internal reflection element (IRE)	PS701	Thorlabs, Inc.	- Size: 10.0 mm - Shape: Right angle prism - Weight: 0.02 kg

APPENDIX B

COMPONENTS OF DRYING SYSTEM

Component	Model	Manufacturer	Specifications
Ceramic heater	101	Lasco	- Rated power: 200 W
Heater controller	-	-	- Type : voltage regulator module - Max power: 2000 W - Material : electronic components & plastic
Drying chamber	-	workshop	- Material: aluminum - Size: 155mm x 87mm x 80mm (LxWxH) - Volume: 1078800 mm^3
IRE Gasket	-	Stockwell elastomerics	- Material : Silicone rubber - Dimensions: 14.80 mm x 10.80 mm x 0.81 mm (LxWxH)

APPENDIX C

PARTS CATALOGUES

C-1. LED34-TEC

LIGHT EMITTING DIODES 1.6÷4.6 μm

Model LED34-TEC 3.4 μm 24 μW

•Light Emitting Diodes ***LED34-TEC*** are designed for emitting at a spectral range around 3400 nm. Thermocooler and thermoresistor are mounted inside 9 mm package TO-5. Heterostructures (HS) are grown on InAs substrates

•Light Emitting Diodes ***LED34-TEC*** are developed for using in optical gas sensors and medical diagnostics. Such construction gives possibility for temperature stabilization of LED parameters. Lifetime is more then 10000 hours.

•Related products: ***LED34*** can be used in optical pair with our photodiodes ***PD36***. Our standard ***LED Driver*** provides power supply of ***LED34-TEC*** in two recommended here regimes (Quasi-CW and Pulsed).

Parameters	Min	Typ	Max
Wavelength, μm	3.30	3.40	3.50
FWHM, μm	0.60	0.70	0.80
Optical Power, μW Quasi-CW @ 200 mA Pulsed@2A	20 320	24 400	28 480
Switching Time, ns	10	30	50
Range of temperature control °C	-10÷+60		
Emitting Area, μm	300x300		
Soldering temperature	95 °C		
Package	TO-5 with thermocooler and thermistor		

Recommended regimes of LED operation

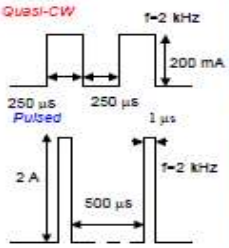

Main thermocooler parameters (without load)

I_{max} (Amps)	Q_{max} (Watts)	U_{max} (Volts)	ΔT_{max} °C
0.7	0.4	1.0	67

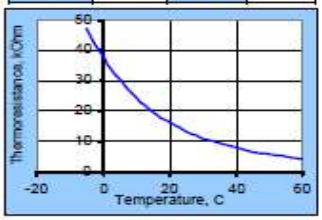

Package TO-5

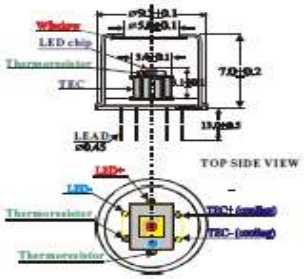

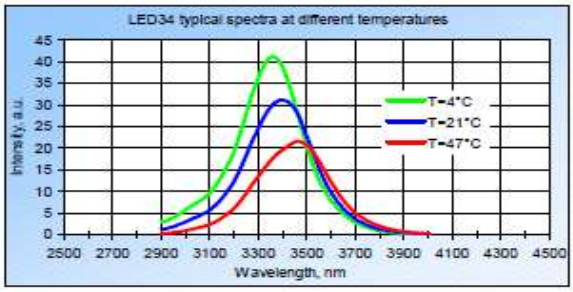

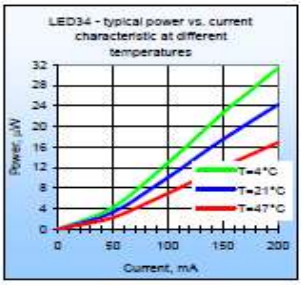

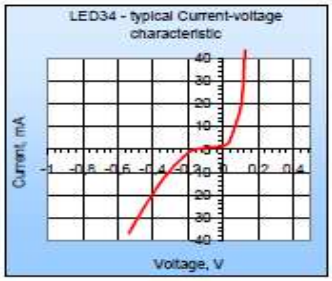

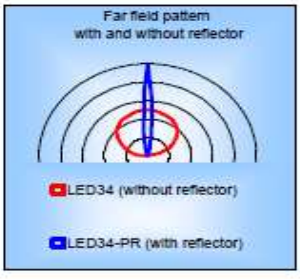

C-2. PD36-03-TEC

Mid infrared IBSG Optoelectronics

PHOTODIODE with TEC
PD36-03-TEC
1.5 - 3.8 µm

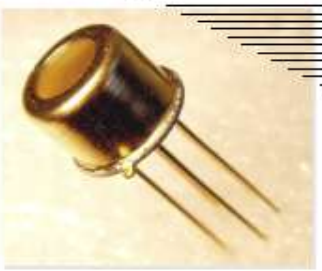

Features

- High reliability
- Superior linearity
- Thermo stability
- Easy-to-use detector/amplifier modules are also available

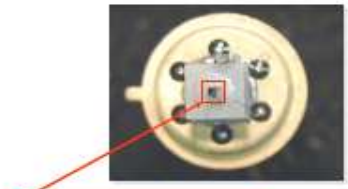

Photodiode CHIP

Applications

- Invironment measurements
- Infared spectrophotometry
- Laser detection
- Analytical instruments

Accessories (optional)

- Amplifier with temperature controller AMT-07M

Description

Photodiode **PD36-03-TEC** is a model of photodetector for detection of radiation at room temperature in the Middle Infrared (Mid-IR) spectral range from 1500 to 3800 nm.

Photodiode **PD36-03-TEC** has thermo electric cooler (**TEC**) and termistor for a control of temperature. Components are integrated inside the standard 9.2 mm TO-5 package with **TEC**.

Diameter of the photosensitive area of **PD36-03-TEC** is 300 µm. High speed of response makes it possible for detection of modulated radiation of laser diodes (LDs) and light-emitting diodes (LEDs).

Related products: **PD36-03-TEC** can be used in optical pair with our **LED185**...**LED36**.

General characteristics

Package	Parameter	Symbol	Value	Unit
TO-5 with TEC	Sensitive area diameter	d	0.3	mm
	Weight	m	1.15	g
	Operating temperature	T_{opr}	− 20...+ 40	°C
	Window material	sapphire glass		
	Cooling	one-stage TE-cooled		
	Soldering temperature	T_s	+ 230	°C
	Storage temperature	T_{stg}	− 20...+ 50	°C
	Maximum reverse bias voltage	V_b	− 1.0	V
	Size	D	9.2	mm
		H	20.2	

IBSG Co., Ltd.,
26 Polytekhnicheskaya str.,
Saint Petersburg,
194021
RUSSIA

Ta: +7 (812) 292 7929,
Fax: +7 (812) 297 0006,
E-mail: ioffe@mail.ioffe.ru
IBSG.inform@gmail.com
www.ibsg-st-petersburg.com

Electrical and optical characteristics

Parameter	Symbol	Condition	Element temperature			Unit
			− 20 °C	0 °C	+ 20 °C	
Spectral sensitivity range	λ	at level 10%	1.5* - 3.6	-	1.5* - 3.8	μm
Peak sensitivity wavelength	λ_p	at level 90%	2.5 - 3.3	-	2.6 - 3.4	μm
Photo sensitivity	S	at λ_p	1.0 - 1.2			A/W
Detectivity	D*	at λ_p	$[0.6 - 1.0]\cdot10^{10}$	-	$[3 - 5]\cdot10^{9}$	$cm\cdot Hz^{1/2}\cdot W^{-1}$
Dark current	I_d	V_b = − 0.2 V	40 - 90	-	150 - 350	μA
		V_b = − 0.4 V	90 - 150	-	200 - 500	
Capacitance	C	V_b = 0 V, f = 1 MHz	70 - 1000			pF
Rise time	t_r	V_b = 0 V, R_L = 50 Ω	20 - 120			ns
Fall time	t_f					
Shunt resistance	R_0	$V_b \approx \pm$ [5 - 10] mV	900 - 6700	-	100 - 1200	Ω
Noise equivalent power	NEP	at λ_p	-	-	-	$W\cdot Hz^{-1/2}$

TEC *TO506.1MC0400710.TB103* parameters (without load)

Parameter	Symbol	Condition	Value	Unit
Current power	I_{max}	ΔT_{max}	1.50	A
Voltage	U_{max}	ΔT_{max}	0.80	V
Cooling energy	Q_{max}	-	1.30	W
Temperature range	ΔT_{max}	vacuum	70	K
Termistor resistance	R_t	at + 20 °C	10.00	kΩ

* Not at level 10%

IBSG Co., Ltd.,
26 Polytekhnicheskaya str.,
Saint Petersburg,
194021
RUSSIA

Tel: +7 (812) 292 7929,
Fax: +7 (812) 297 0006,
E-mail: kuhlis@iropt9.ioffe.ru
IBSG.inform@gmail.com
www.ibsg-st-petersburg.com

Mid infrared IBSG Optoelectronics

PHOTODIODE with TEC
PD36-03-TEC
1.5 - 3.8 μm

Spectral response

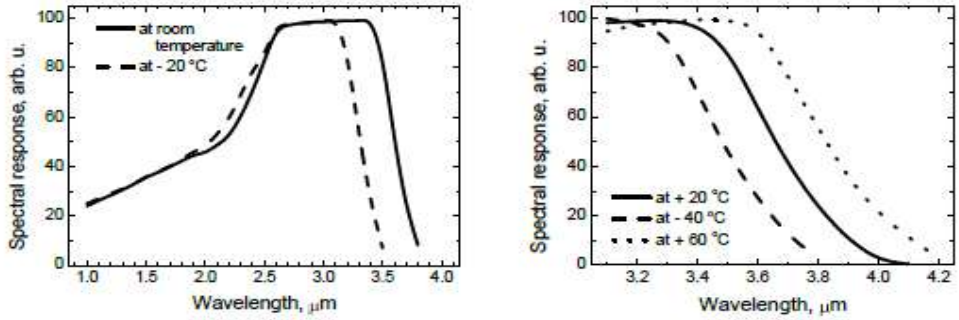

Shunt resistance vs. element temperature

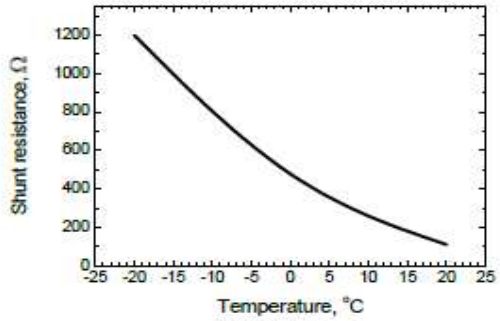

Capacitance vs. reverse voltage

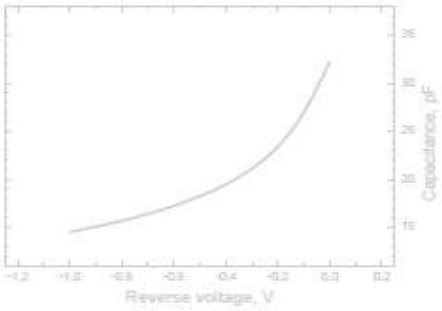

IBSG Co., Ltd.,
26 Polytekhnicheskaya str.,
Saint Petersburg,
194021
RUSSIA

Te: +7 (812) 292 7929,
Fax: +7 (812) 297 0006,
E-mail: kuntis@inopt9.ioffe.ru
IBSG.inform@gmail.com
www.ibsg-st-petersburg.com

Dark current vs. reverse voltage

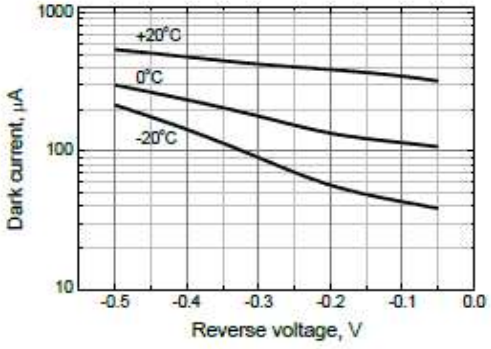

Thermoresistance vs. temperature

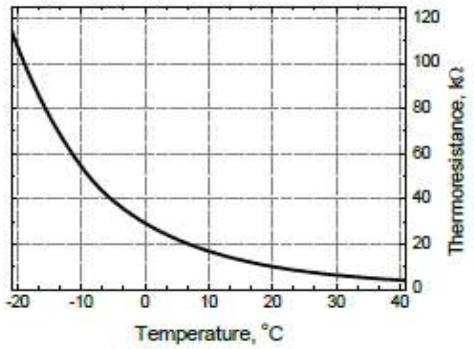

C-3. ZnSe RIGHT ANGLE PRISM

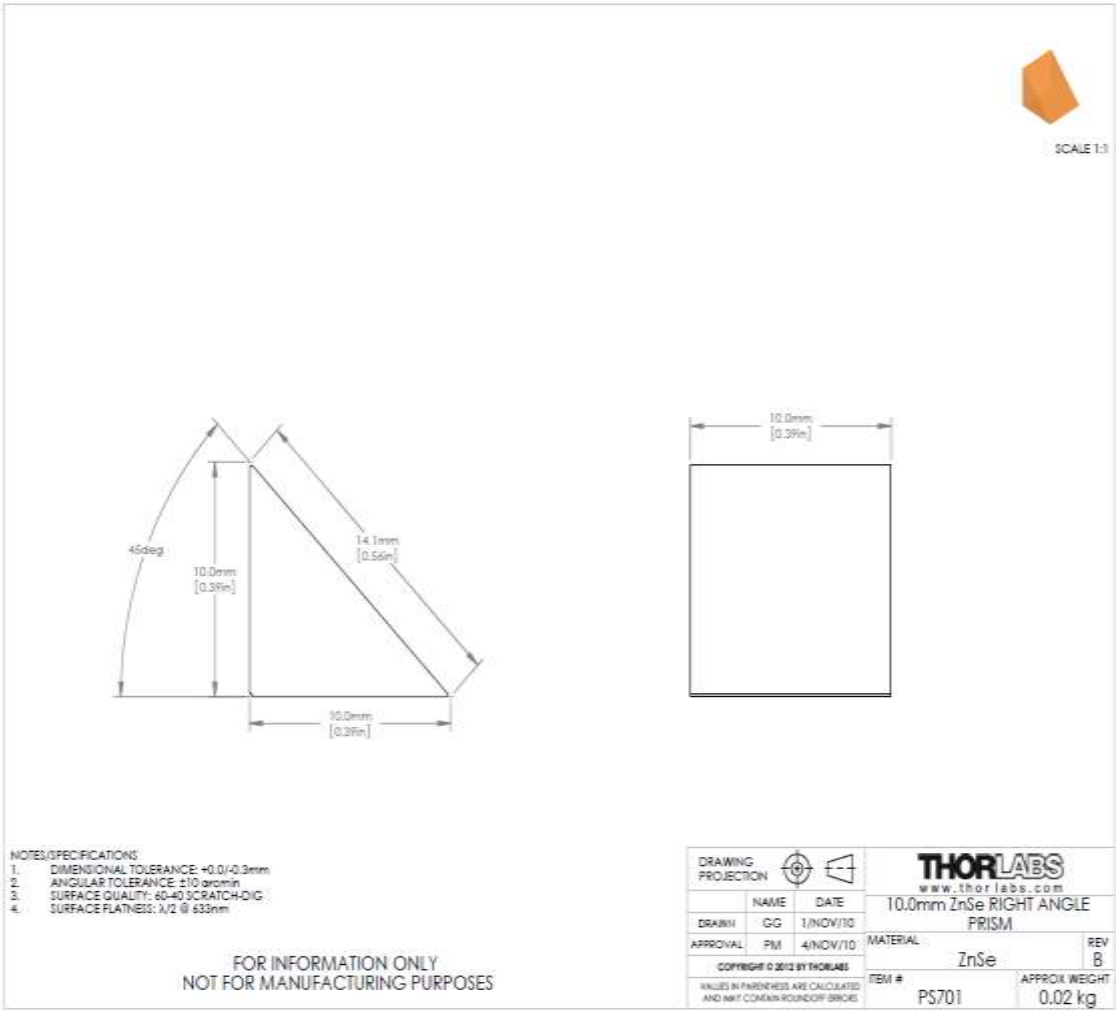

APPENDIX D

SAMPLES OF SOLIDWORKS® DRAWINGS FOR THE SENSOR DESIGN

D-1. TOP SURFACE

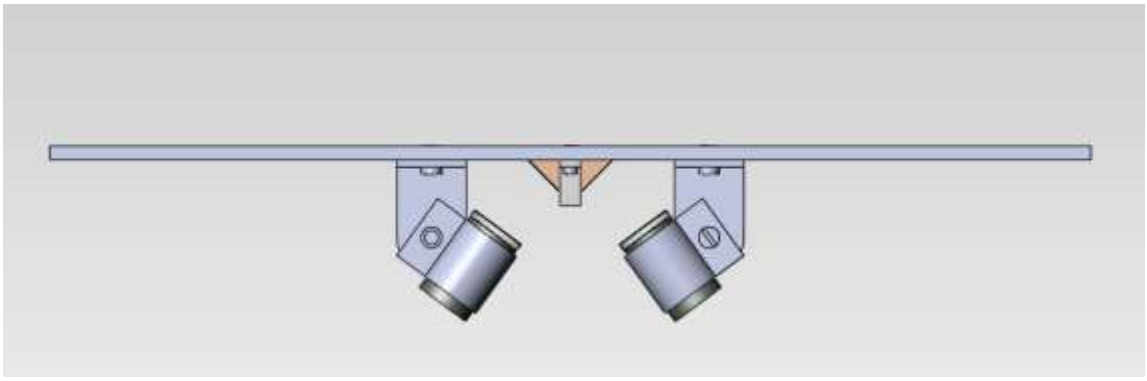

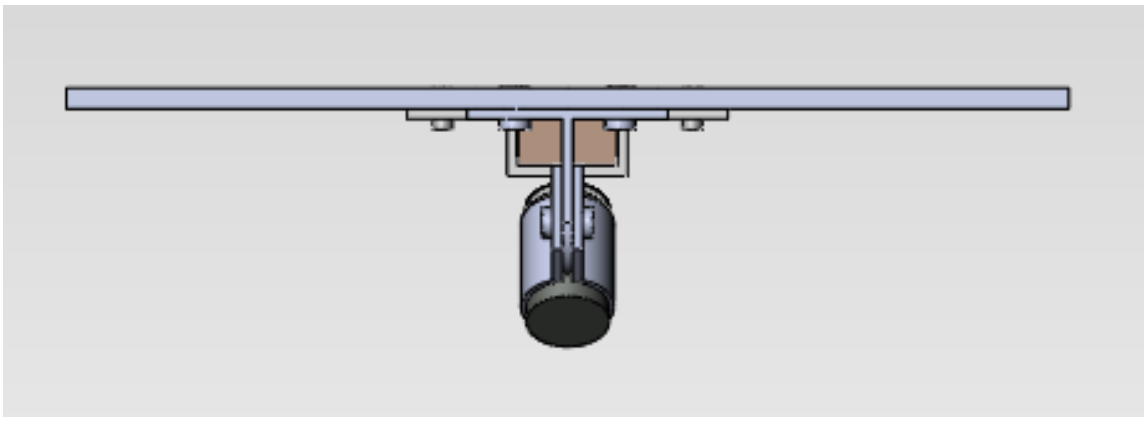

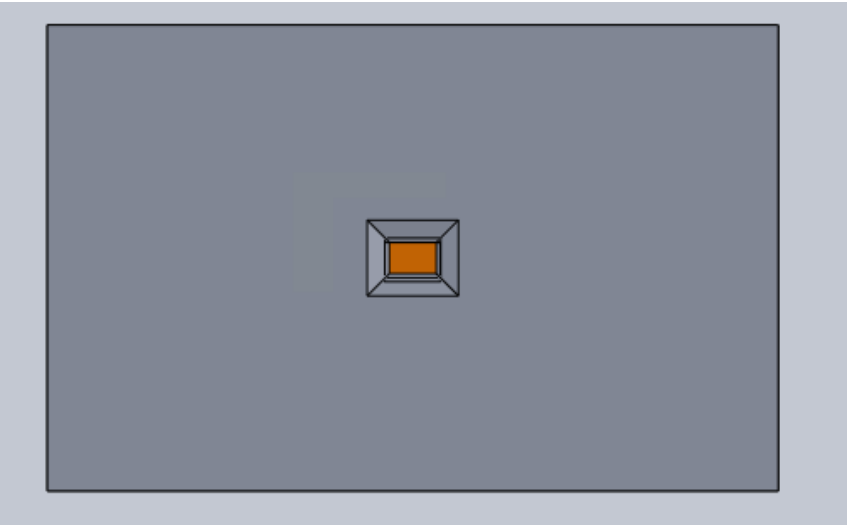

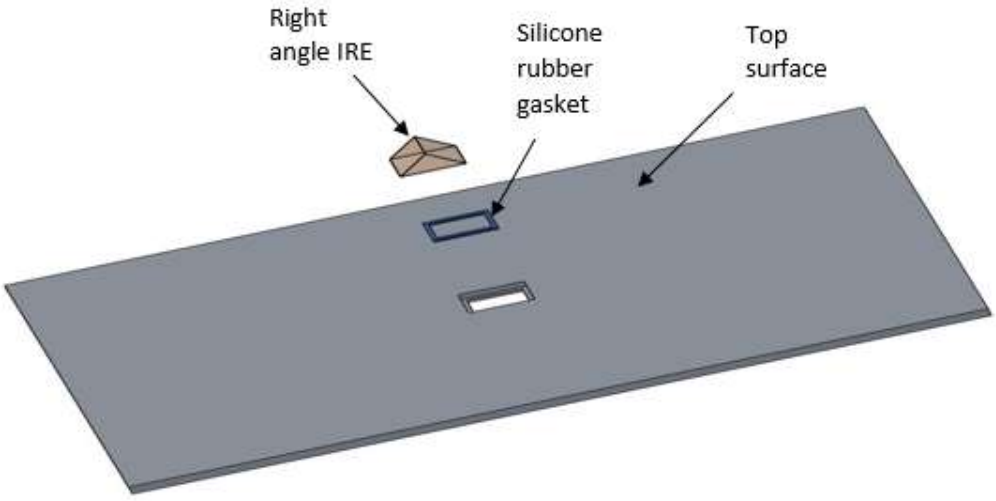
Right
angle IRE
Silicone
rubber
gasket
Top
surface

D-2. DRYING CHAMBER

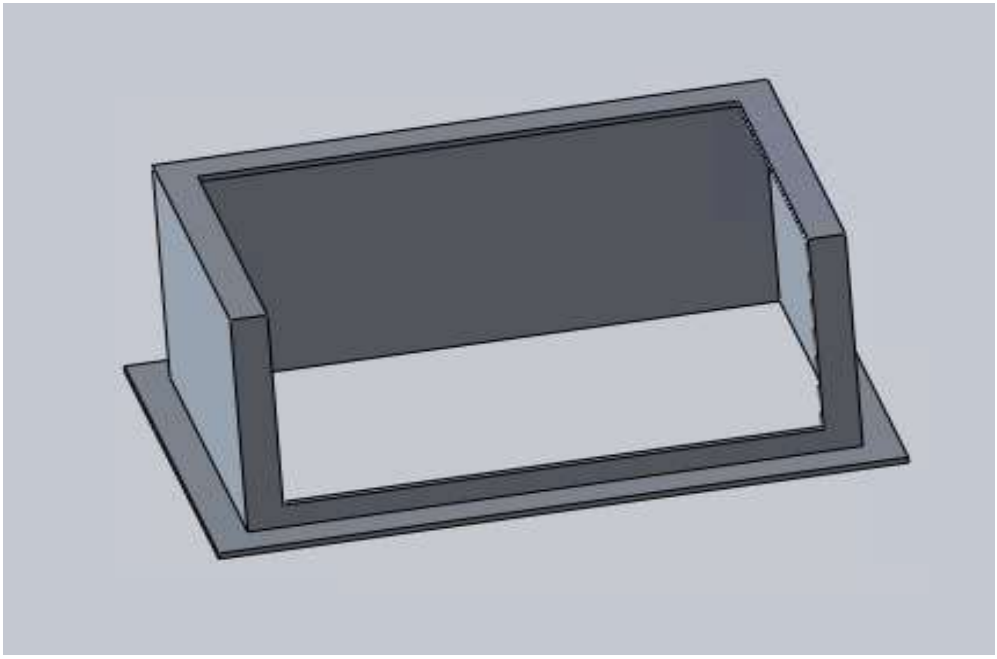

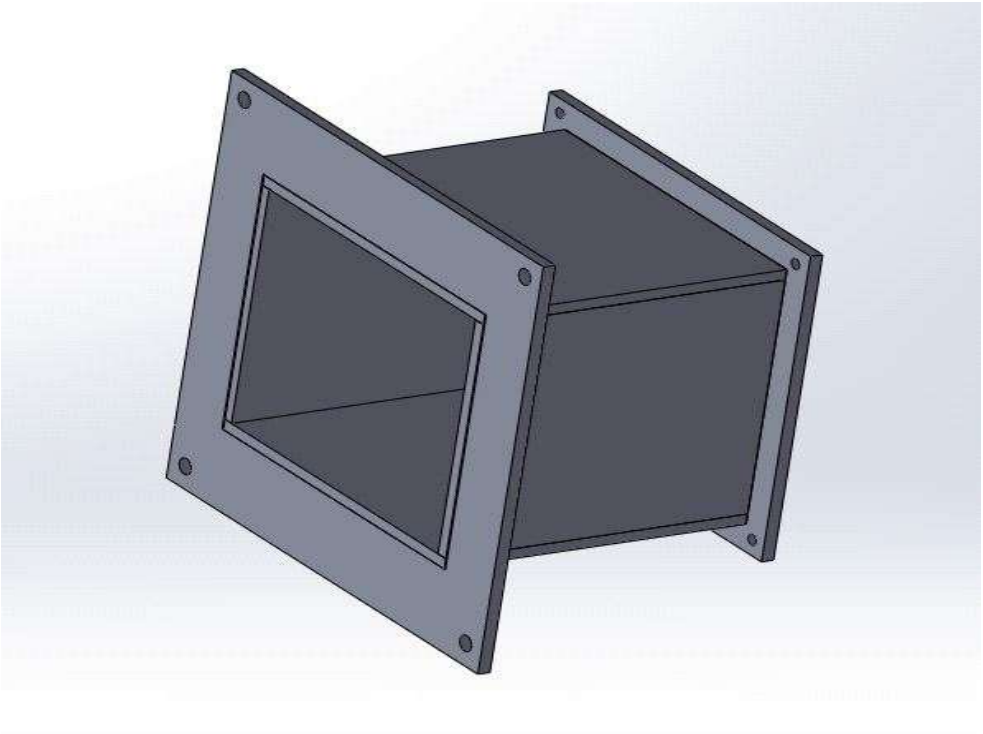

APPENDIX E

REGRESSION ANALYSES FOR USING THE NICOLET 6700 ATR-FTIR SPECTROMETR TO MEASURE NEUTRAL LIPIDS IN MICROALGAE

E-1. NANNOCHLORIS OCULATA

Best Subsets Regression: Lipid content versus 2920 cm-1, 2855 cm-1,1742 cm-1

```
Response is Lipid content [mg/g]
28 cases used, 2 cases contain missing values

                                                          2 2 1
                                                          9 8 7
                                                          2 5 4
                                                          0 5 2

                                                          c c c
                                                          m m m
                R-Sq             R-Sq  Mallows           - - -
Vars  R-Sq   (adj)    PRESS   (pred)       Cp       S   1 1 1
   1  42.7   40.5  50044.5    34.6      3.1  41.081       X
   1  37.1   34.6  56091.5    26.7      5.8  43.048     X
   2  49.0   44.9  50035.2    34.6      2.1  39.511     X X
   2  45.5   41.2  51574.9    32.6      3.8  40.830   X   X
   3  49.3   42.9  52670.8    31.2      4.0  40.223   X X X
```

Regression Analysis: Lipid content [mg/g] versus 2855 cm-1, 1742 cm-1

```
Method

Rows unused  2


Analysis of Variance

Source       DF  Seq SS  Contribution  Adj SS  Adj MS  F-Value  P-Value
Regression    2   37515        49.01%   37515   18758    12.02    0.000
  2855 cm-1   1   28361        37.05%    4852    4852     3.11    0.090
  1742 cm-1   1    9154        11.96%    9154    9154     5.86    0.023
Error        25   39027        50.99%   39027    1561
Total        27   76542       100.00%


Model Summary

      S    R-sq  R-sq(adj)    PRESS  R-sq(pred)
39.5106  49.01%     44.93%  50035.2      34.63%
```

Coefficients

Term	Coef	SE Coef	95% CI	T-Value	P-Value	VIF
Constant	67.3	16.9	(32.5, 102.0)	3.98	0.001	
2855 cm-1	245	139	(-41, 531)	1.76	0.090	1.67
1742 cm-1	363	150	(54, 672)	2.42	0.023	1.67

Regression Equation

Lipid content [mg/g] = 67.3 + 245 2855 cm-1 + 363 1745 cm-1

Residual Plots for Lipid content [mg/g]

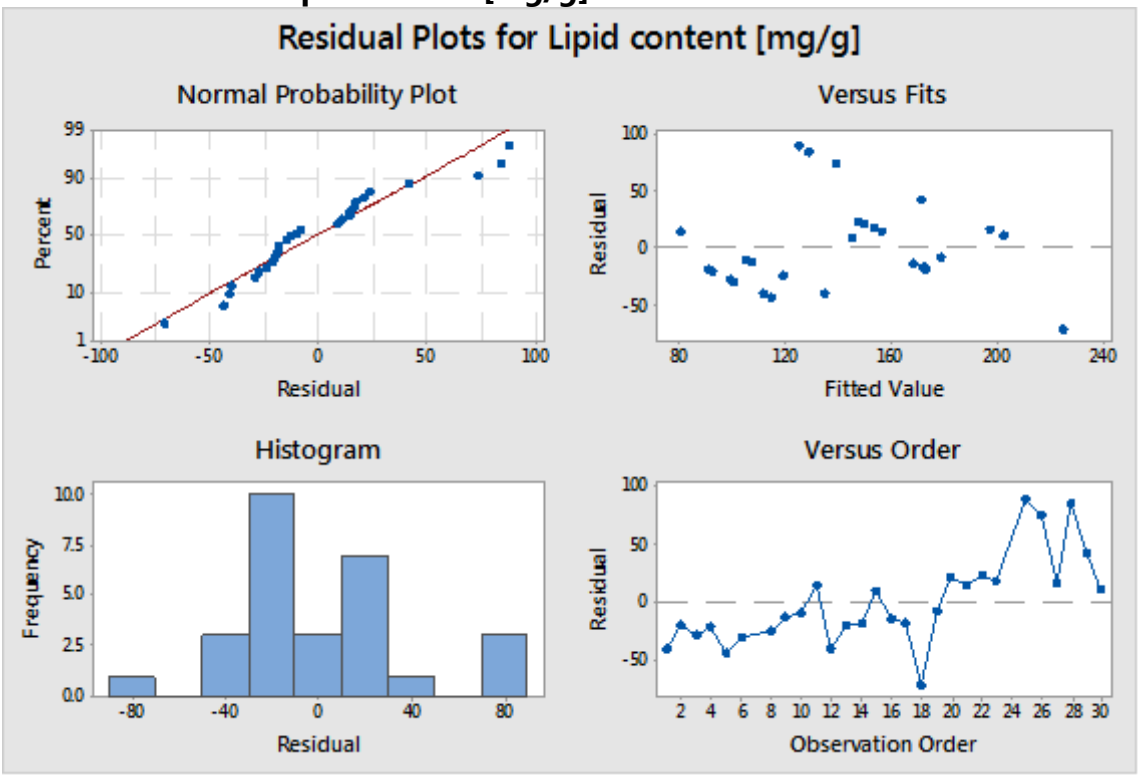

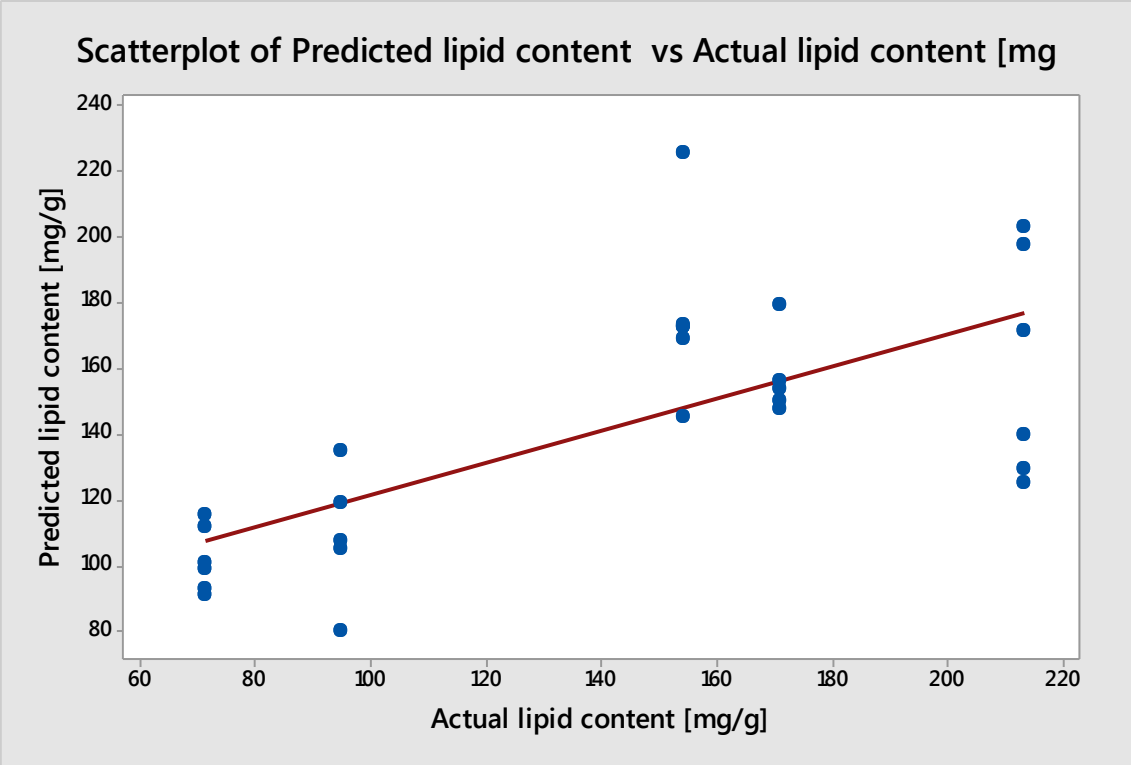

E-2. DESMID MICROALGAE

Best Subsets Regression: Lipid conten versus 2920 cm-1, 2855 cm-1,1742 cm-1

```
Response is Lipid content [mg/g]
29 cases used, 1 cases contain missing values

                                                2 2 1
                                                9 8 7
                                                2 5 4
                                                0 5 2

                                                c c c
                                                m m m
                 R-Sq     R-Sq  Mallows          - - -
Vars   R-Sq    (adj)    (pred)       Cp       S  1 1 1
   1   52.7     50.9     46.6      7.5  57.229  X
   1   49.6     47.7     43.3      9.6  59.076    X
   2   61.9     58.9     54.2      3.2  52.370  X X
   2   58.5     55.3     51.1      5.5  54.645  X   X
   3   63.6     59.3     51.5      4.0  52.158  X X X
```

Regression Analysis: Lipid content [mg/g] versus 2920 cm-1, 2855 cm-1

Method

Rows unused 1

Analysis of Variance

Source	DF	Adj SS	Adj MS	F-Value	P-Value
Regression	2	115633	57817	21.08	0.000
2920 cm-1	1	22923	22923	8.36	0.008
2855 cm-1	1	17121	17121	6.24	0.019
Error	26	71307	2743		
Total	28	186941			

Model Summary

S	R-sq	R-sq(adj)	R-sq(pred)
52.3697	61.86%	58.92%	54.16%

Coefficients

Term	Coef	SE Coef	T-Value	P-Value	VIF
Constant	59.0	20.9	2.82	0.009	
2920 cm-1	136.1	47.1	2.89	0.008	1.75
2855 cm-1	1033	414	2.50	0.019	1.75

Regression Equation

Lipid content [mg/g] = 59.0 + 136.1 2920 cm-1 + 1033 2855 cm-1

Residual Plots for Lipid content [mg/g]

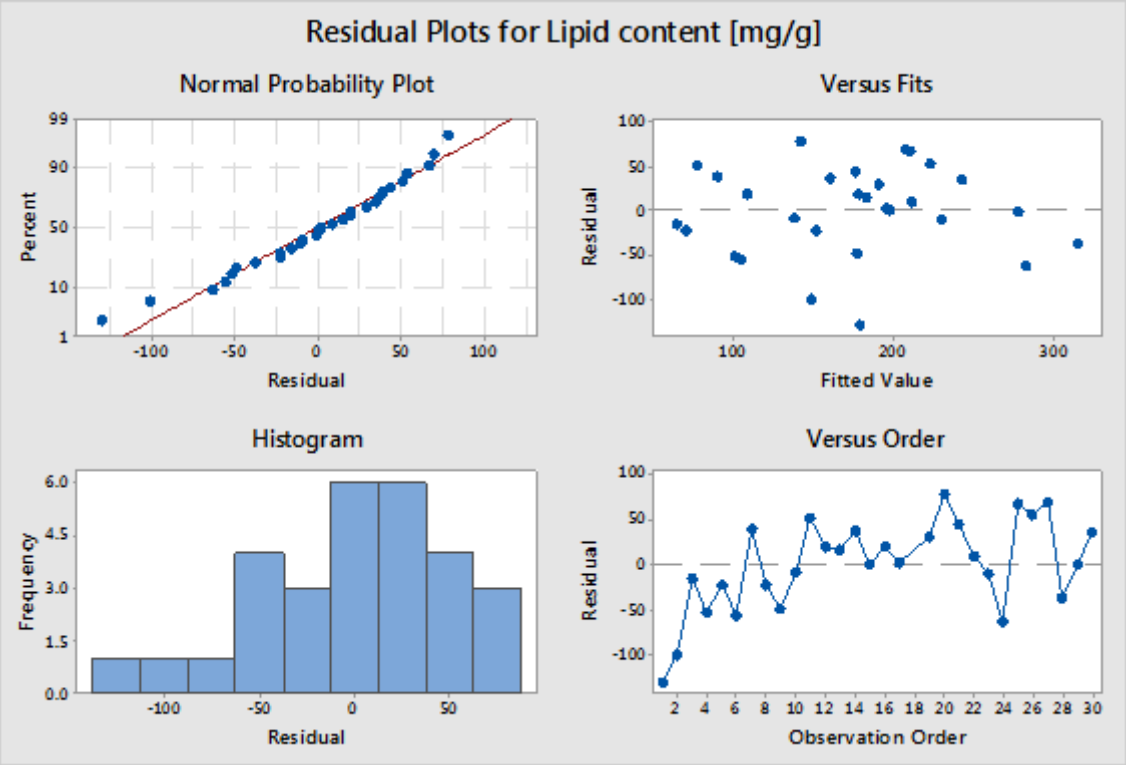
Residual Plots for Lipid content [mg/g]
Normal Probability Plot
Percent
Residual
Versus Fits
Residual
Fitted Value
Histogram
Frequency
Residual
Versus Order
Residual
Observation Order

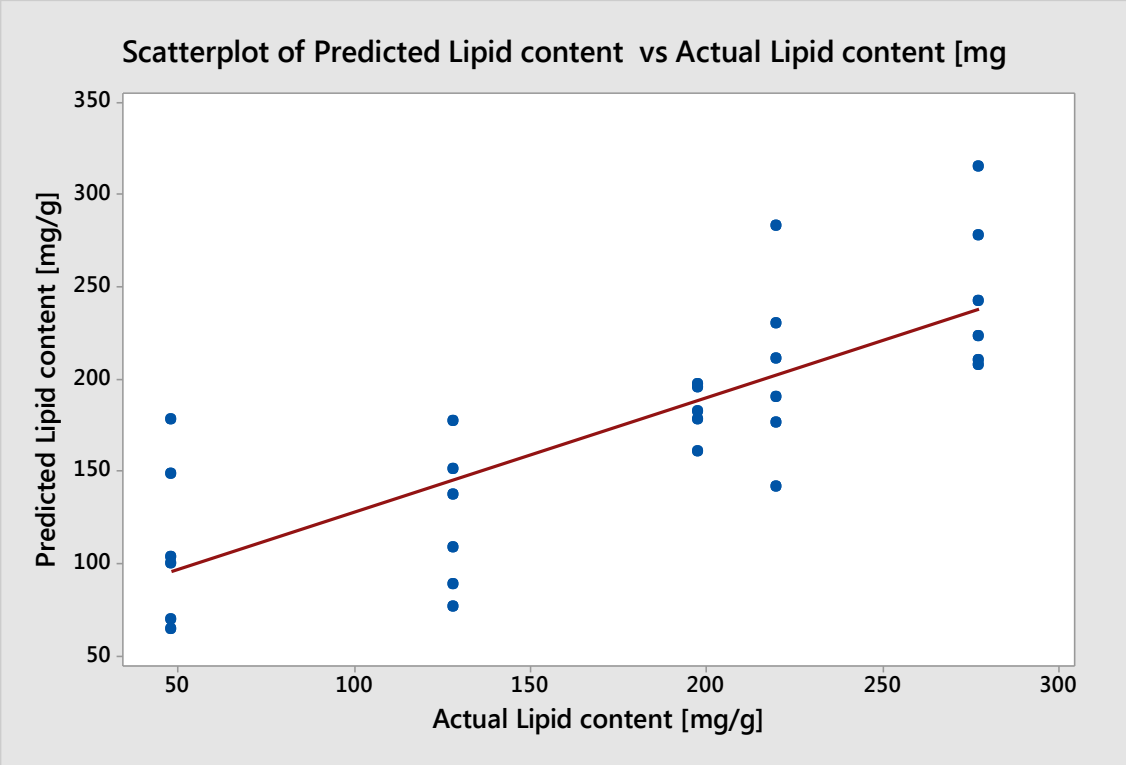
Scatterplot of Predicted Lipid content vs Actual Lipid content [mg
Predicted Lipid content [mg/g]
Actual Lipid content [mg/g]

E-3. MIXED SPECIES (GENERALIZED MODEL)

Best Subsets Regression: Lipid conten versus 2920 cm-1, 2855 cm-1, 1742 cm-1

```
Response is Lipid content [mg/g]
57 cases used, 3 cases contain missing values

                                                    2 2 1
                                                    9 8 7
                                                    2 5 4
                                                    0 5 2

                                                    c c c
                                                    m m m
             R-Sq              R-Sq  Mallows         - - -
Vars  R-Sq  (adj)     PRESS  (pred)       Cp       S 1 1 1
   1  21.6   20.2  229622.3    17.4      4.3  62.958     X
   1  21.5   20.1  233243.7    16.1      4.3  62.993 X
   2  27.1   24.4  217992.7    21.6      2.3  61.277 X   X
   2  27.0   24.3  218373.4    21.5      2.3  61.307   X X
   3  27.4   23.3  223949.2    19.5      4.0  61.705 X X X
```

Regression Analysis: Lipid content [mg/g] versus 2920 cm-1, 1742 cm-1

```
Method

Rows unused  2


Analysis of Variance

Source       DF  Seq SS  Contribution  Adj SS  Adj MS  F-Value  P-Value
Regression    2   77055        27.33%   77055   38527    10.34    0.000
  2920 cm-1   1   61454        21.80%   15766   15766     4.23    0.044
  1742 cm-1   1   15601         5.53%   15601   15601     4.19    0.046
Error        55  204900        72.67%  204900    3725
Total        57  281955       100.00%


Model Summary

      S    R-sq  R-sq(adj)   PRESS  R-sq(pred)
61.0365  27.33%     24.69%  220019      21.97%


Coefficients

Term        Coef  SE Coef      95% CI     T-Value  P-Value   VIF
Constant   106.1     16.0  (73.9, 138.2)     6.61    0.000
2920 cm-1   65.6     31.9  ( 1.7, 129.5)     2.06    0.044  1.54
1742 cm-1  122.1     59.7  ( 2.5, 241.6)     2.05    0.046  1.54


Regression Equation

Lipid content [mg/g] = 106.1 + 65.6 2920 cm-1 + 122.1 1742 cm-1
```

Residual Plots for Lipid content [mg/g]

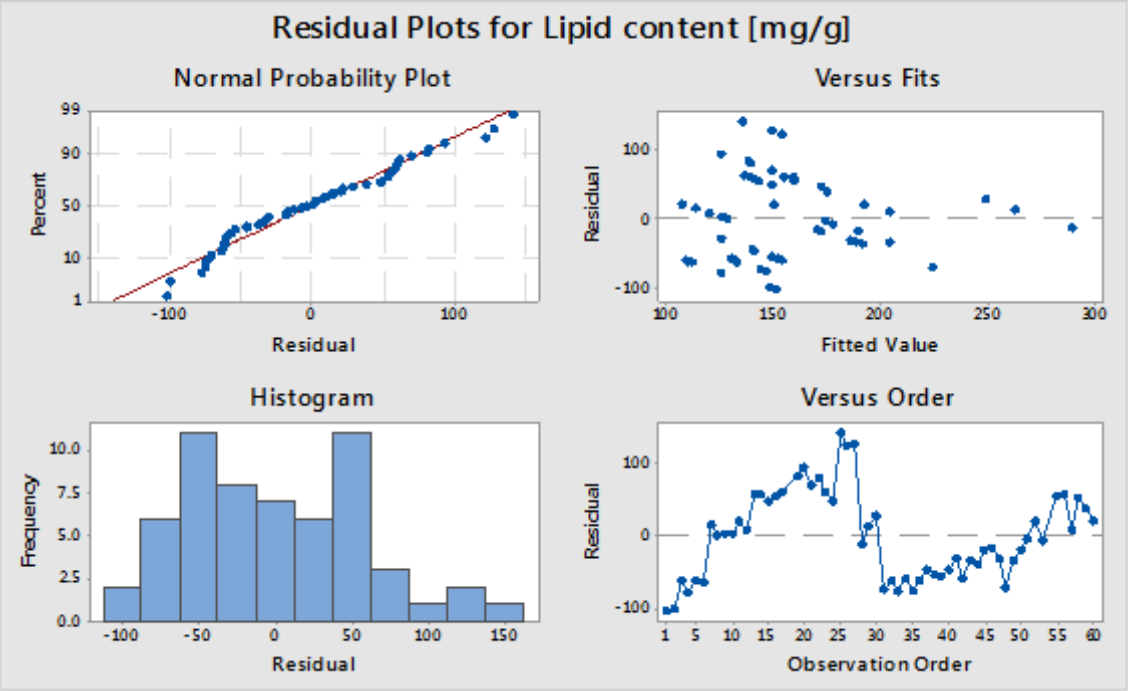

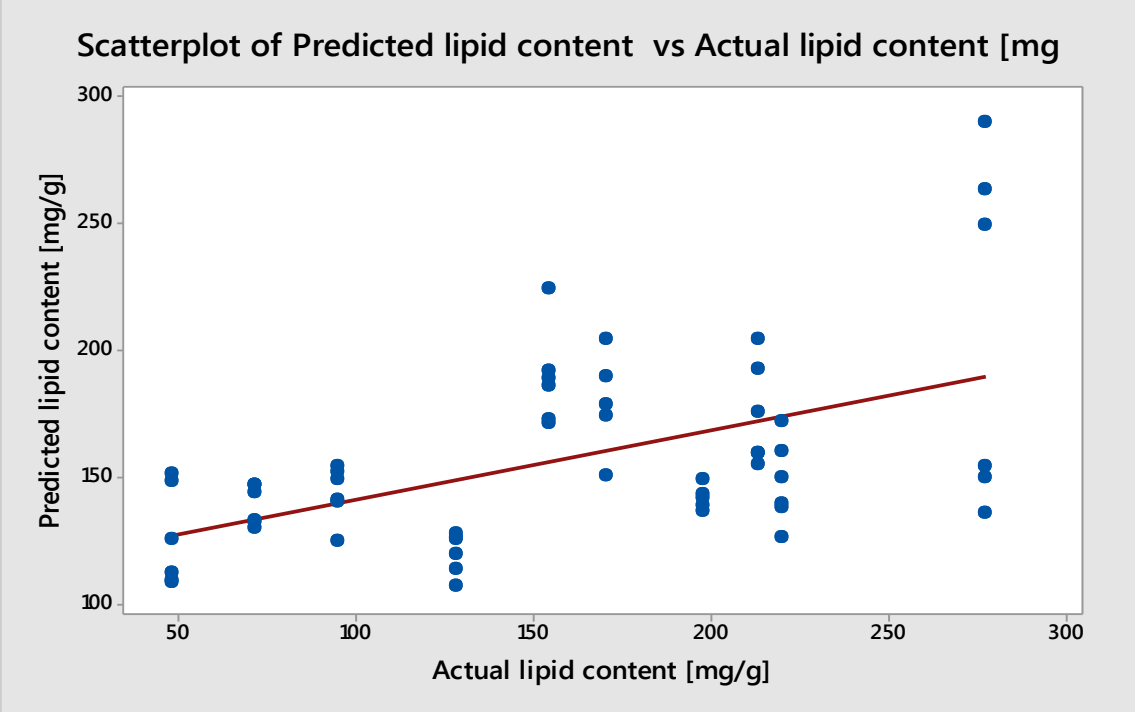

APPENDIX F

ACUIRED SPECTRA OF NANNOCHLORIS OCULATA AND DESMID USING THE NICOLET 6700 ATR-FTIR SPECTROMETER

F-1. NANNOCHLORIS OCULATA

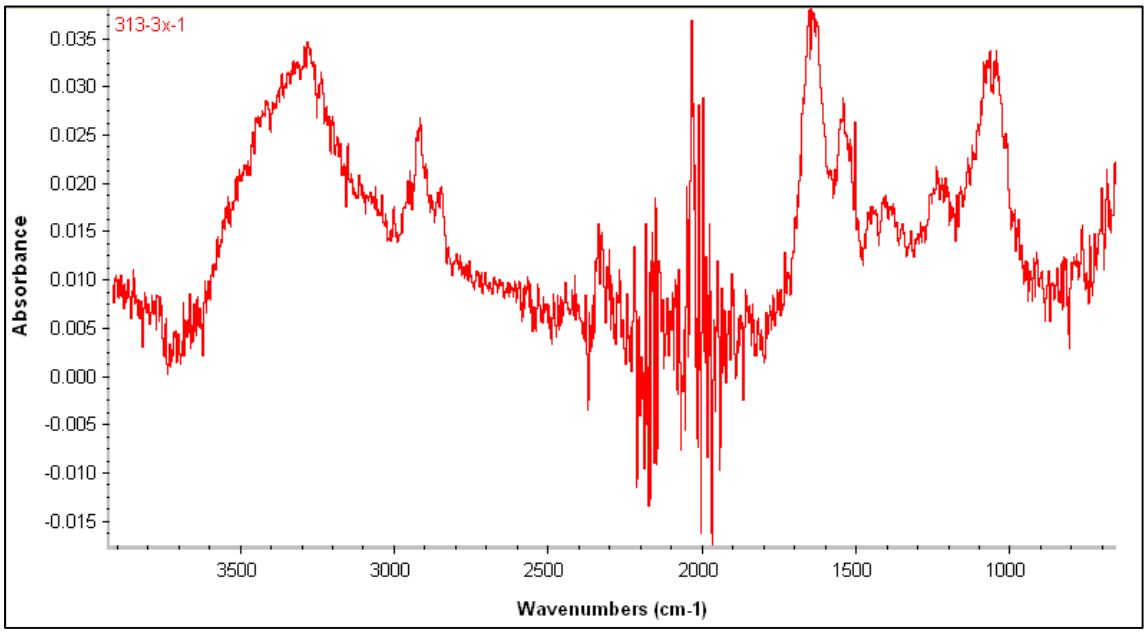

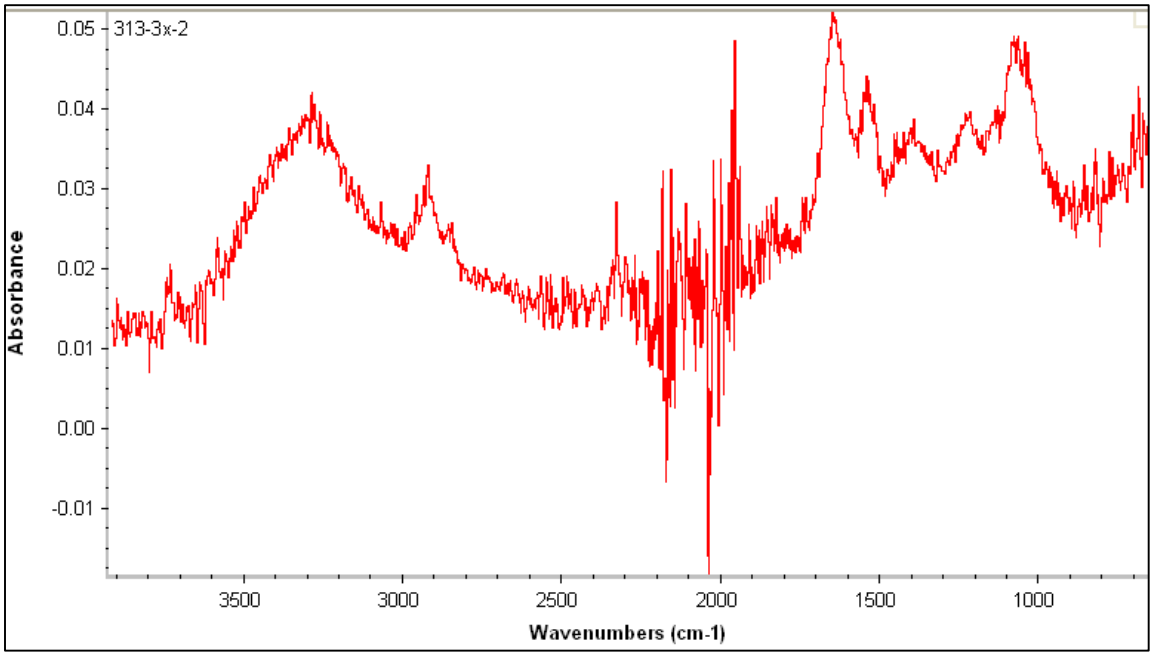
313-3x-2
0.05
0.04
0.03
0.02
0.01
0.00
-0.01
Absorbance
3500
3000
2500
2000
1500
1000
Wavenumbers (cm-1)

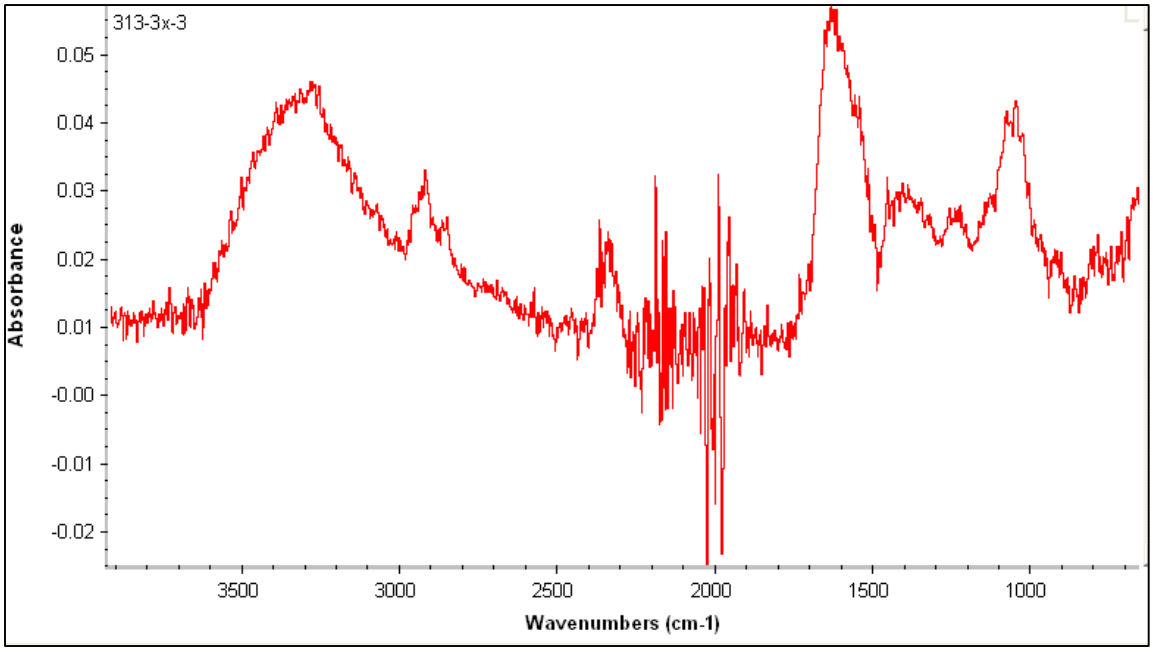
313-3x-3
0.05
0.04
0.03
0.02
0.01
-0.00
-0.01
-0.02
Absorbance
3500
3000
2500
2000
1500
1000
Wavenumbers (cm-1)

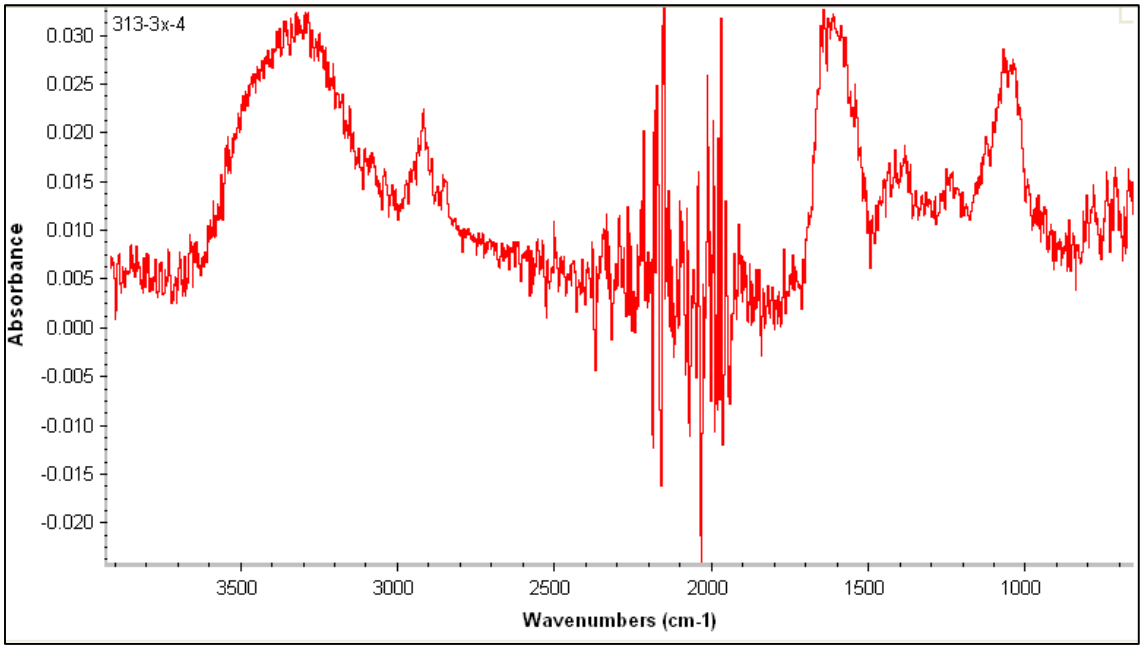
313-3x-4
0.030
0.025
0.020
0.015
0.010
0.005
0.000
-0.005
-0.010
-0.015
-0.020
Absorbance
3500
3000
2500
2000
1500
1000
Wavenumbers (cm-1)

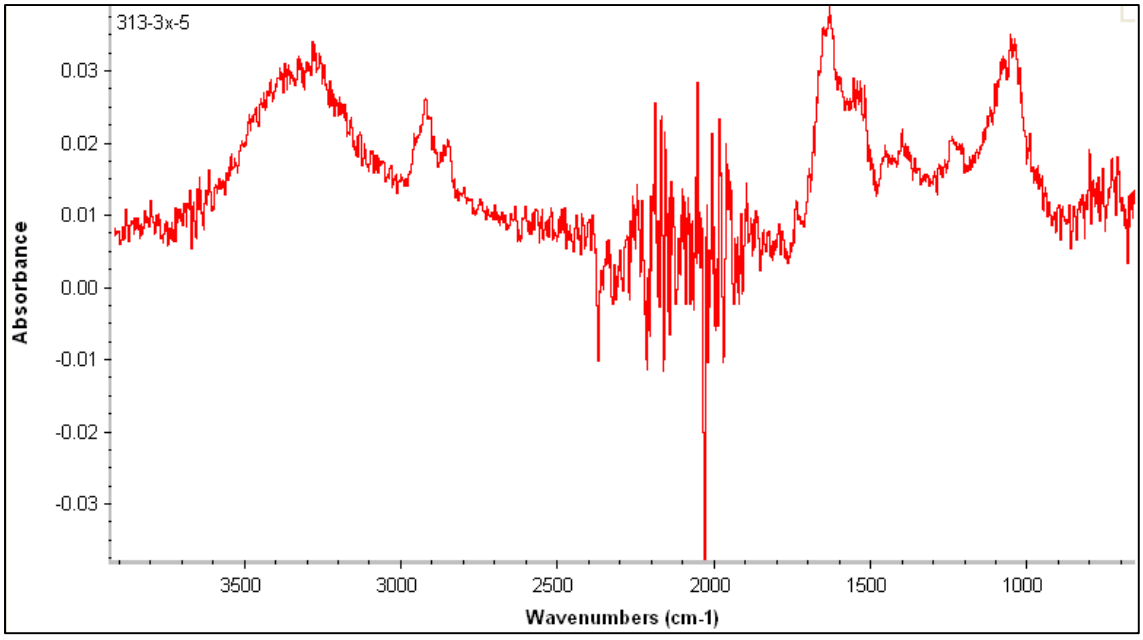
313-3x-5
0.03
0.02
0.01
0.00
-0.01
-0.02
-0.03
Absorbance
3500
3000
2500
2000
1500
1000
Wavenumbers (cm-1)

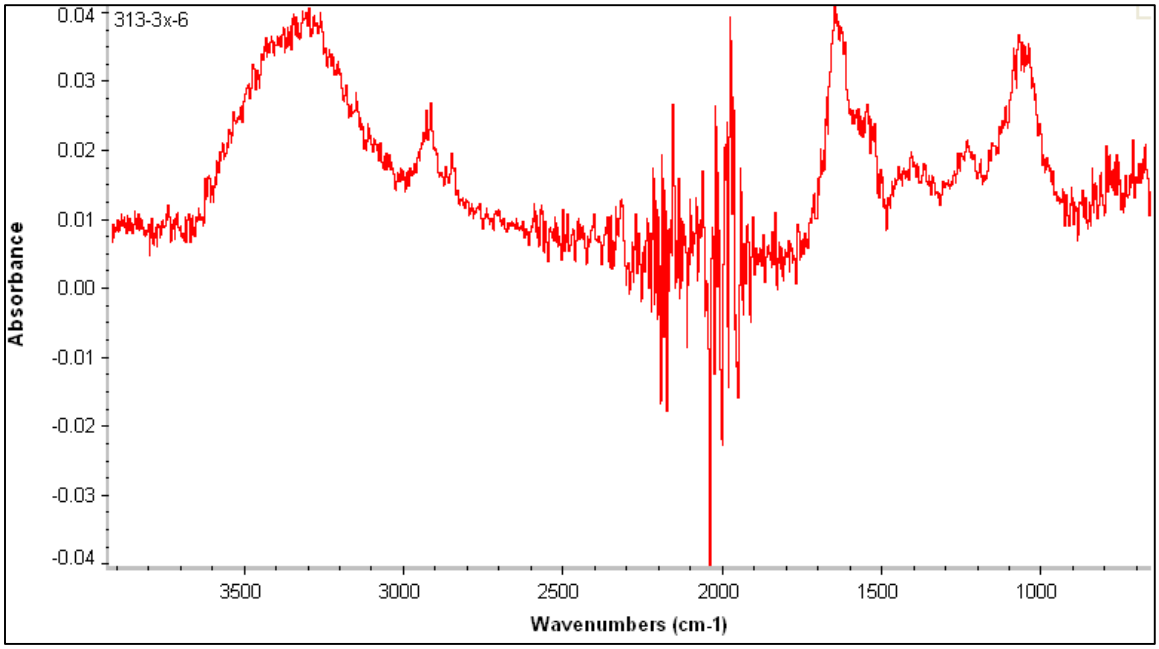
313-3x-6
0.04
0.03
0.02
0.01
0.00
-0.01
-0.02
-0.03
-0.04
Absorbance
3500
3000
2500
2000
1500
1000
Wavenumbers (cm-1)

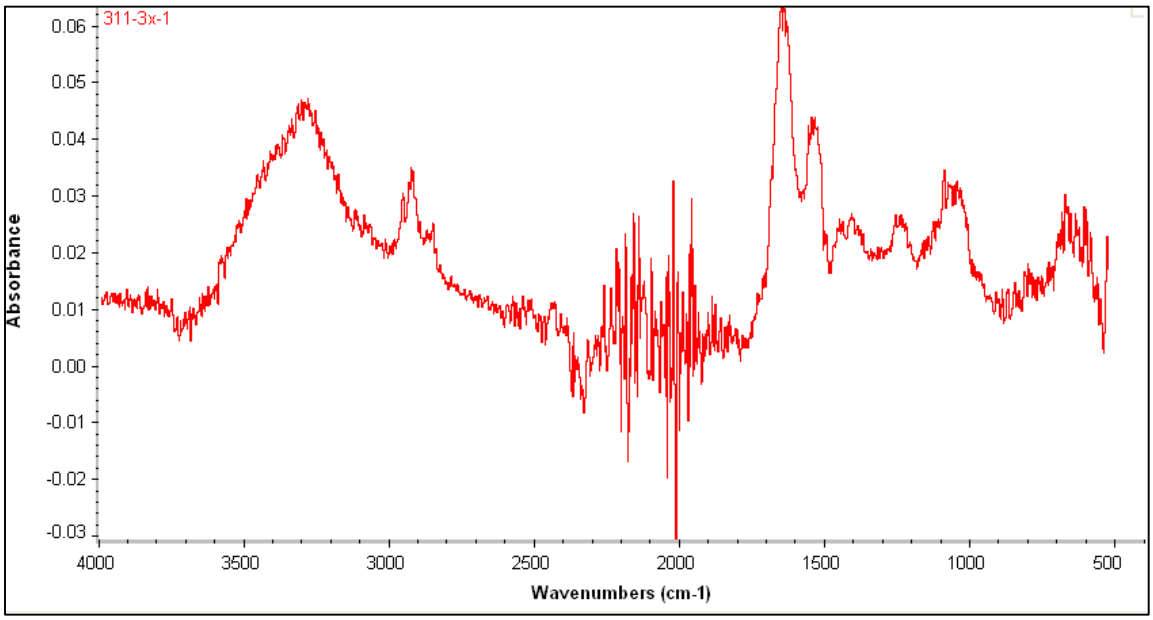
311-3x-1
0.06
0.05
0.04
0.03
0.02
0.01
0.00
-0.01
-0.02
-0.03
Absorbance
4000
3500
3000
2500
2000
1500
1000
500
Wavenumbers (cm-1)

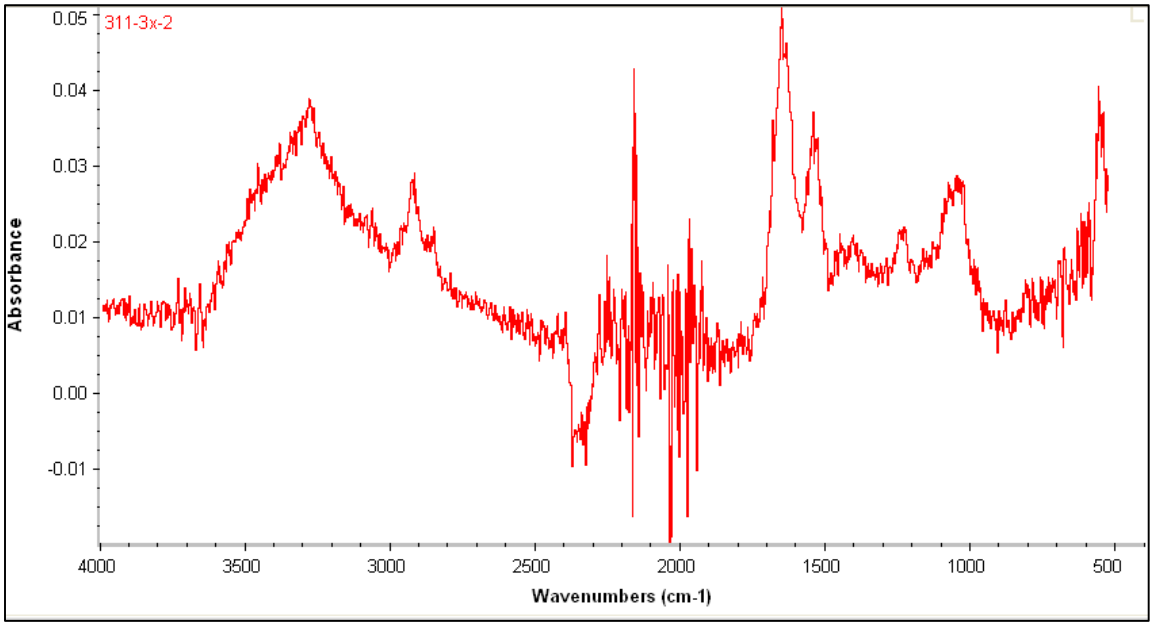
311-3x-2
0.05
0.04
0.03
0.02
0.01
0.00
-0.01
Absorbance
4000
3500
3000
2500
2000
1500
1000
500
Wavenumbers (cm-1)

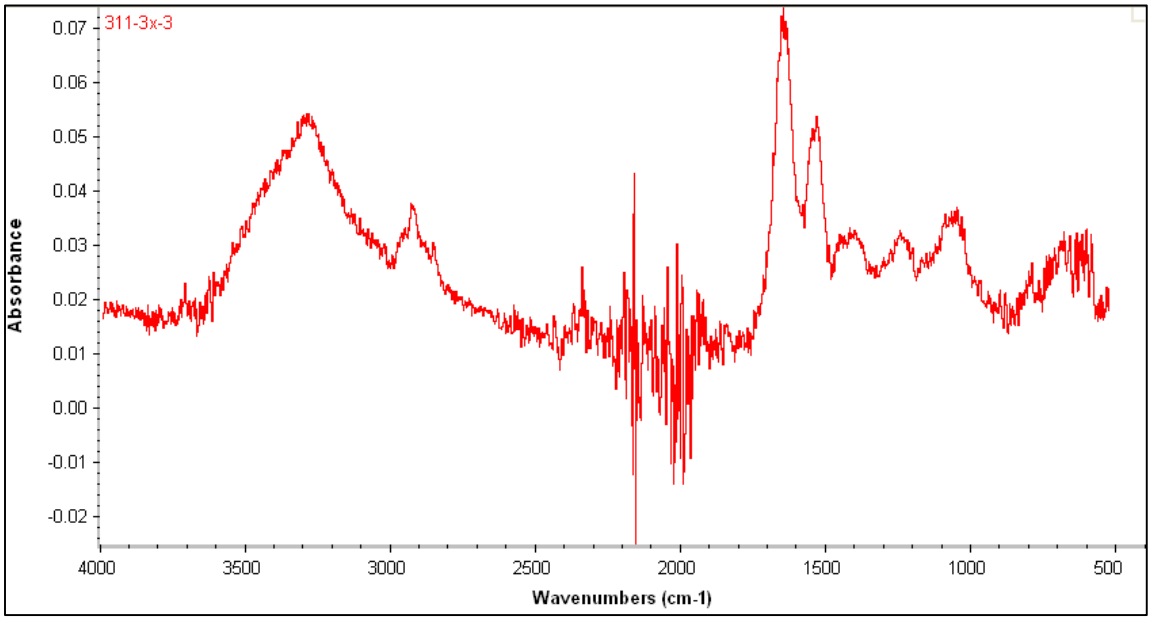
311-3x-3
0.07
0.06
0.05
0.04
0.03
0.02
0.01
0.00
-0.01
-0.02
Absorbance
4000
3500
3000
2500
2000
1500
1000
500
Wavenumbers (cm-1)

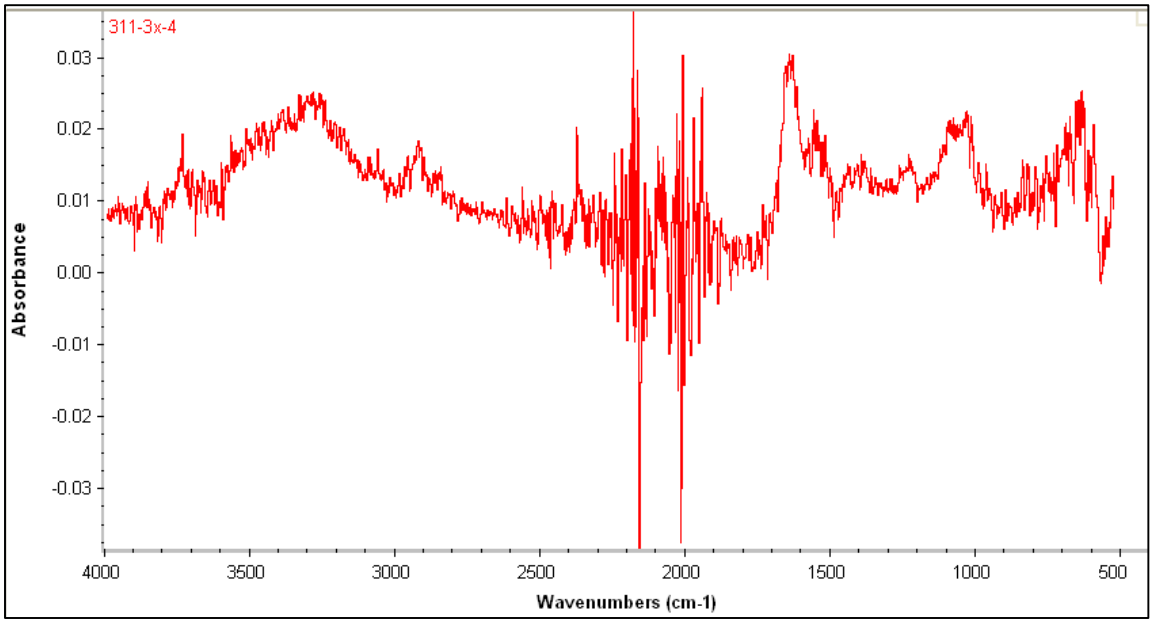
311-3x-4
0.03
0.02
0.01
0.00
-0.01
-0.02
-0.03
Absorbance
4000
3500
3000
2500
2000
1500
1000
500
Wavenumbers (cm-1)

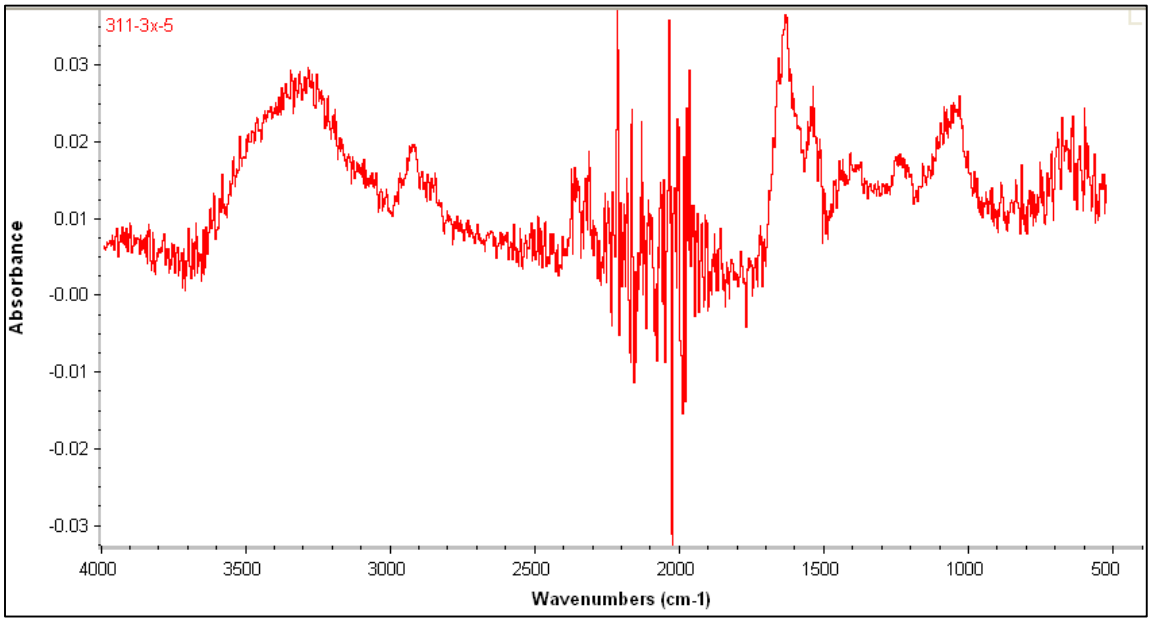
311-3x-5
0.03
0.02
0.01
-0.00
-0.01
-0.02
-0.03
Absorbance
4000
3500
3000
2500
2000
1500
1000
500
Wavenumbers (cm-1)

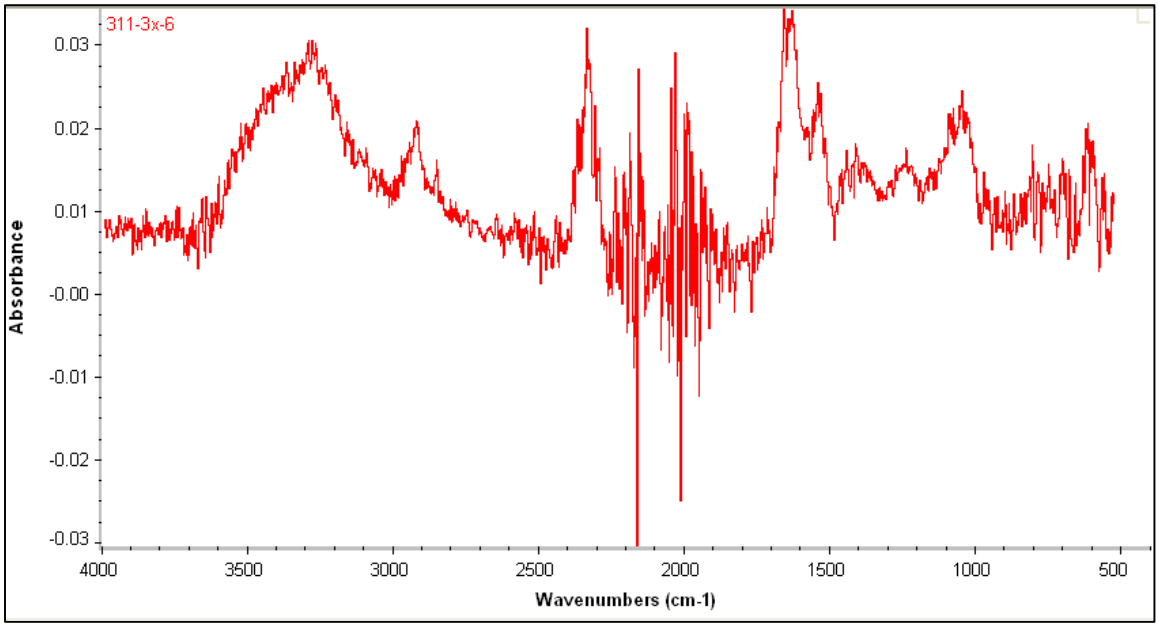
311-3x-6
0.03
0.02
0.01
-0.00
-0.01
-0.02
-0.03
Absorbance
4000
3500
3000
2500
2000
1500
1000
500
Wavenumbers (cm-1)

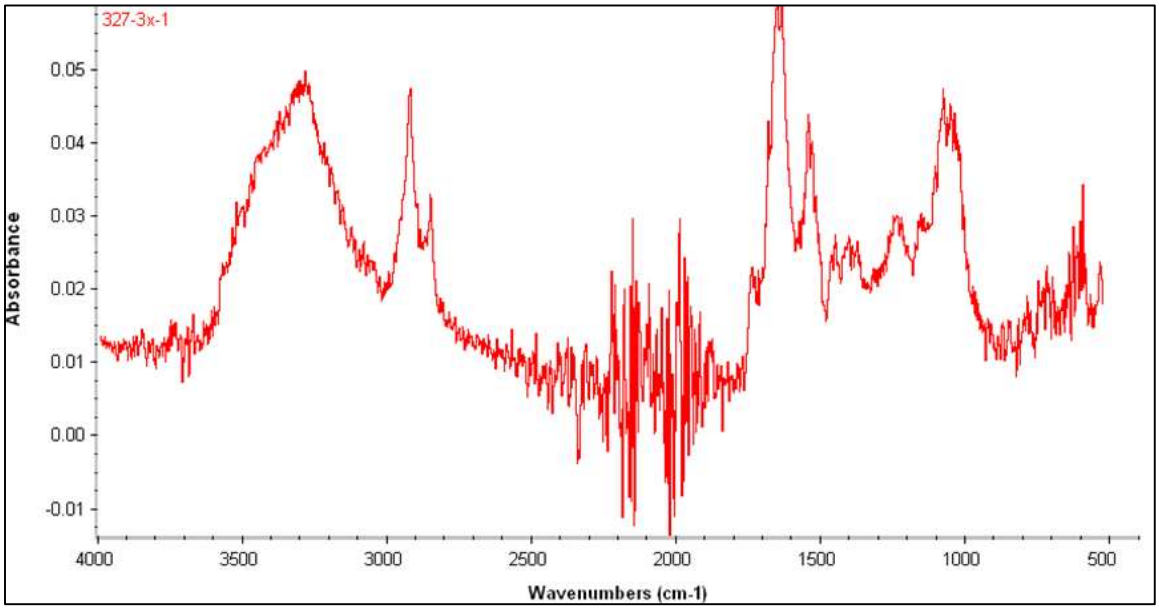
327-3x-1
0.05
0.04
0.03
0.02
0.01
0.00
-0.01
Absorbance
4000
3500
3000
2500
2000
1500
1000
500
Wavenumbers (cm-1)

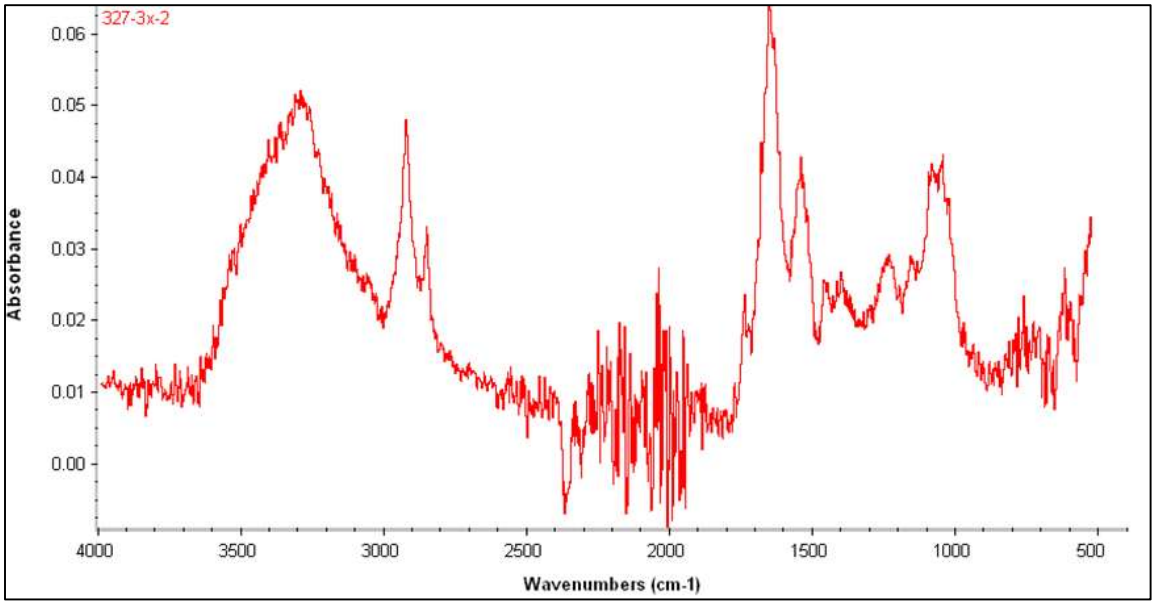
327-3x-2
Absorbance
0.06
0.05
0.04
0.03
0.02
0.01
0.00
4000
3500
3000
2500
2000
1500
1000
500
Wavenumbers (cm-1)

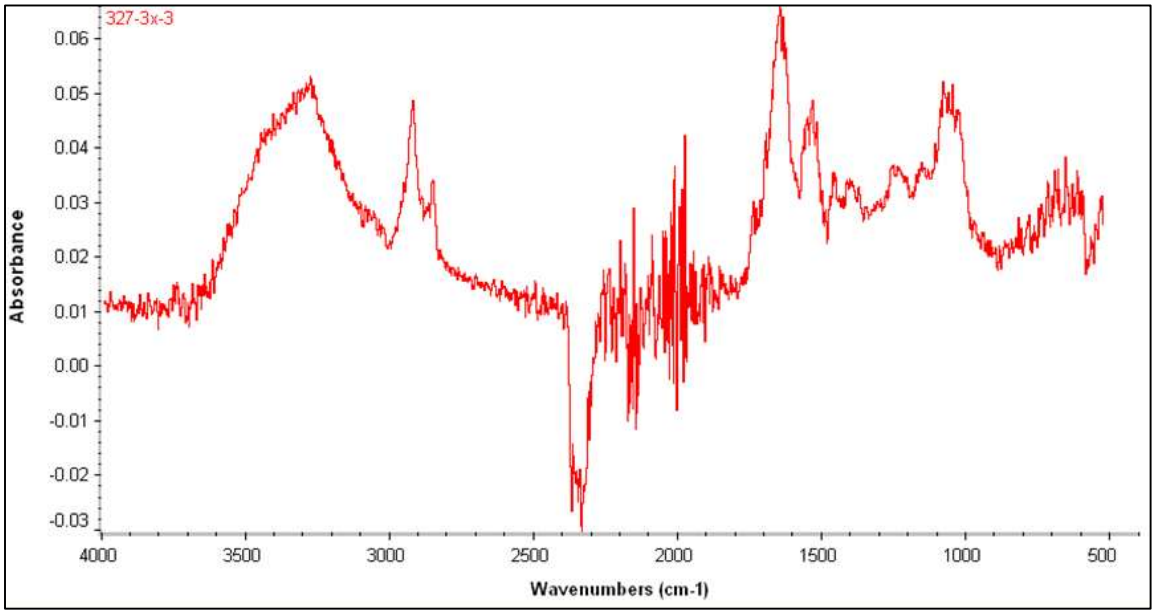
327-3x-3
Absorbance
0.06
0.05
0.04
0.03
0.02
0.01
0.00
-0.01
-0.02
-0.03
4000
3500
3000
2500
2000
1500
1000
500
Wavenumbers (cm-1)

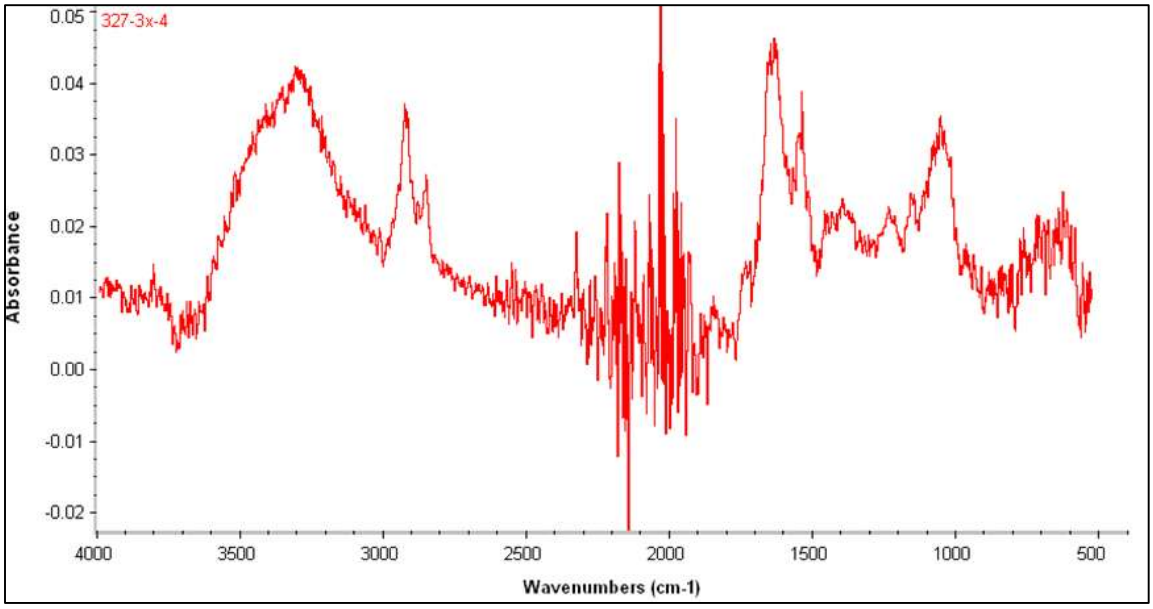
327-3x-4
Absorbance
0.05
0.04
0.03
0.02
0.01
0.00
-0.01
-0.02
4000
3500
3000
2500
2000
1500
1000
500
Wavenumbers (cm-1)

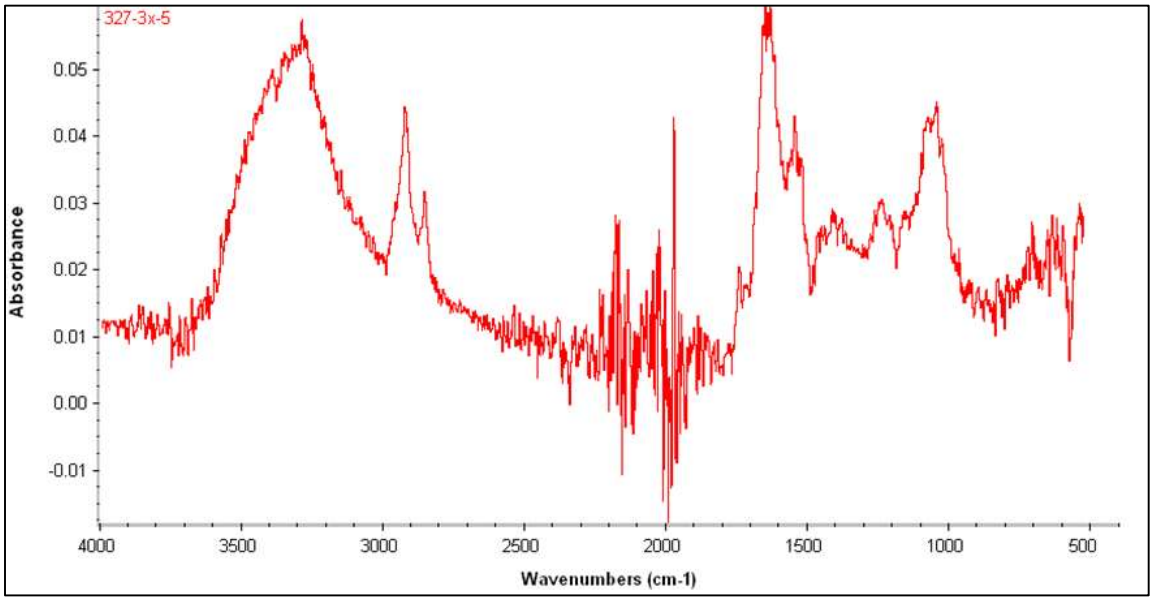
327-3x-5
Absorbance
0.05
0.04
0.03
0.02
0.01
0.00
-0.01
4000
3500
3000
2500
2000
1500
1000
500
Wavenumbers (cm-1)

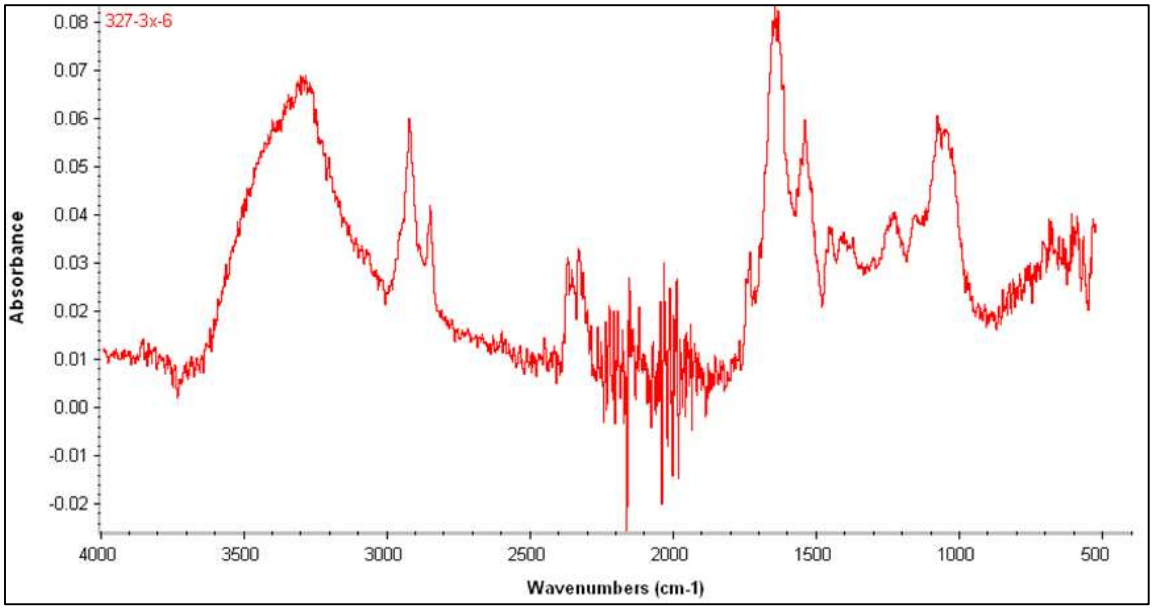
327-3x-6
Absorbance
0.08
0.07
0.06
0.05
0.04
0.03
0.02
0.01
0.00
-0.01
-0.02
4000
3500
3000
2500
2000
1500
1000
500
Wavenumbers (cm-1)

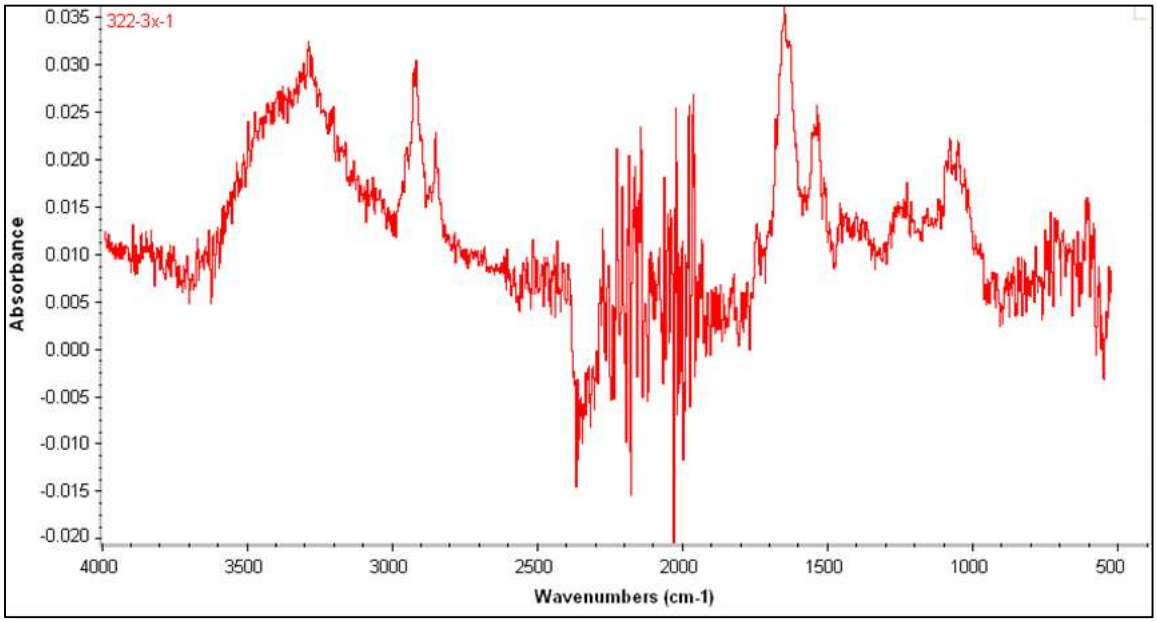
322-3x-1
Absorbance
0.035
0.030
0.025
0.020
0.015
0.010
0.005
0.000
-0.005
-0.010
-0.015
-0.020
4000
3500
3000
2500
2000
1500
1000
500
Wavenumbers (cm-1)

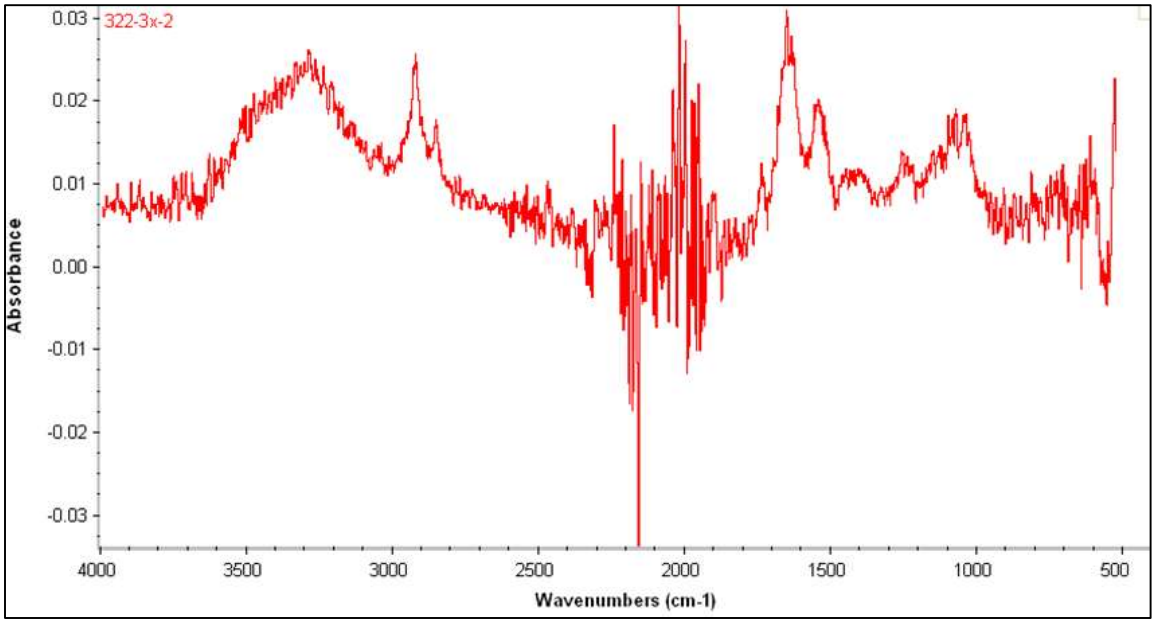
322-3x-2
0.03
0.02
0.01
0.00
-0.01
-0.02
-0.03
Absorbance
4000
3500
3000
2500
2000
1500
1000
500
Wavenumbers (cm-1)

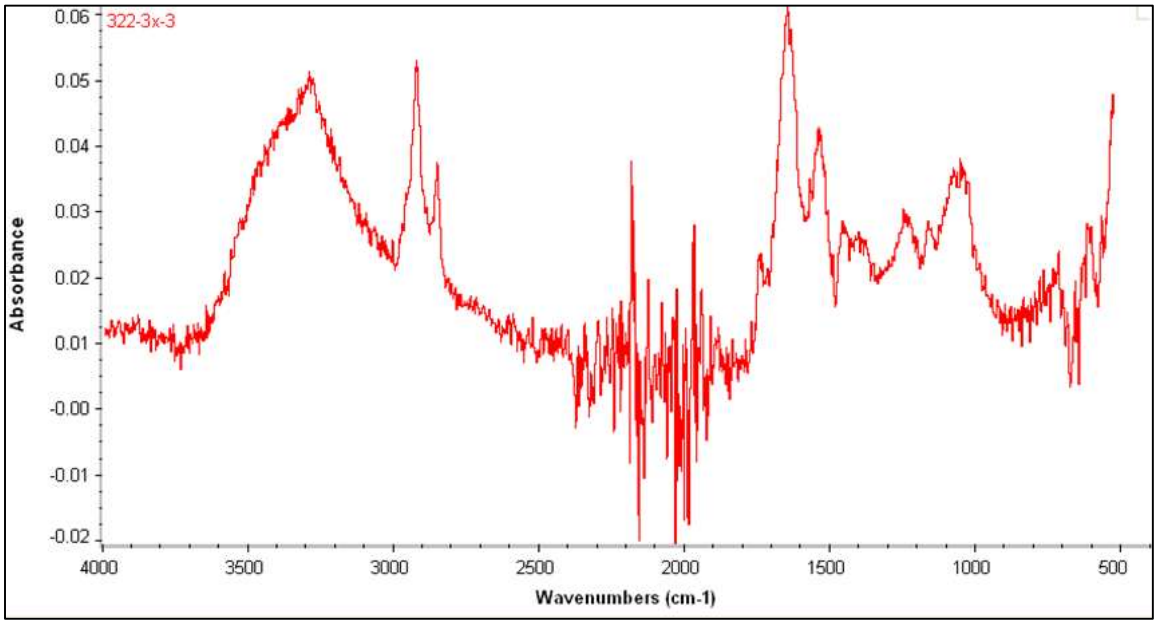
322-3x-3
0.06
0.05
0.04
0.03
0.02
0.01
-0.00
-0.01
-0.02
Absorbance
4000
3500
3000
2500
2000
1500
1000
500
Wavenumbers (cm-1)

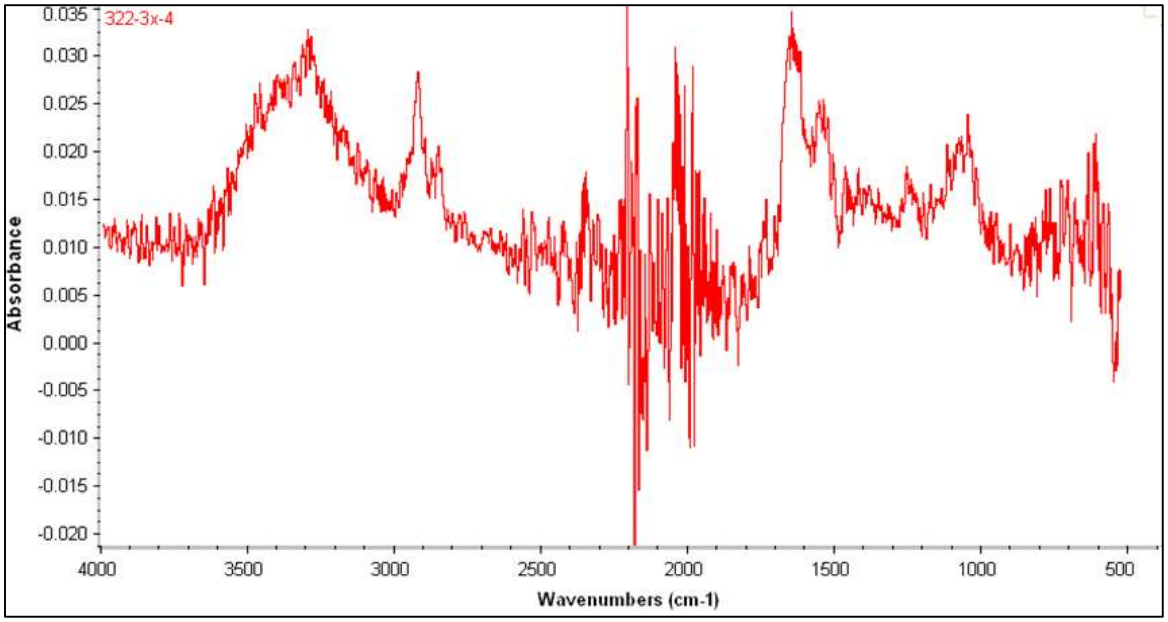
322-3x-4
Absorbance
0.035
0.030
0.025
0.020
0.015
0.010
0.005
0.000
-0.005
-0.010
-0.015
-0.020
4000
3500
3000
2500
2000
1500
1000
500
Wavenumbers (cm-1)

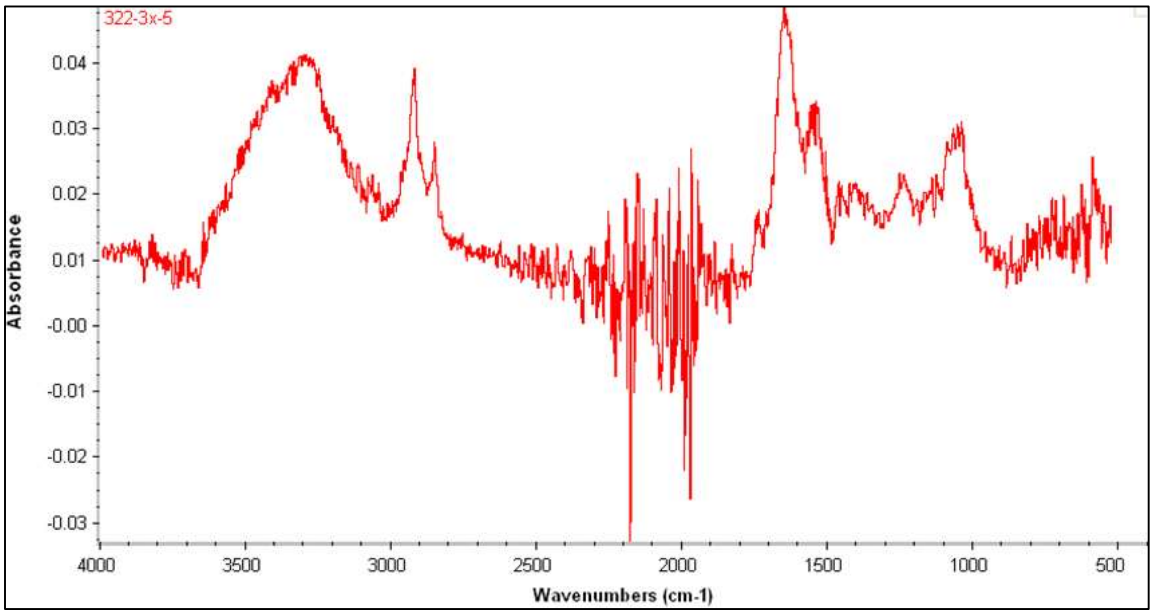
322-3x-5
Absorbance
0.04
0.03
0.02
0.01
-0.00
-0.01
-0.02
-0.03
4000
3500
3000
2500
2000
1500
1000
500
Wavenumbers (cm-1)

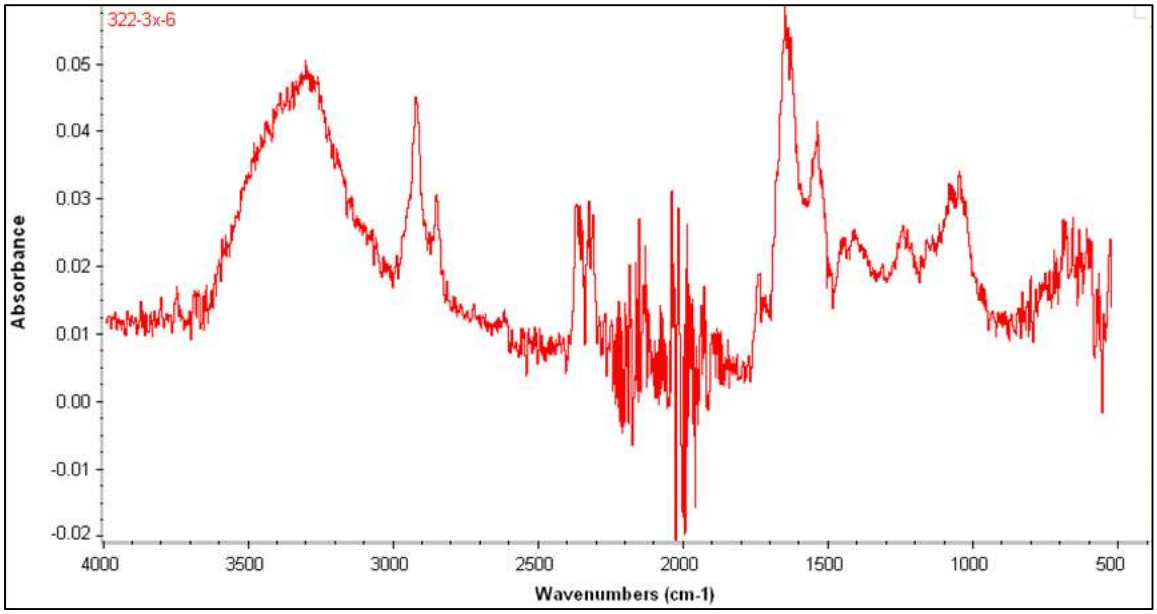
322-3x-6
Absorbance
0.05
0.04
0.03
0.02
0.01
0.00
-0.01
-0.02
4000
3500
3000
2500
2000
1500
1000
500
Wavenumbers (cm-1)

F-2. DESMID

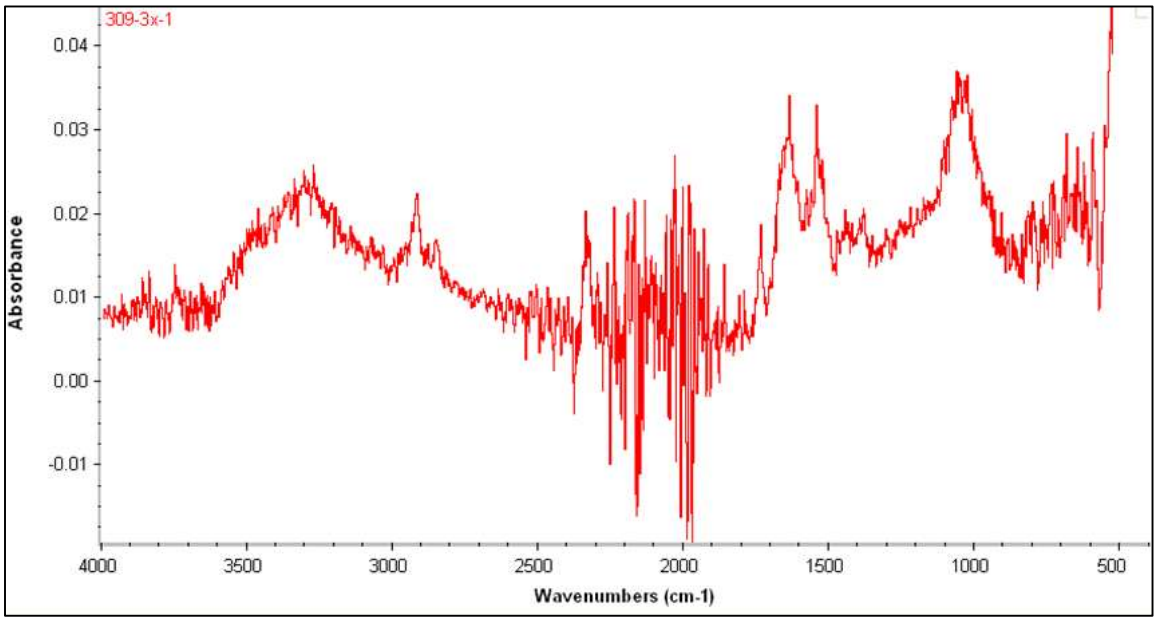
309-3x-1
Absorbance
0.04
0.03
0.02
0.01
0.00
-0.01
4000
3500
3000
2500
2000
1500
1000
500
Wavenumbers (cm-1)

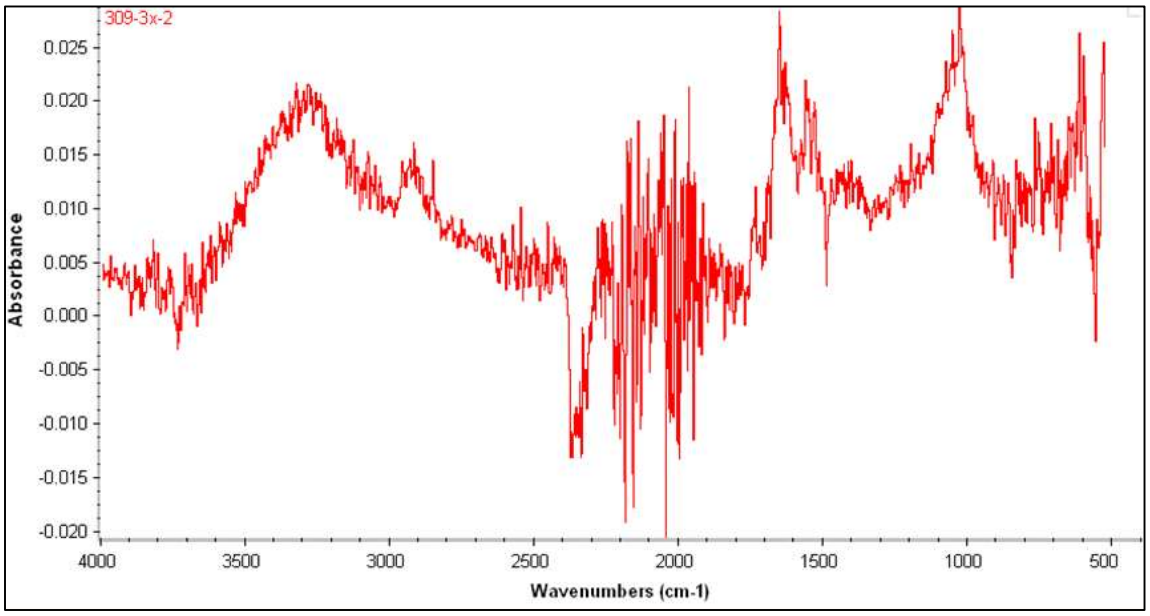
309-3x-2
Absorbance
0.025
0.020
0.015
0.010
0.005
0.000
-0.005
-0.010
-0.015
-0.020
4000
3500
3000
2500
2000
1500
1000
500
Wavenumbers (cm-1)

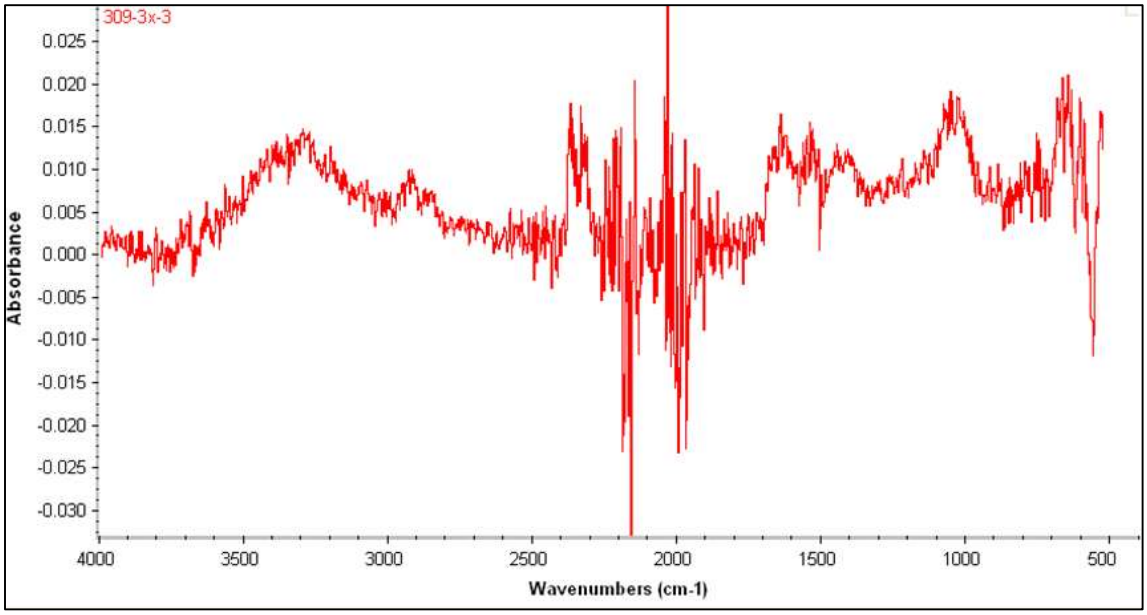
309-3x-3
Absorbance
0.025
0.020
0.015
0.010
0.005
0.000
-0.005
-0.010
-0.015
-0.020
-0.025
-0.030
4000
3500
3000
2500
2000
1500
1000
500
Wavenumbers (cm-1)

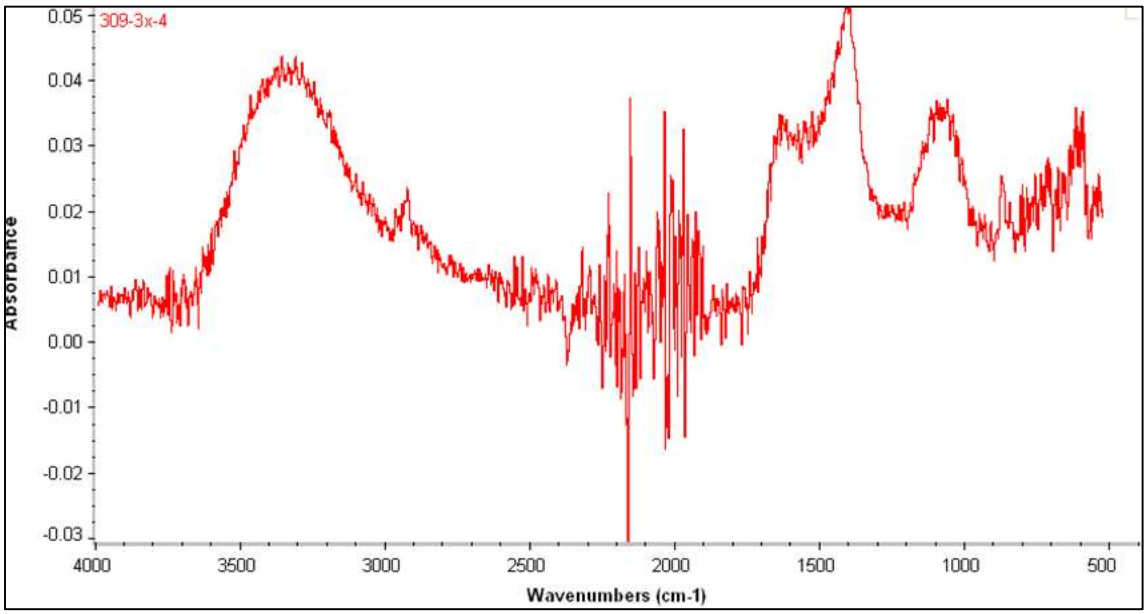
309-3x-4
Absorbance
0.05
0.04
0.03
0.02
0.01
0.00
-0.01
-0.02
-0.03
4000
3500
3000
2500
2000
1500
1000
500
Wavenumbers (cm-1)

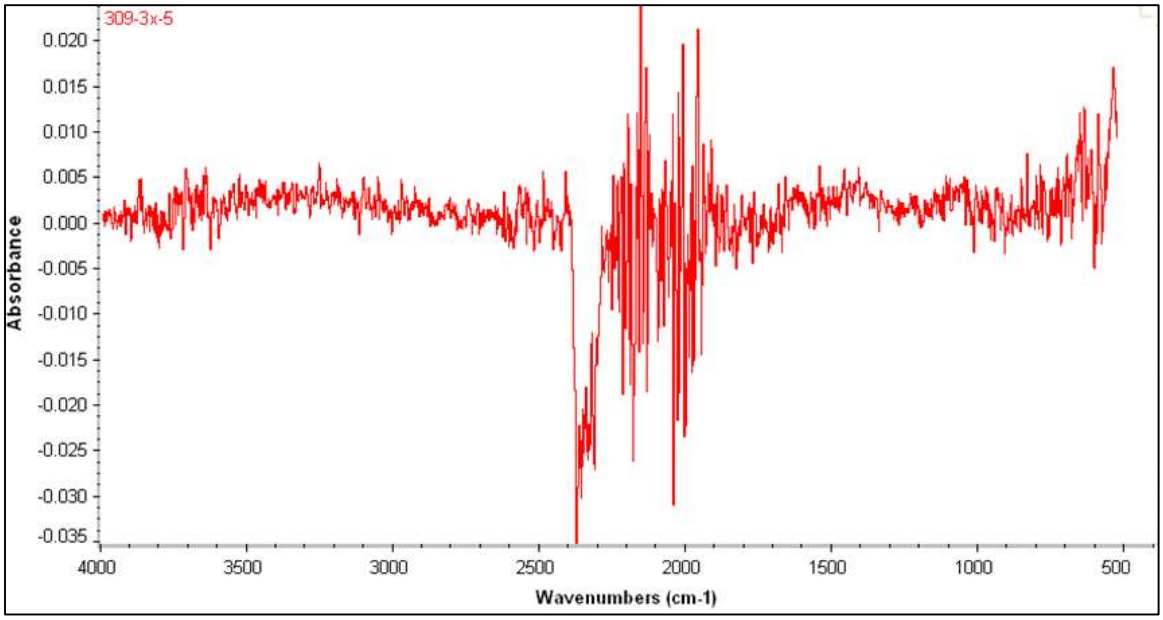
309-3x-5
Absorbance
0.020
0.015
0.010
0.005
0.000
-0.005
-0.010
-0.015
-0.020
-0.025
-0.030
-0.035
4000
3500
3000
2500
2000
1500
1000
500
Wavenumbers (cm-1)

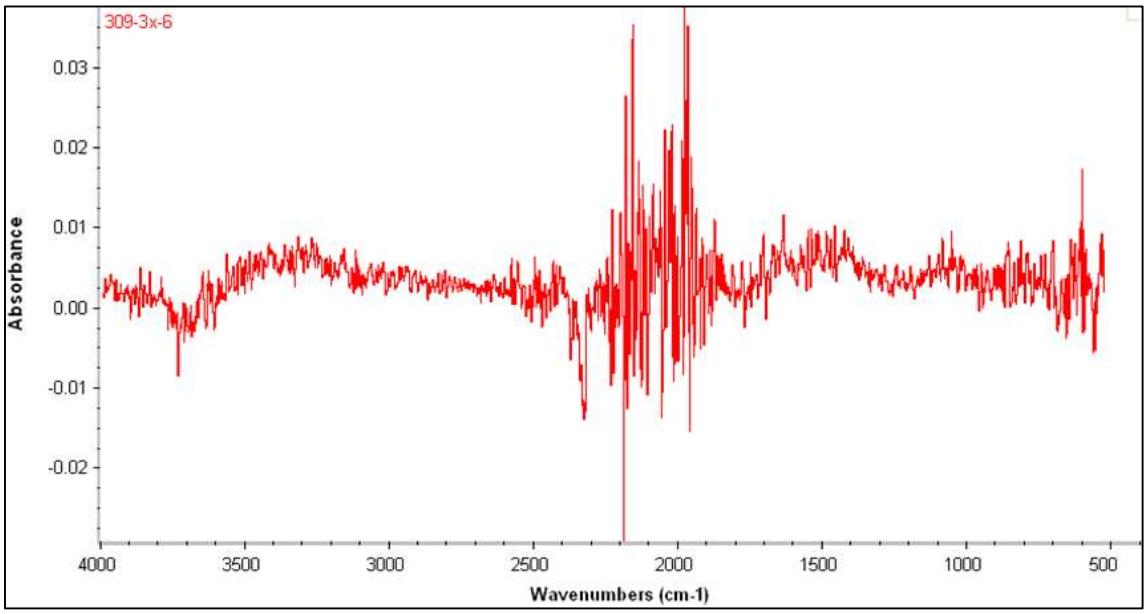
309-3x-6
Absorbance
0.03
0.02
0.01
0.00
-0.01
-0.02
4000
3500
3000
2500
2000
1500
1000
500
Wavenumbers (cm-1)

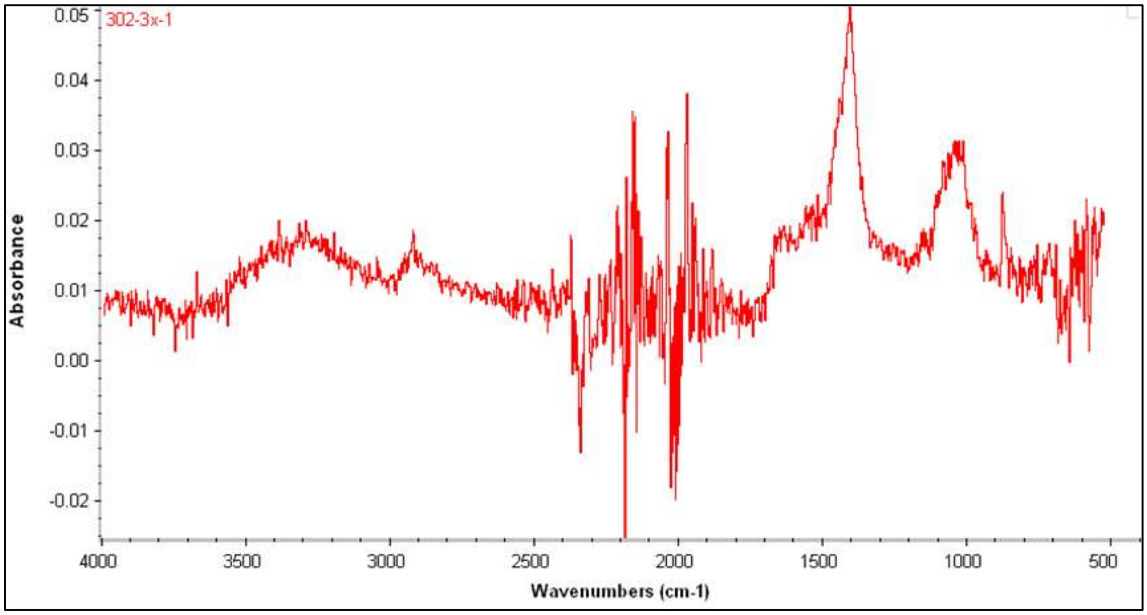
302-3x-1
Absorbance
0.05
0.04
0.03
0.02
0.01
0.00
-0.01
-0.02
4000
3500
3000
2500
2000
1500
1000
500
Wavenumbers (cm-1)

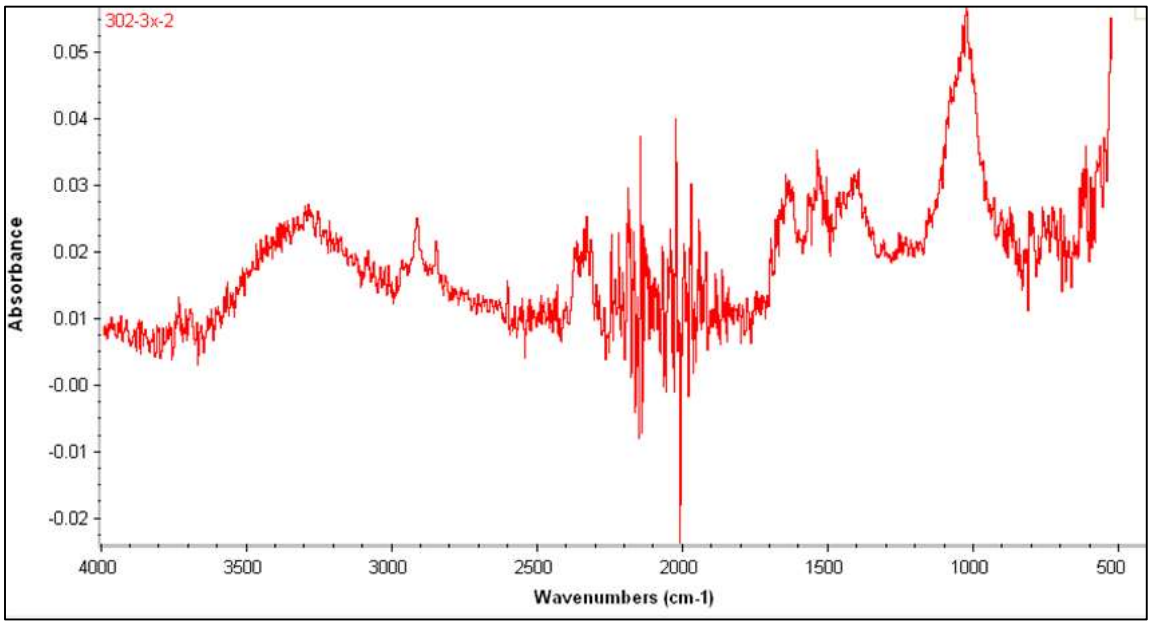
302-3x-2
Absorbance
0.05
0.04
0.03
0.02
0.01
-0.00
-0.01
-0.02
4000
3500
3000
2500
2000
1500
1000
500
Wavenumbers (cm-1)

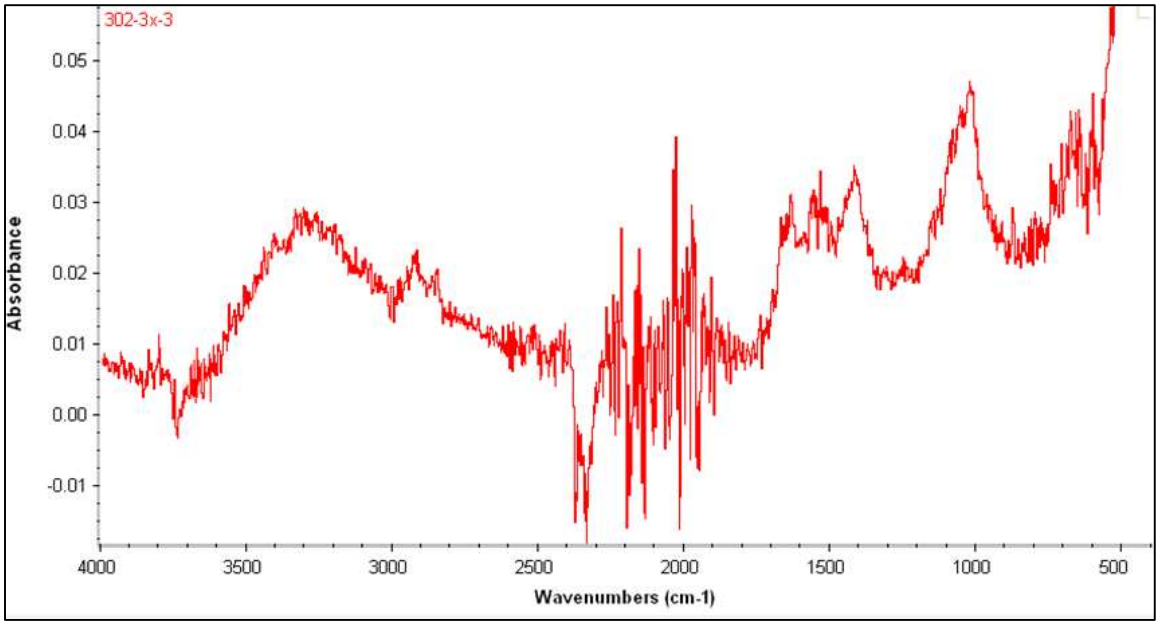
302-3x-3
0.05
0.04
0.03
0.02
0.01
0.00
-0.01
Absorbance
4000
3500
3000
2500
2000
1500
1000
500
Wavenumbers (cm-1)

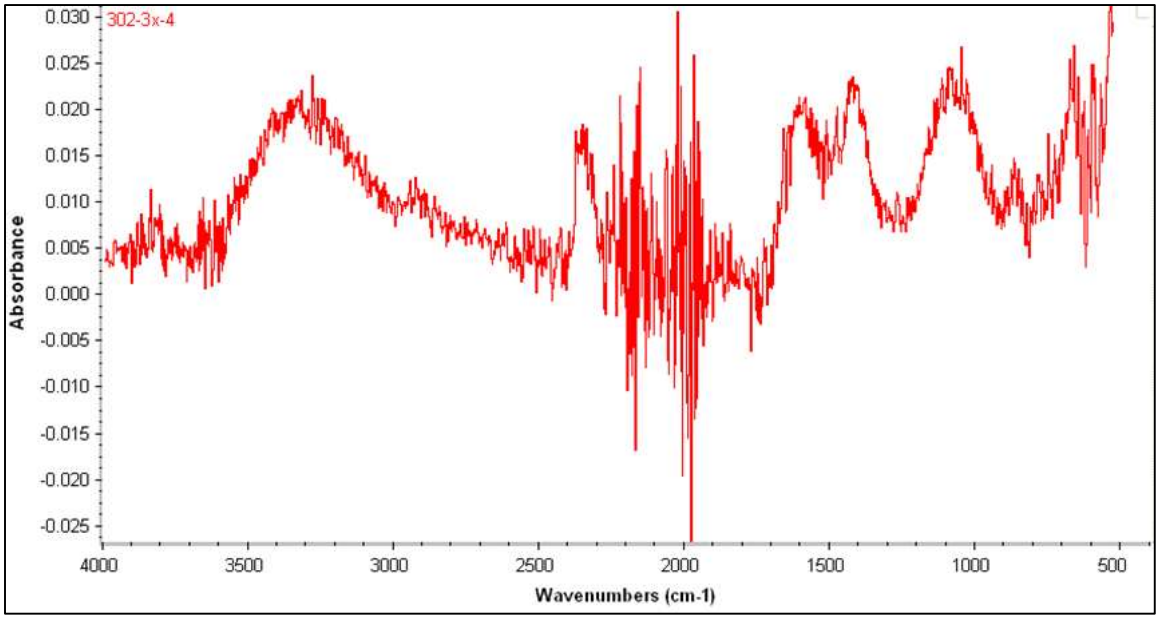
302-3x-4
0.030
0.025
0.020
0.015
0.010
0.005
0.000
-0.005
-0.010
-0.015
-0.020
-0.025
Absorbance
4000
3500
3000
2500
2000
1500
1000
500
Wavenumbers (cm-1)

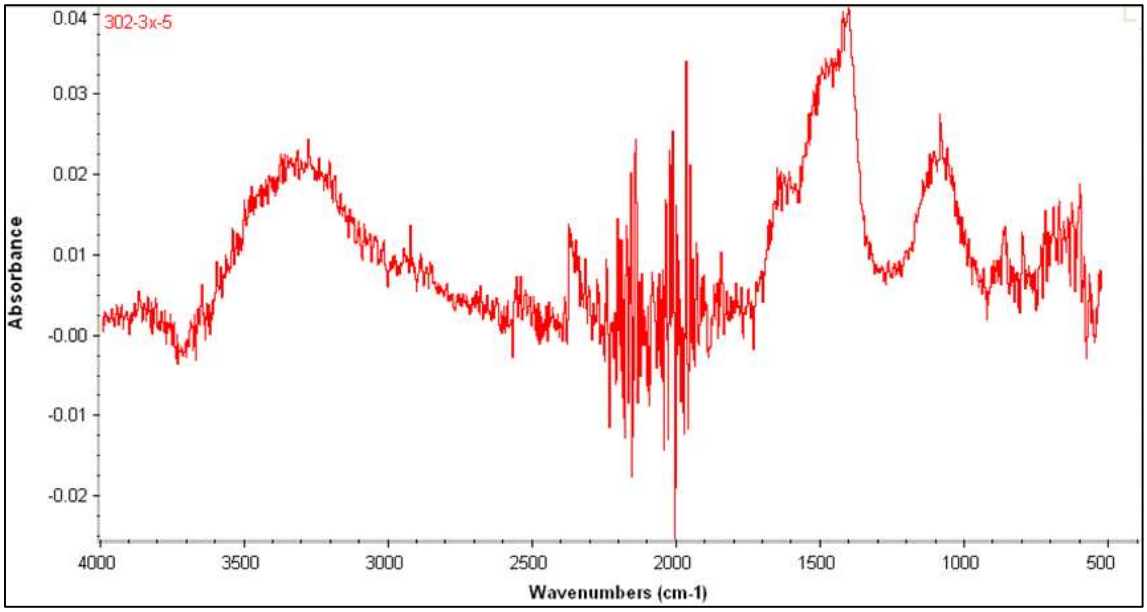
302-3x-5
Absorbance
0.04
0.03
0.02
0.01
-0.00
-0.01
-0.02
4000
3500
3000
2500
2000
1500
1000
500
Wavenumbers (cm-1)

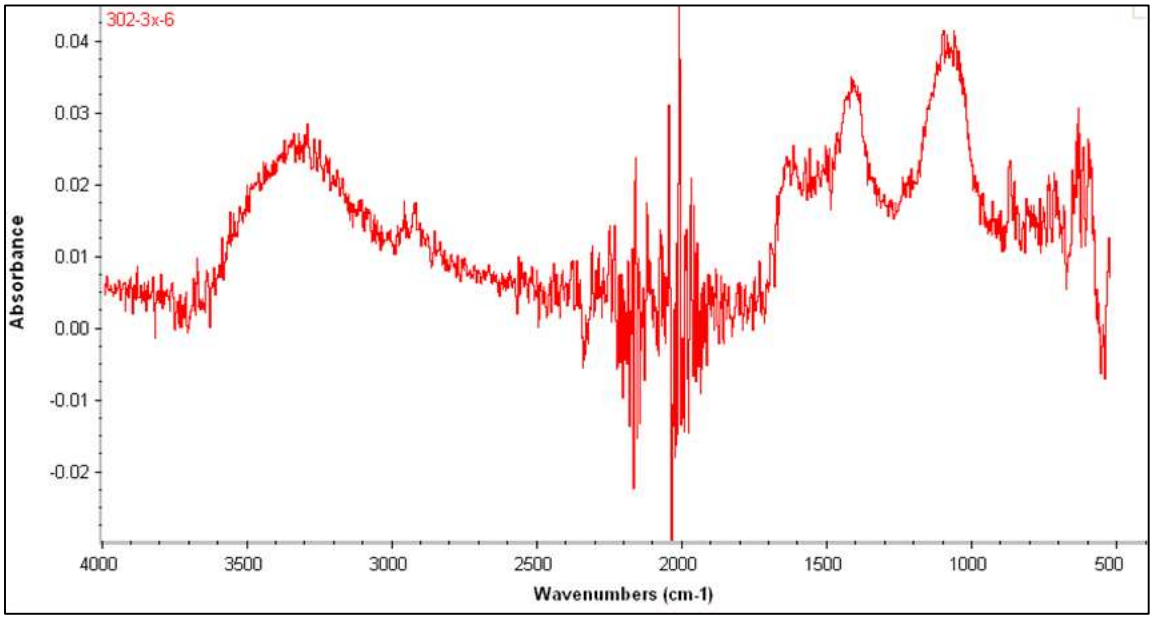
302-3x-6
Absorbance
0.04
0.03
0.02
0.01
0.00
-0.01
-0.02
4000
3500
3000
2500
2000
1500
1000
500
Wavenumbers (cm-1)

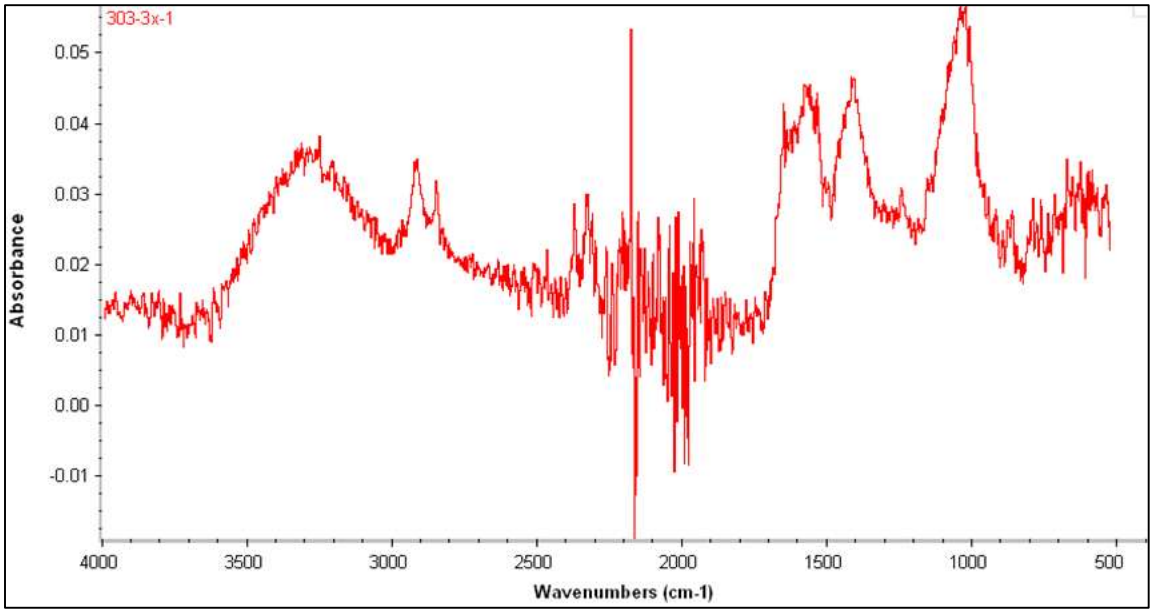
303-3x-1
Absorbance
0.05
0.04
0.03
0.02
0.01
0.00
-0.01
4000
3500
3000
2500
2000
1500
1000
500
Wavenumbers (cm-1)

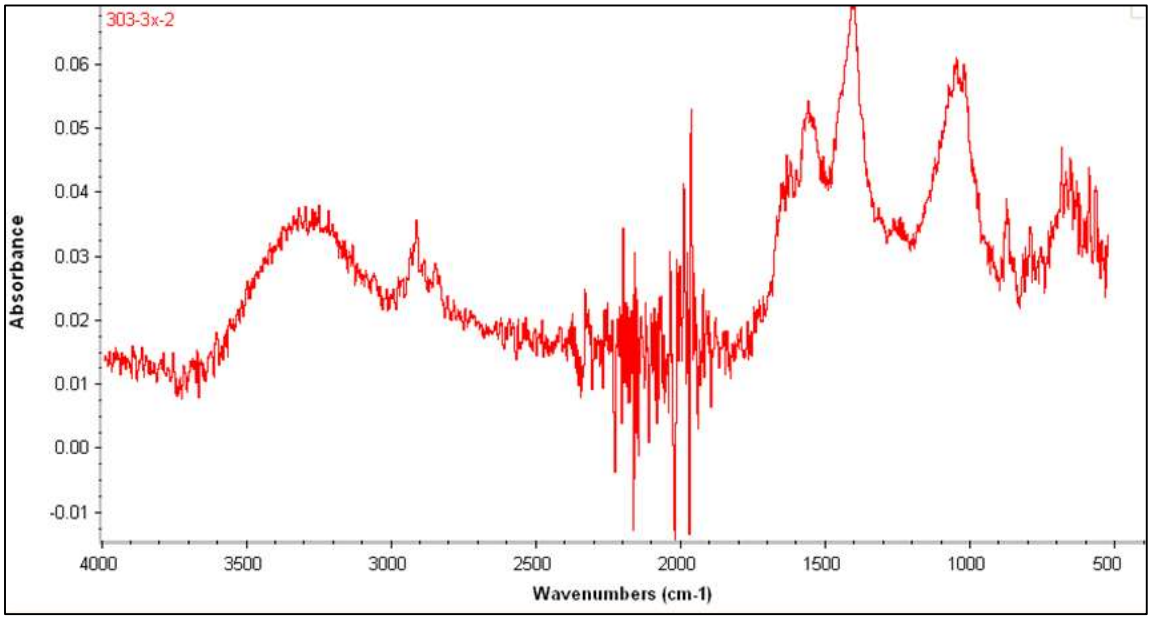
303-3x-2
Absorbance
0.06
0.05
0.04
0.03
0.02
0.01
0.00
-0.01
4000
3500
3000
2500
2000
1500
1000
500
Wavenumbers (cm-1)

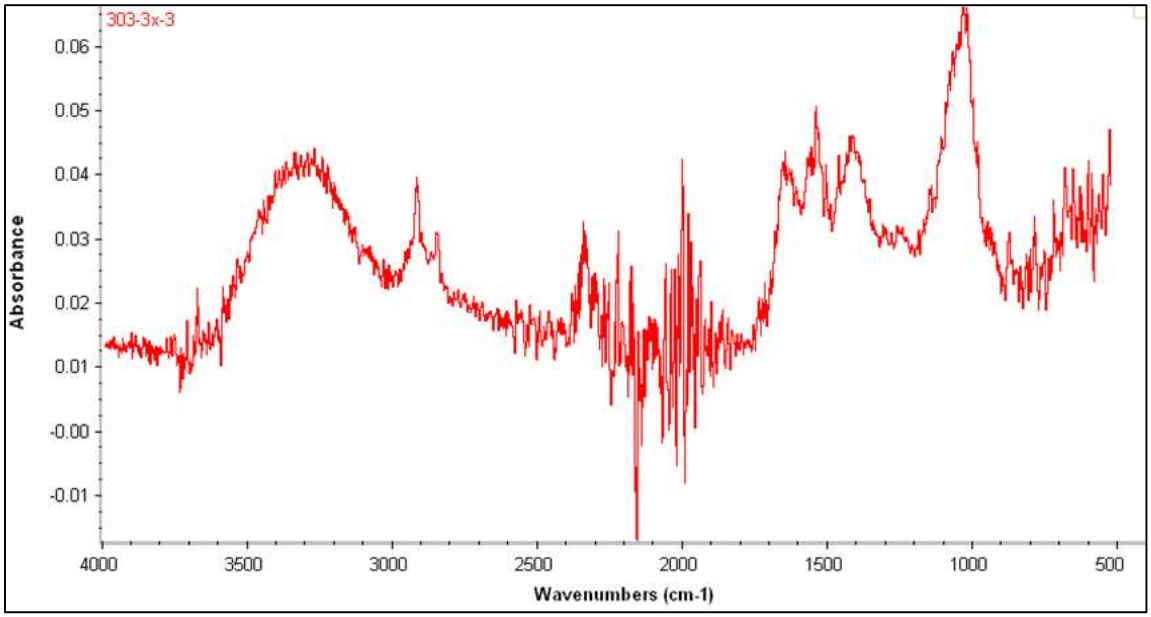
303-3x-3
Absorbance
0.06
0.05
0.04
0.03
0.02
0.01
-0.00
-0.01
4000
3500
3000
2500
2000
1500
1000
500
Wavenumbers (cm-1)

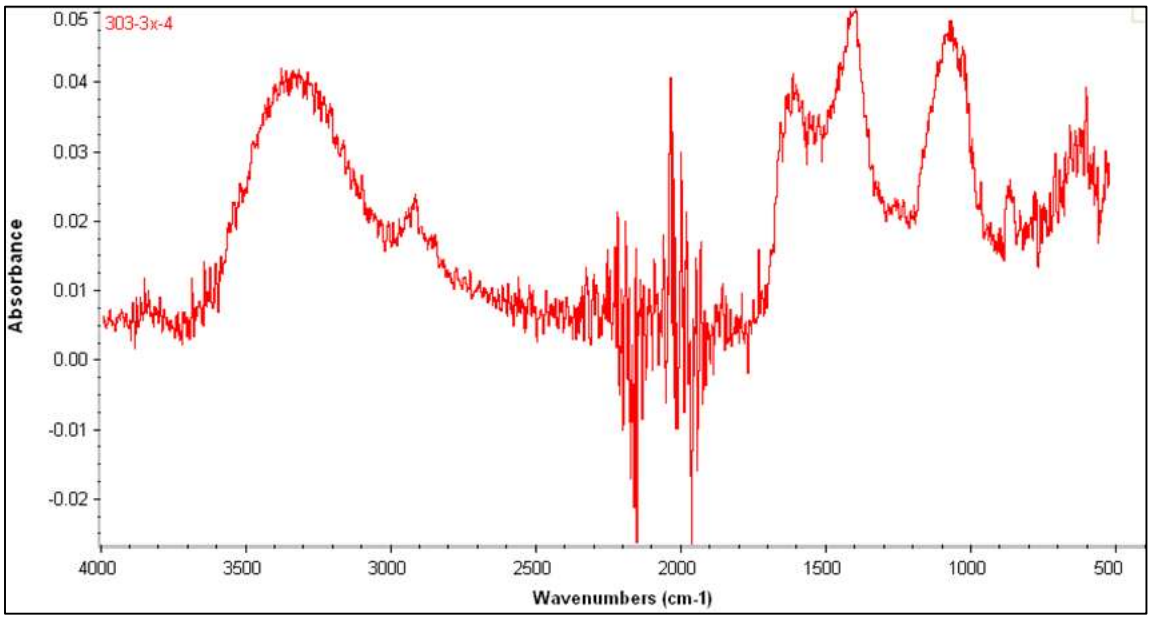
303-3x-4
Absorbance
0.05
0.04
0.03
0.02
0.01
0.00
-0.01
-0.02
4000
3500
3000
2500
2000
1500
1000
500
Wavenumbers (cm-1)

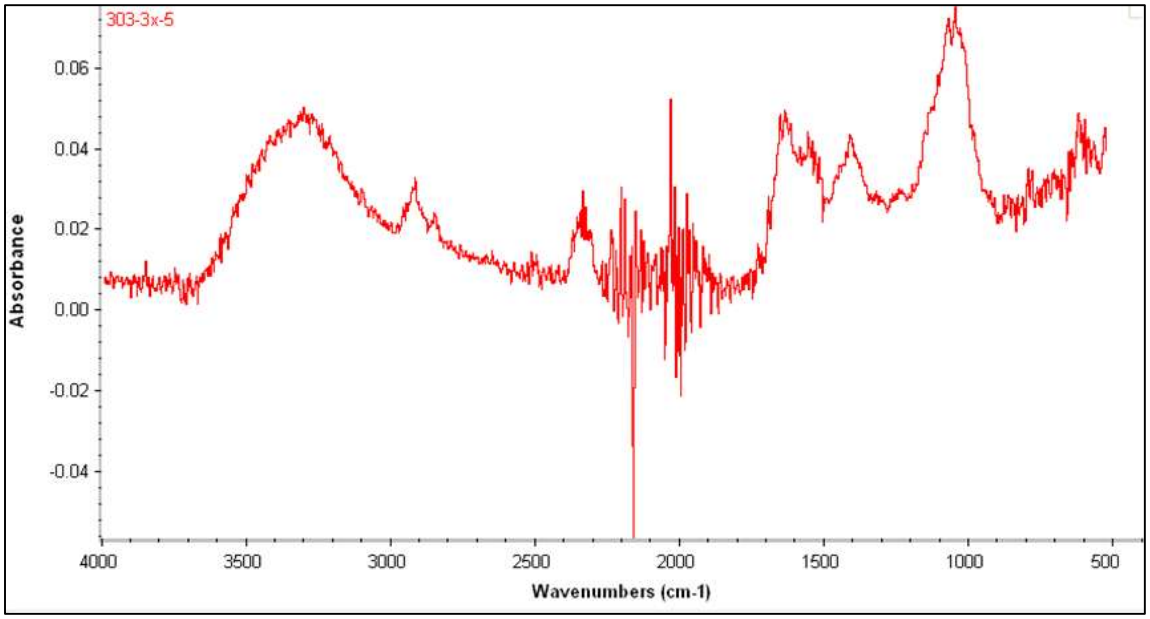
303-3x-5
0.06
0.04
0.02
0.00
-0.02
-0.04
Absorbance
4000
3500
3000
2500
2000
1500
1000
500
Wavenumbers (cm-1)

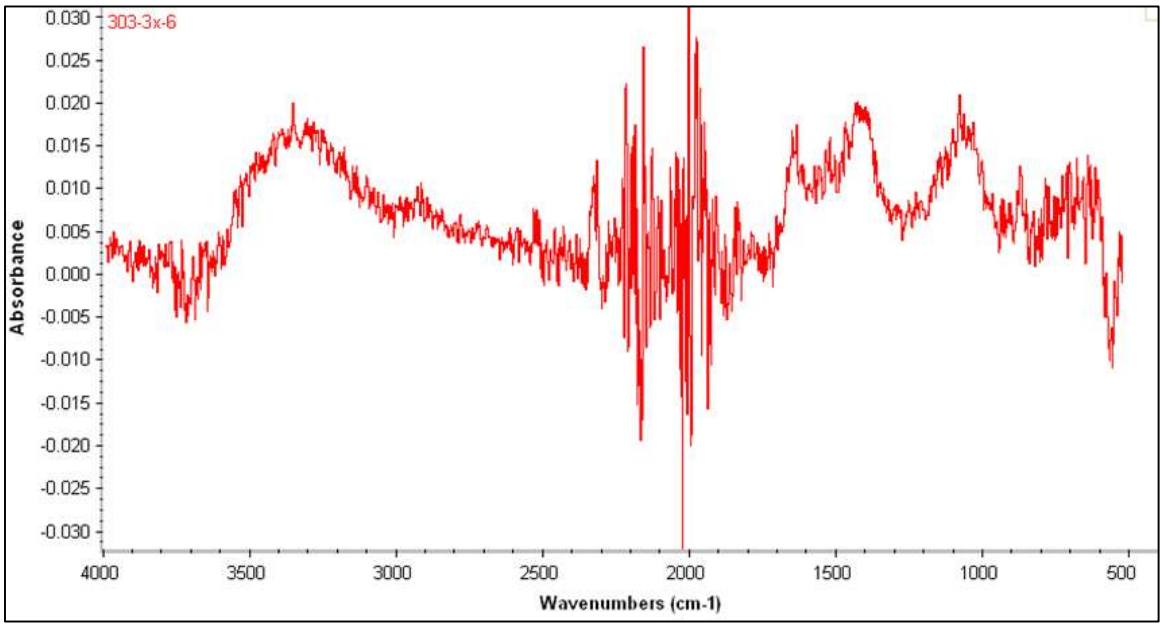
303-3x-6
0.030
0.025
0.020
0.015
0.010
0.005
0.000
-0.005
-0.010
-0.015
-0.020
-0.025
-0.030
Absorbance
4000
3500
3000
2500
2000
1500
1000
500
Wavenumbers (cm-1)

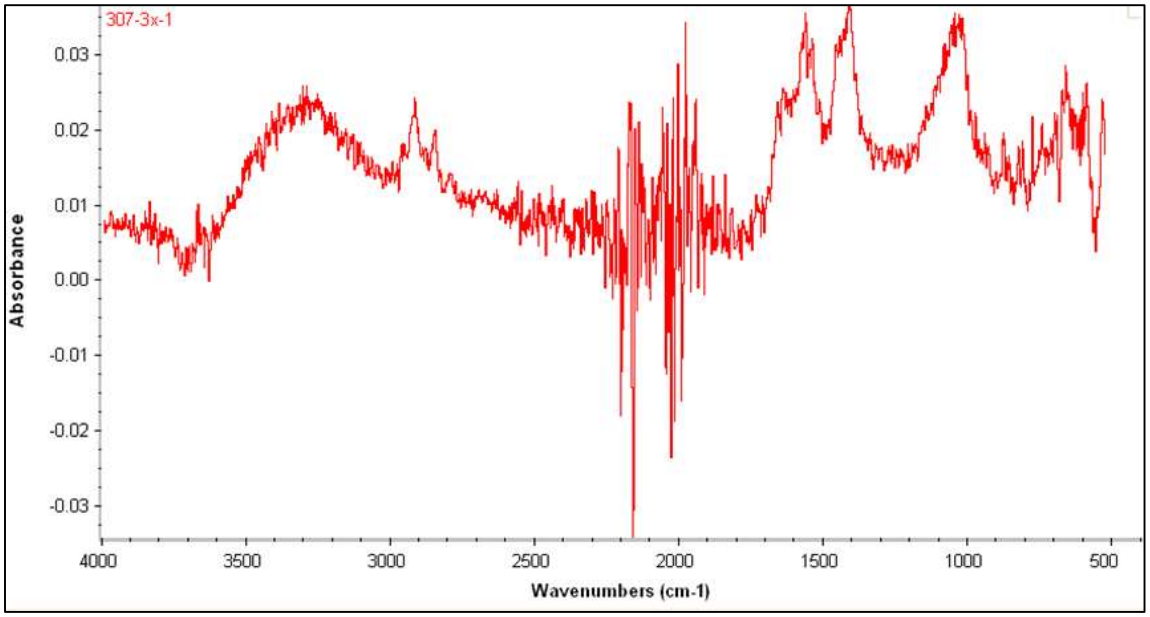
307-3x-1
Absorbance
0.03
0.02
0.01
0.00
-0.01
-0.02
-0.03
4000
3500
3000
2500
2000
1500
1000
500
Wavenumbers (cm-1)

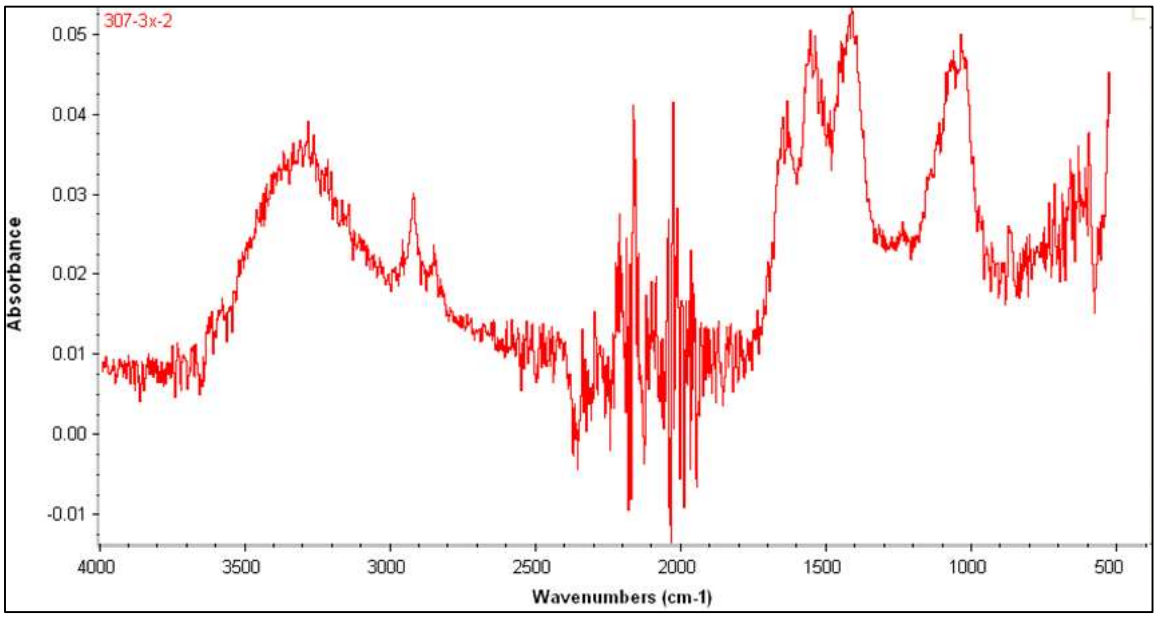
307-3x-2
Absorbance
0.05
0.04
0.03
0.02
0.01
0.00
-0.01
4000
3500
3000
2500
2000
1500
1000
500
Wavenumbers (cm-1)

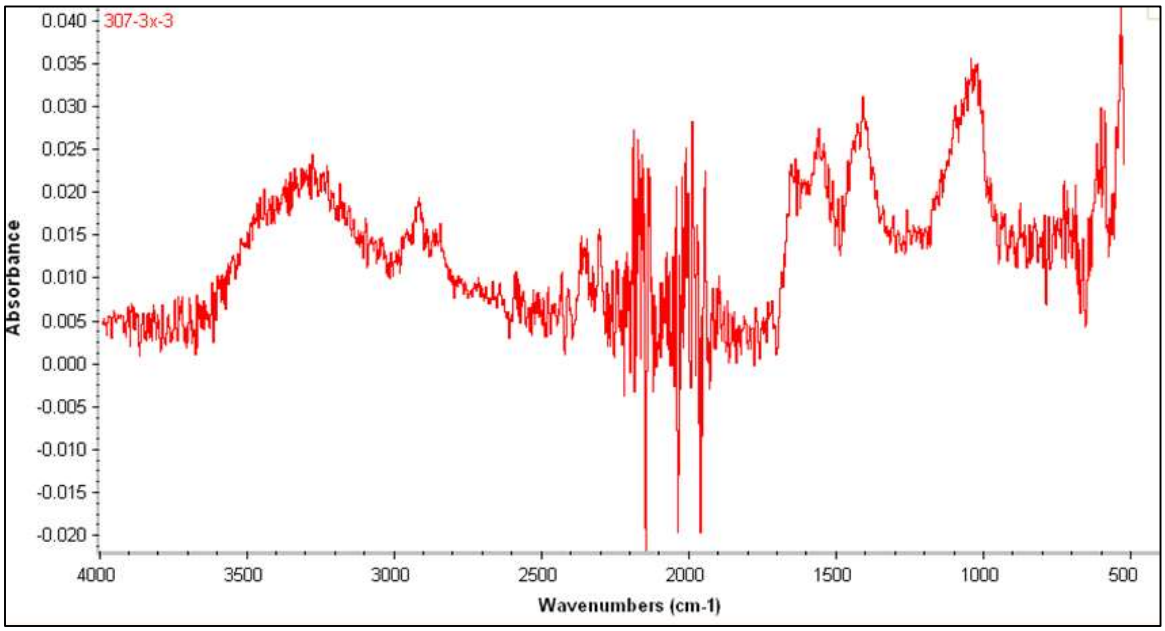
307-3x-3
Absorbance
0.040
0.035
0.030
0.025
0.020
0.015
0.010
0.005
0.000
-0.005
-0.010
-0.015
-0.020
4000
3500
3000
2500
2000
1500
1000
500
Wavenumbers (cm-1)

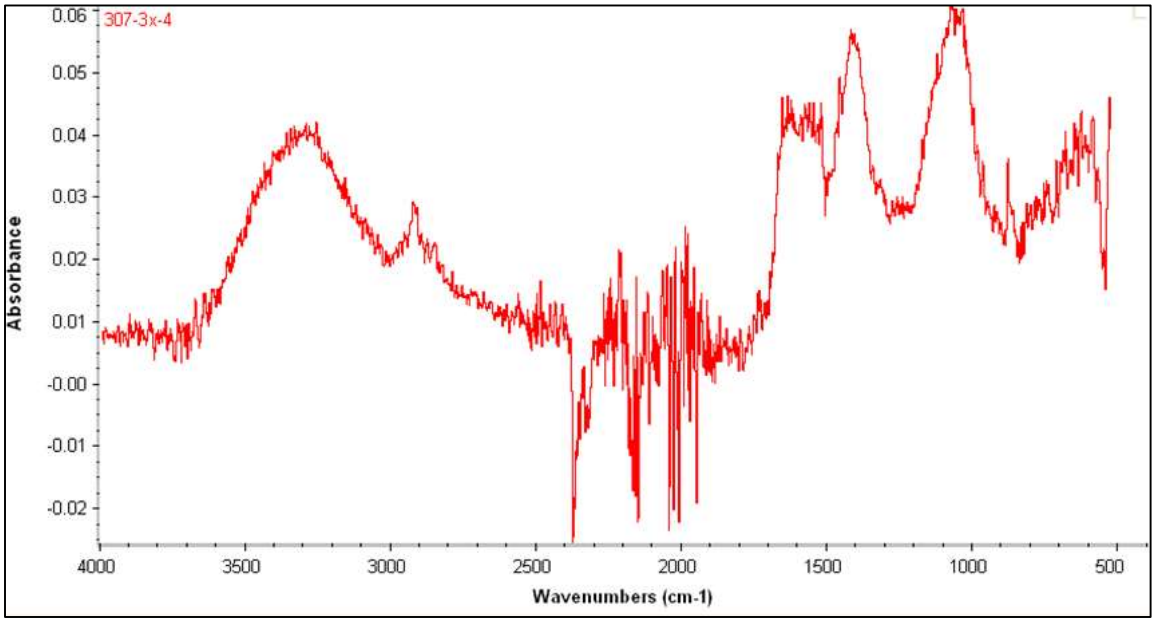
307-3x-4
Absorbance
0.06
0.05
0.04
0.03
0.02
0.01
-0.00
-0.01
-0.02
4000
3500
3000
2500
2000
1500
1000
500
Wavenumbers (cm-1)

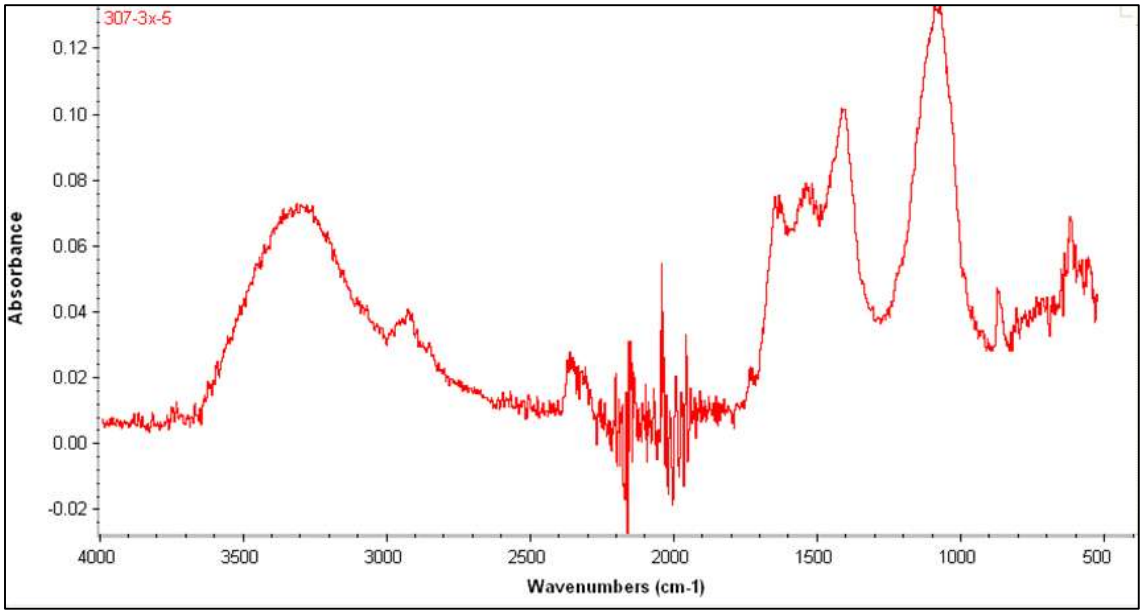
307-3x-5
Absorbance
0.12
0.10
0.08
0.06
0.04
0.02
0.00
-0.02
4000
3500
3000
2500
2000
1500
1000
500
Wavenumbers (cm-1)

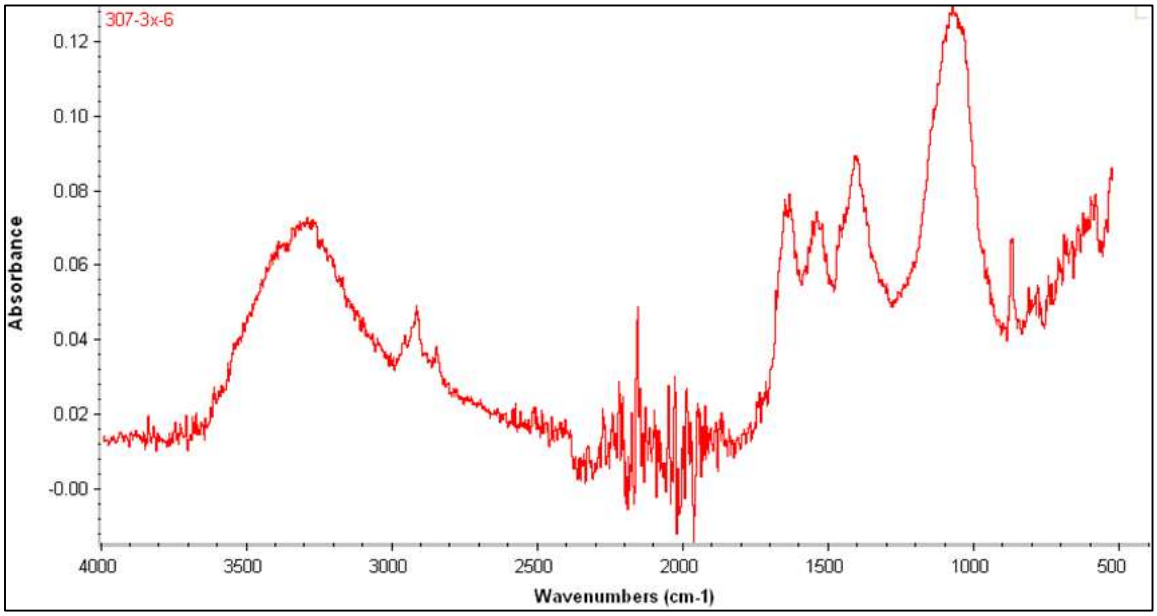
307-3x-6
Absorbance
0.12
0.10
0.08
0.06
0.04
0.02
-0.00
4000
3500
3000
2500
2000
1500
1000
500
Wavenumbers (cm-1)

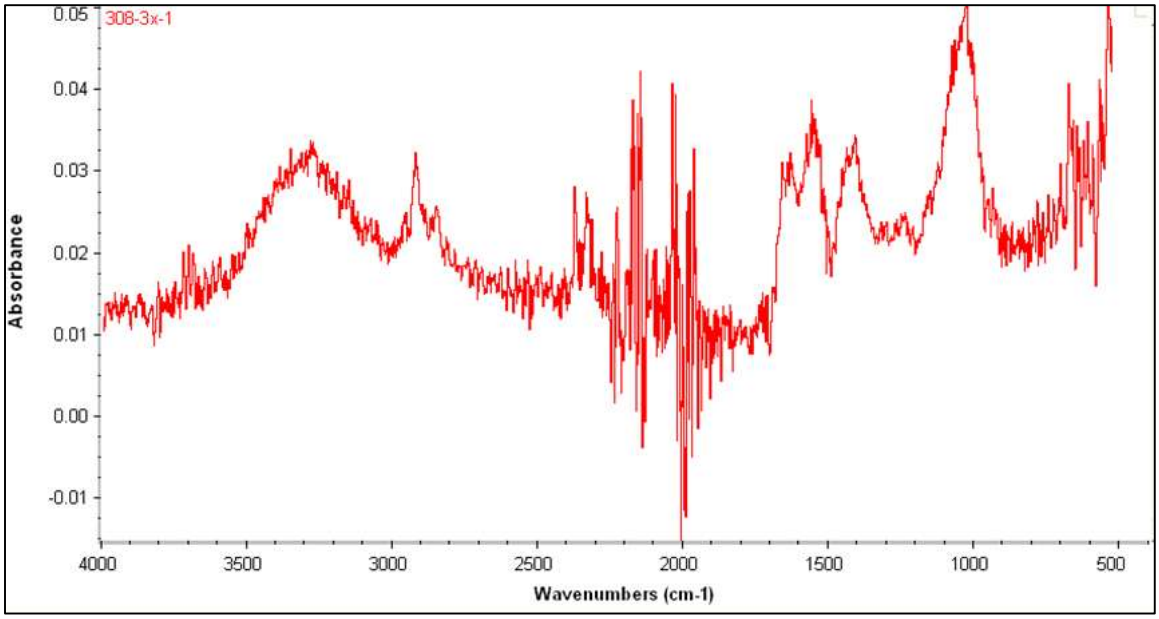
308-3x-1
Absorbance
0.05
0.04
0.03
0.02
0.01
0.00
-0.01
4000
3500
3000
2500
2000
1500
1000
500
Wavenumbers (cm-1)

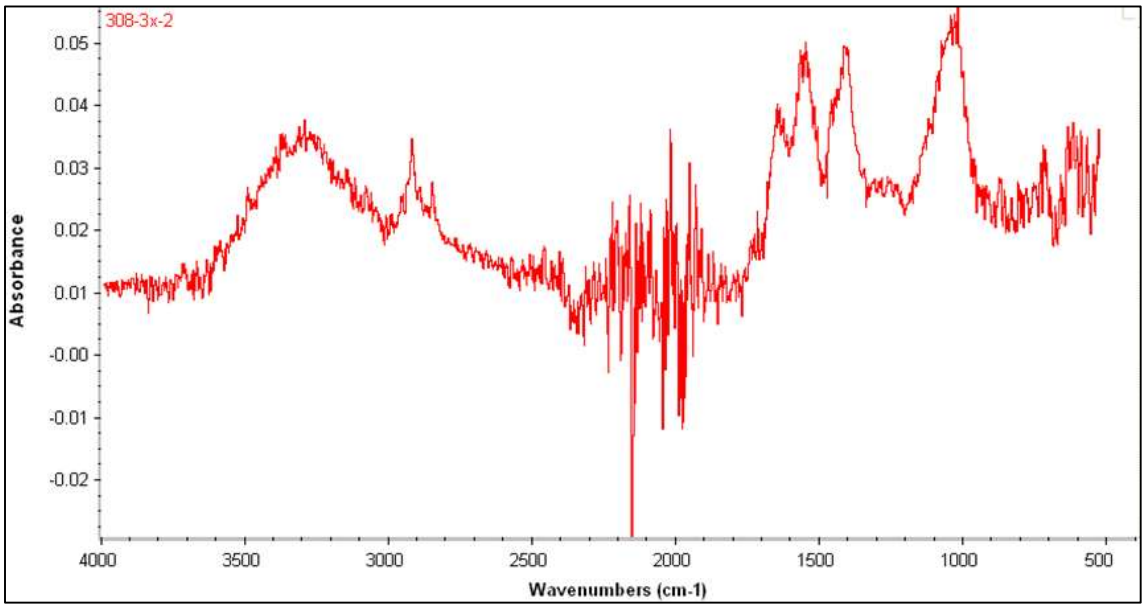
308-3x-2
Absorbance
0.05
0.04
0.03
0.02
0.01
-0.00
-0.01
-0.02
4000
3500
3000
2500
2000
1500
1000
500
Wavenumbers (cm-1)

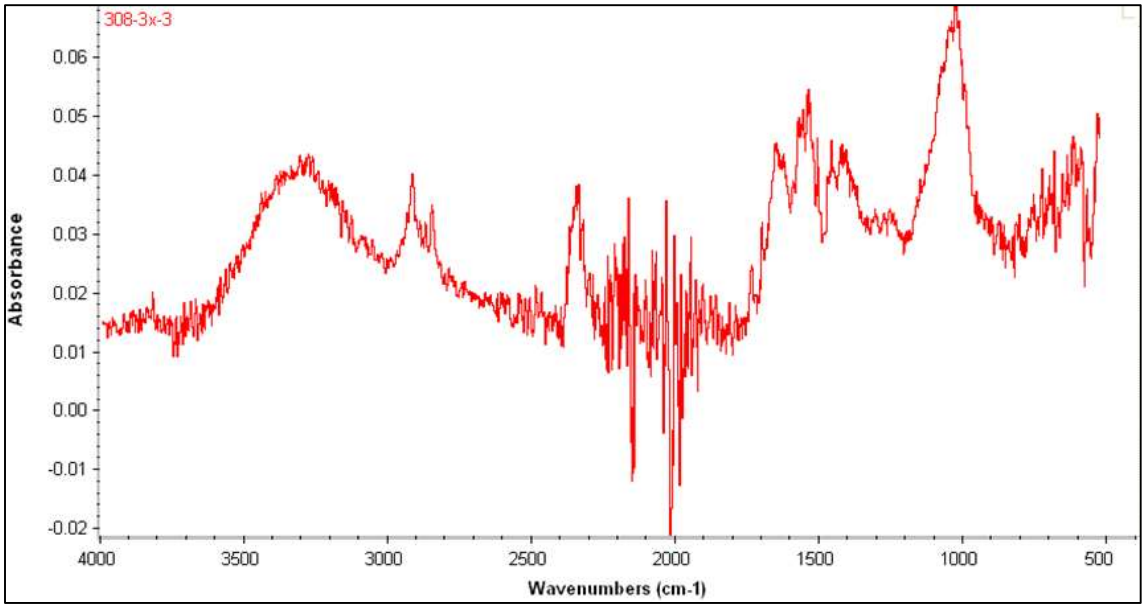
308-3x-3
Absorbance
0.06
0.05
0.04
0.03
0.02
0.01
0.00
-0.01
-0.02
4000
3500
3000
2500
2000
1500
1000
500
Wavenumbers (cm-1)

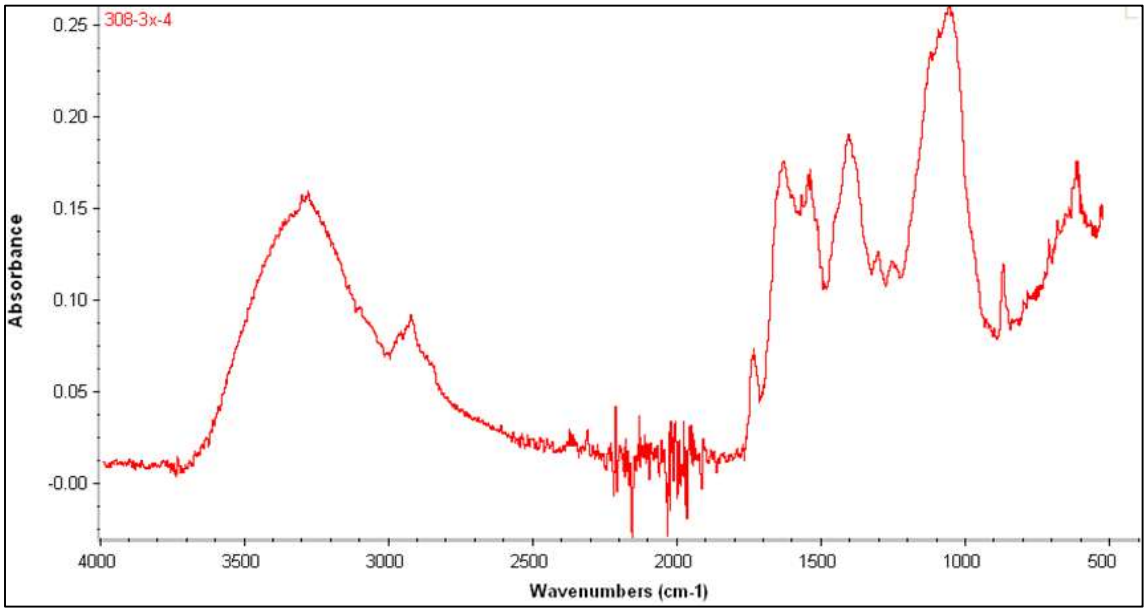
308-3x-4
Absorbance
0.25
0.20
0.15
0.10
0.05
-0.00
4000
3500
3000
2500
2000
1500
1000
500
Wavenumbers (cm-1)

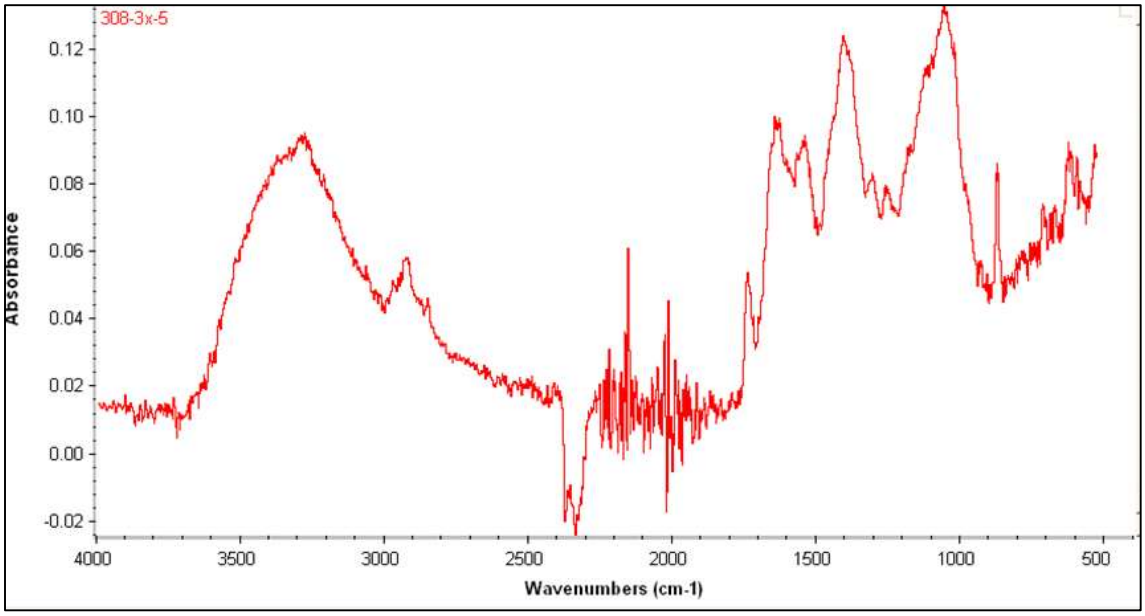
308-3x-5
Absorbance
0.12
0.10
0.08
0.06
0.04
0.02
0.00
-0.02
4000
3500
3000
2500
2000
1500
1000
500
Wavenumbers (cm-1)

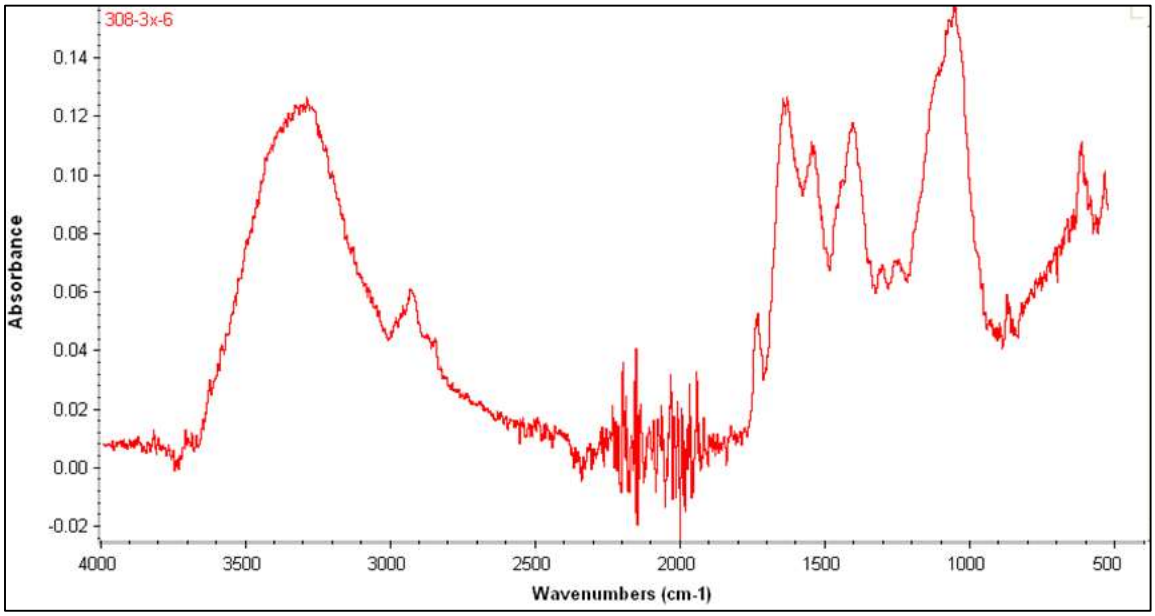
308-3x-6
Absorbance
0.14
0.12
0.10
0.08
0.06
0.04
0.02
0.00
-0.02
4000
3500
3000
2500
2000
1500
1000
500
Wavenumbers (cm-1)